2019

Developing a Rational Peptide Ligand Design Method Using CD13 as a Prototype Target Receptor

Md Zahir Uddin
University of the Pacific, zahirshohag@yahoo.com

DEVELOPING A RATIONAL PEPTIDE LIGAND DESIGN METHOD USING CD13 AS A PROTOTYPE TARGET RECEPTOR

by

Md Zahir Uddin

A Dissertation Submitted to the

Graduate School

In Partial Fulfillment of the

Requirements for the Degree of

DOCTOR OF PHILOSOPHY

Thomas J. Long School of Pharmacy and Health Sciences
Pharmaceutical and Chemical Sciences

University of the Pacific
Stockton, California

2019

DEVELOPING A RATIONAL PEPTIDE LIGAND DESIGN METHOD USING CD13 AS A PROTOTYPE TARGET RECEPTOR

by

Md Zahir Uddin

APPROVED BY:

Dissertation Advisor: Bhaskara R. Jasti, Ph.D.

Dissertation Co-Advisor: Xiaoling Li, Ph.D.

Committee Member: Jerry Tsai, Ph.D.

Committee Member: Xin Guo, Ph.D.

Committee Member: John Livesey, Ph.D.

Department Chair: William K. Chan, Ph.D.

Dean of Graduate School: Thomas Naehr, Ph.D.

DEVELOPING A RATIONAL PEPTIDE LIGAND DESIGN METHOD USING CD13 AS A PROTOTYPE TARGET RECEPTOR

By

Md Zahir Uddin

DEDICATION

This dissertation is dedicated to my father Zamal Uddin Ahmed, mother Salma Zamal, wife Farjana Akther and our son Azan Zahir.

ACKNOWLEDEGEMENTS

I would like to express my sincere gratefulness to my advisor Dr. Bhaskara Jasti for giving me the opportunity to work with him. I thank Dr. Jasti, for his continuous support, guidance, and suggestions throughout the course of Ph.D. I gratefully thank Dr. Xiaoling Li, for his valuable guidance, help and suggestions. I would also like to thank Dr. Jerry Tsai and Dr. Hyun Joo for their help and guidance in designing the peptide ligands for this study. I thank Dr. Xin Guo, for his suggestions and for being on the committee. I would like to thank Dr. Livesey for his suggestions and serving on the committee. I appreciate Dr. Mamoun Alhamadsheh for letting me work in his laboratory. I would like to thank Drs Ren, Wrischinik, Livesey for letting me use the mass spectrometer, confocal microscope, and microplate reader in their laboratories. I thank Drs John Wang, Xuan Gao, Guoying Jiang, Arturo Orjalo, Alexis Dunkle, and Shrenik Mehta for their help during my internship at Genentech. I would like to thank Ms. Kathy Kassab and Lynda Davis for all their help during my course of study. My appreciation goes to the University of the Pacific Holmok Cancer Research Grant for the project. I would also like to appreciate the Board of Directors of Pacific Pharmacy Associates for the prestigious Carl Riedesel Endowed Graduate Scholarship. I thank AAPS-DDDI section, and Formurex Inc. for the travel awards and Drs Ravindra Vasavada, Madhukar and Kishori Chaubal for providing me the scholarships. I would like to thank my previous and current lab mates Dr. Yoshiko Katori Stowell, Dr. Yu Zheng, Dr. Poonam Saraf, Dr. Sameer Sachdeva, Dr. Dan Su, Dr. Wabel, Poonam, Jingda, Xingchen, Lavanya, Yan, Ryan, and Margrit for their support. I appreciate Dr. Patrick Batoon, Yuntao, and Yadwinder for their help in mass spectrometry. I thank my friends Mezbah, Dip, Anis, Nayeem, and Anik for always being there for me. I would like to appreciate Arindom, Tuhin, Razan, and Toufiq for their support and friendship.

Finally, I would thank my parents, my wife, our son, my sisters, and my parents in law for their help and support that made all this possible. They are the most important persons in my life. My dad always wanted me to see as a doctorate. So, here it is dad and it's for you. I have a lot of things to say when we meet again. I do not know how can I thank my mom. She made me what I am today. I love you mom. I would not be able to do all this without the support of my friend/ my love/ my wife, Farjana. Thank you Farjana for tolerating me, and keep it on; I love you. I know you are always there for me. I would like to especially mention about our son, Azan Zahir. He is the best thing that has happened in my life. Azan, I want to see you healthy and happy always; keep exploring son and may almighty bless you to be a good human being.

Developing a Rational Peptide Ligand Design Method Using CD13 as a Prototype Target Receptor

Abstract

By Md Zahir Uddin

University of the Pacific
2019

Structure based computational peptide design methods have gained significant interest in recent years with the availability of structural insights of protein-protein interactions obtained from the crystal structures. Most of these approaches design new peptide ligands by connecting the crucial amino acid residues from the protein interface and are generally not based on any predicted receptor-ligand interaction. In this work, a peptide design method based on the Knob-Socket model was used to identify the specific ligand residues packing into the receptor interface. This method enables rational peptide ligand design by predicting amino acid residues that will fit best at the binding site of the receptor protein. Specific peptide ligands for the model receptor CD13 that are overexpressed in several cancer types were designed in this study. From the initial library of designed peptides, three potential candidates were selected based on simulated energies in the CD13 binding site using the programs Molecular Operating Environment (MOE) and AutoDock Vina. In the CD13 enzymatic activity inhibition assay, the three identified peptides exhibited 2.7 to 7.4 times lower IC_{50} values (GYPAY, 227 μM; GFPAY, 463 μM; GYPAVYLF, 170 μM) when compared to the known peptide ligand CNGRC(C1-C5) (1260 μM). The binding affinities of the peptides (GYPAY, K_i = 54.0 μM; GFPAY, K_i = 74.3 μM; GYPAVYLF, K_i = 38.8 μM) were 10 to 20 times higher than that of CNGRC (C1-C5) (K_i = 773 μM). The double reciprocal plots from the steady state enzyme

kinetic assays confirmed the binding of the peptides to the intended active site of CD13. The cell binding and confocal microscopy assays showed that the designed peptides selectively bind to the CD13 on cell surface. The designed peptide-drug conjugates (PDCs) showed lower in vitro cytotoxicity and slightly better in vivo antitumor efficacy as compared to a model drug MMAE. However, the PDCs contributed to much lower weight loss in mice indicating lower side effects in vivo.

This study demonstrated the feasibility of a Knob-Socket based rational design of novel peptides ligands in improving the identification of specific binding in comparison to the labor intensive current methods.

TABLE OF CONTENTS

LIST OF TABLES

Table

LIST OF FIGURES

Figure

Chapter 1: Introduction

The pharmacological properties of a drug determine the resulting biological effects in patients. These biological effects are generally produced by the interaction of the drug molecule with its receptors at the site of action. The drug-target interaction efficacy remains undermined unless the drug gets delivered to the action site at a concentration that causes maximum therapeutic effect and minimum side-effects (1). However, the activity of majority of the currently used pharmaceuticals is not based on their ability to accumulate specifically in the pathological site. Typically, the active agent uniformly distributed throughout the body, has to cross numerous bio-barriers, like other organs, membranes and intracellular compartments before it reaches the site of action. During this process, the molecule can get inactivated or exhibit undesirable effect in tissues not involved in the pathological process. Consequently, the drug needs to be administered in high amounts to achieve the required therapeutic concentration in the pathological body compartment. Thus, a large portion of the administered dose is just wasted in healthy normal tissues. Moreover, this nonselective distribution, antigenic and/or cytotoxic drugs may lead to many negative side effects (2). Drug targeting, i.e. predominant drug accumulation in the target organ or tissue, is one feasible option to tackle many of these challenges.

1.1 Drug Targeting

Drug targeting can be defined as the ability of a drug to selectively accumulate in the target organ or tissue in a manner that the drug concentration at the pathological site is high, while the concentration in the healthy non-target body parts is low, to prevent any peripheral toxic effect. The key advantages of drug targeting are: (a) simplified drug administration protocol, (b) reduced quantity of drug required for therapeutic effect and lower cost of therapy,

and (c) achieving markedly increased drug concentration at target site without negative side reactions in non-target body compartments. The same targeting strategy can also be applied to a great extent for the diagnostic molecules (3).

The concept of drug targeting is not new. It was first suggested by Paul Ehrlich almost a century ago when he introduced the hypothetical entity - "magic bullet" comprising of two components – first one to recognize and bind to the target and the second one which will impart the therapeutic effect. In current concept the targeted drugs have three coordinated components: (a) the drug molecule, (b) the targeting moiety/ligand, (c) pharmaceutical carrier to deliver multiple drug molecules per targeting moiety. Targeting can be applied on whole organ level, on cellular level specific for a certain organ, or even on the subcellular level such as, cell surface antigens (2, 4, 5).

The most widely used targeting strategy is based on the knowledge that every organ or tissue contains certain molecules/biomarkers (antigens) that are specific for the organ of interest. To successfully deliver a drug to the target organ, another molecule (targeting moiety) can be used as a cargo unit which has the capability to specifically recognize and interact with the target antigen. Based on this principle, many targeted drug delivery systems have been constructed that can deliver pharmaceuticals to various organs and tissues. However in many cases, certain physical principles or physiological features of the target organ can be used for effective targeting of pharmaceuticals (6-9).

1.2 Drug Targeting Strategies

The principal drug targeting strategies which have been investigated in different experimental and clinical settings are: (a) direct application of the drug into the target organ or tissue, (b) passive accumulation of the drug molecule through leaky vasculature (passive

targeting), (c) physical targeting utilizing the differential pH and/or temperature at the target pathological compartment, or using paramagnetic drug carrier under the action of outside magnetic field, (d) targeting with the aid of ligand molecules (active targeting) having specific affinity towards the target site (2, 3).

1.2.1 Direct application of drug into the target site. In some cases, drug targeting can be achieved by simply administering the drug into the organ of interest. Although it sounds like a simple technique but the applicability is very limited and developing the formulation for direct application can be very complicated (2, 3). Notable examples of this technique include intra-articular application of methotrexate using liposomal formulation for arthritis (10), ophthalmic administration of carteolol loaded in nanoparticles to treat intraocular hypertension (11), and infusion of thrombolytic enzymes in coronary for the treatment of thrombus induced myocardial infarction (12).

1.2.2 Passive targeting. The blood vessel might become leaky under certain pathological states. Highly permeable leaky vascular endothelium was observed in tumors (13), oxygen deficient areas of infarcted myocardium (14), and inflammation (3). In those areas with high vascular permeability, relatively large nanoparticles like liposomes or micelles (size ranging from 10 to 500 nm) can penetrate and embedded inside interstitium. These nanoparticles can carry the drug to the leaky area and release the drug by conventional carrier degradation. The size of the nanocarriers can be adjusted to modulate the efficacy of the passive targeting system. This passive or spontaneous drug delivery is also known as ‘enhanced permeability and retention’ (EPR) effect (Figure 1.1) and is mostly used for targeting cancers (2, 15). The prerequisite for this type of targeted delivery system is that the carriers used should be able to circulate in the blood for long enough duration to allow drug accumulation. An excellent

example of this EPR based targeting is the commercial drug formulation, Doxil, which is long circulating polyethylene glycol (PEG) coated liposomes carrying doxorubicin (16). Long circulating micellar system with smaller cut-off size was also shown to deliver the drug effectively into the tumor (17). Long circulating liposomes may also be used to deliver drugs in myocardial infarction area (18).

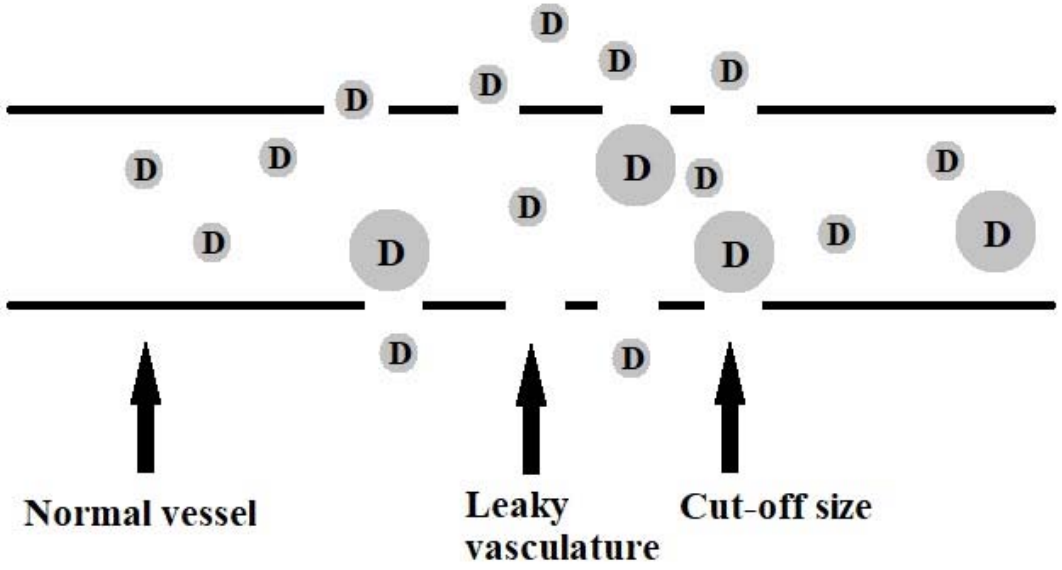

Figure 1.1: Schematic representation of the passive targeting of drugs/drug carriers in leaky vascular area and the role of cut-off size

1.2.3 Physical targeting. Different physical factors of both endogenous and exogenous origin have been explored for targeted drug delivery. In the first case, targeting relies on pathological areas have different characteristics, like temperature, pH and/or redox potential when compared to normal areas. It has been observed that the inflamed or neoplastic tissues generally exhibit lower pH and some degree of hyperthermia. This allows the use of stimuli-responsive drug transporters which degrade at higher temperature or lower pH than the normal

physiological range, releasing the entrapped drug. Although the delivery systems are uniformly distributed throughout the body but they will only disintegrate and release the drug at the target area having abnormal physiological properties (19) (Figure 1.2).

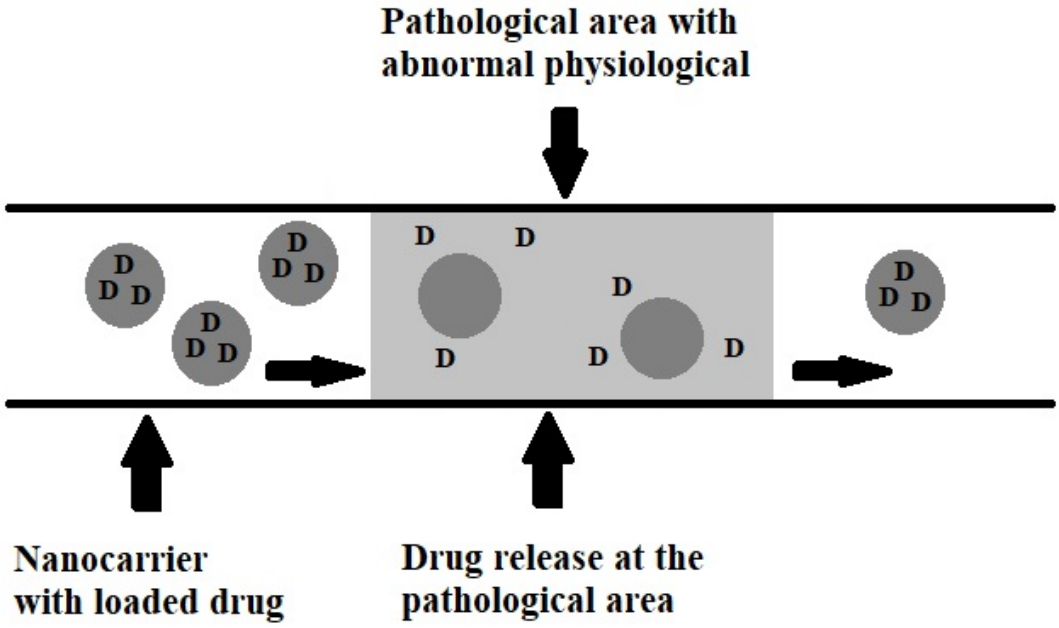

Figure 1.2: Schematic representation of the physical drug targeting

Temperature-sensitive liposomes containing anti-cancer agent methotrexate have been shown to accumulate in tumors significantly faster when intravenously injected into tumor bearing mice. This preferential accumulation was especially prominent when external heat was applied at the tumor region (20). pH sensitive liposomes also achieved similar effects and are currently in use to deliver genetic materials and drugs to the target of interest (21).

An example of drug targeting by external physical force is the magnetic drug delivery. To achieve this, drug is immobilized on a microcarrier with ferromagnetic properties. When

administered intravenously, these carriers can accumulate in the area where an external magnetic field is applied. The magnitude of accumulation will be dependent on the rate of blood flow and the applied magnetic field intensity (22). Streptokinase was delivered in carotid arteries of experimental dogs for targeted lysis of thrombus by immobilizing the streptokinase on dextran coated iron oxide microparticles (23).

1.2.4 Active targeting. The drug targeting approaches described above are not universal. They have some crucial drawbacks. Direct application of drug into the target organ/tissue can be technically challenging, or even the pathological site may be delocalized. In many instances, the pathological area does not exhibit significant difference in terms of vascular leakiness, local pH or temperature, which makes the passive or physical targeting very difficult to achieve. Magnetic drug accumulation is also heavily dependent on the rate of blood flow in the target area. The most common and universal strategy to convey specific affinity towards a target site to a nonspecific drug is the attachment of this drug with another entity (usually called a targeting moiety or ligand molecule) which can selectively recognize and bind to the target site. Direct coupling of the drug to a targeting molecule is the simplest way to construct an active targeted drug delivery system (2) (Figure 1.3).

Immunotoxins is one of the earliest examples of active drug targeting by direct coupling of a drug to a targeting moiety (24). Reservoir type or particulate drug carriers have also been used to load the drug in active targeting. This enables high drug loading, eliminates the need of covalent conjugation, and prevents enzymatic degradation of the drug. This also provides the opportunity to control permeability, size, and circulation time (25).

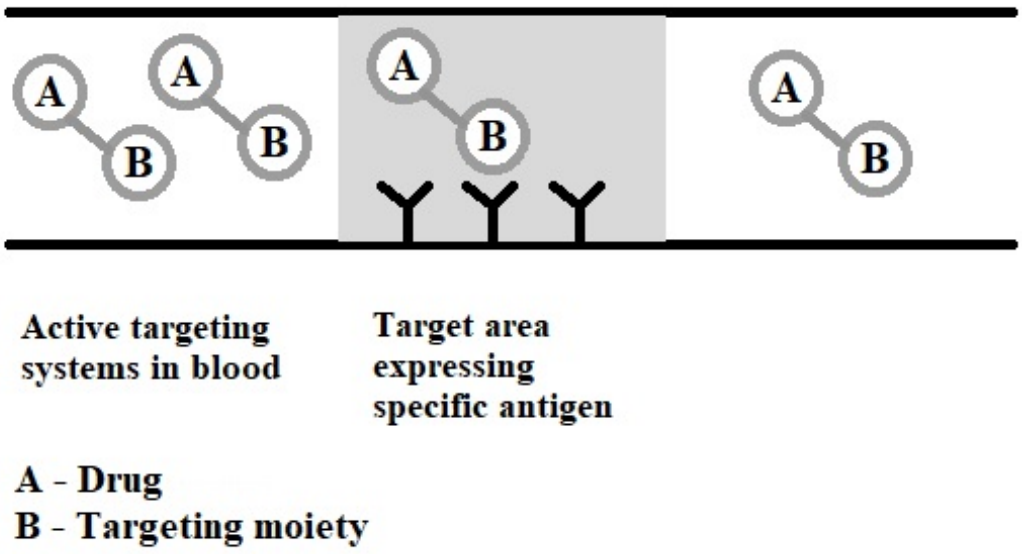

Figure 1.3: Schematic representation of active drug targeting

1.3 Targeting Ligands/Moieties

Targeting ligands can be roughly classified into the following categories: (a) small molecules (small molecule, vitamins, and carbohydrates), (b) antibodies, (c) protein domains, (d) nucleic acid based aptamers, and (e) peptides (26, 27). These commonly used ligands are illustrated in Figure 1.4 in increasing order of their sizes (28-31).

1.3.1 Targeting with small molecules. One of the more customary targeting ligands are small molecules. The main advantages of small molecule as the targeting ligand are good stability profile, straightforward conjugation technique, and low manufacturing cost, considering that it can be synthesized with high yield. But so far there is no systematic protocol to develop such small molecule ligand and many of the already developed ligands do not show high binding affinity and specificity towards the target. Vitamin H, also known as Biotin, was used for

superficial conjugation on nanoparticles having coated streptavidin for in vitro use. The clinical use of this system is very limited because of immunogenicity coming from bacterial origin streptavidin (27).

One of the most extensively investigated small molecule ligand for clinical application is folic acid (vitamin B6). Folic acid binds to the endogenous folate receptors with high affinity. Folate receptors have been reported to be frequently upregulated in many cancer types. A wide range of therapeutic or diagnostic agents have been conjugated to folate for selective drug delivery in tumor site, including chemotherapeutic drugs, protein therapeutics/toxins, gene therapy, oligonucleotides, radio-imaging agents, MRI agents, and drug-loaded nanoparticles (32, 33).

Another type of small molecule ligand which has been studied is benzamide, especially anisamide. The receptor for benzamides is the sigma receptors. Benzamides can target the drug/drug carrier to the tissues which express sigma receptors (34, 35).

Carbohydrates that interact with certain cell surface receptors, can also be used as small molecule targeting ligand. Targeting with carbohydrates uses the concept that endogenous lectin interacts with carbohydrates. This type of targeting requires multiple carbohydrate interactions to establish strong binding. Galactose or galactose-mimics can bind to asialoglycoprotein receptors, which are cell surface lectin receptors heavily expressed on hepatocytes. Lex and ManLAM carbohydrates can be used to target the dendritic cells preferentially expressing DC-SIGN lectin receptors (27, 36).

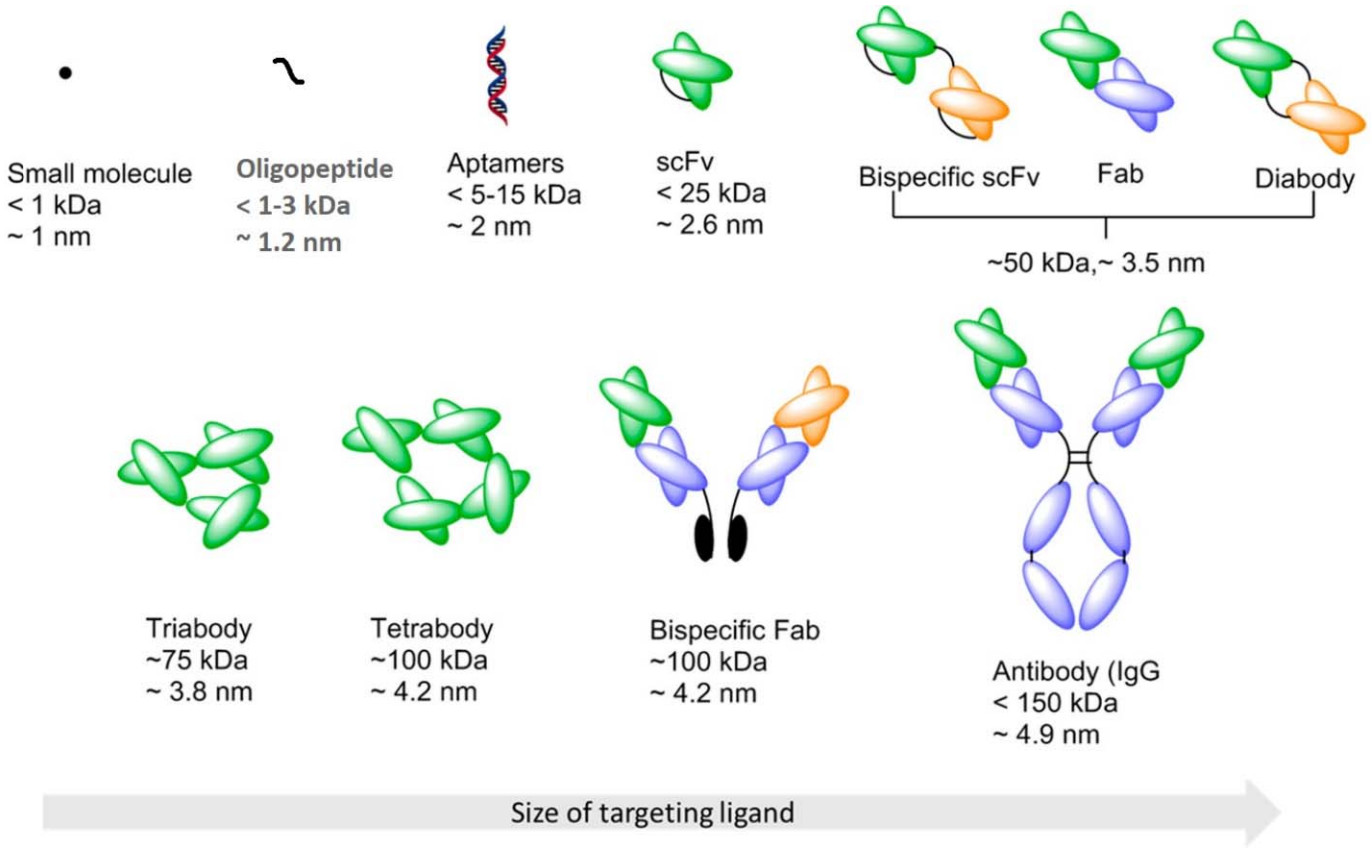

Figure 1.4: Commonly used targeting ligands. Molecular weights and Stokes–Einstein radii are given below the ligand label. Stokes–Einstein radius were estimated using the formula MW (kDa) = $1.32 \times R^3$ (in nm^3). MW is molecular weight; R is Stokes–Einstein radius.

1.3.2 Targeting with antibodies. Antibodies are serum glycoproteins produced by vertebrates, which bind selectively with antigens that induce their production. These (Immunoglobulins -Igs) are Y shaped molecules. Structurally, antibody contains two regions- two fragment antigen binding arms (Fab) and the stem (Fc fragment) connected to the Fabs through a hinge. Based on the constant region, immunoglobulins can be classified into IgA, IgD, IgE, IgM, and IgG and symbolized as α, δ, ε, μ and γ, respectively. Among them IgGs are most extensively used for therapeutic purpose. Polyclonal antibodies are a heterogeneous mixture of antibodies. They are produced from different clones of B cells and thus lack immunochemical similarity. They are active towards multiple epitopes of a single antigen. On the other hand, a monoclonal antibody is homogenous and is active against a single epitope. Monoclonal antibodies (mAb) are produced from single clone of B cell of one animal (37, 38).

There are different mechanisms by which antibodies impart therapeutic efficacy, but in many instances their activity does not produce a lasting effect. Therefore, various strategies have been utilized to augment their activity. Antibody-drug conjugate (ADC) is one such approach, which harness the antibody's specificity and enable the targeted delivery a drug to the pathological site to enhance the activities of both antibody and drug molecule (39).

Antibodies were originally considered as targeting moieties because of their availability and outstanding specificity as in vivo targeting ligand. The extensive use of antibodies in in vivo therapeutics as targeting ligands resulted from many developments that overcame the limitation of cross-species immunogenicity. Most of the current antibodies used for targeting are monoclonal and of murine origin. But those produced from other species and polyclonal antibodies from rabbit have also been very effective. Additionally, there are number of chimeric and humanized antibodies which have been used successfully for targeting. Most of these

antibodies impart targeting by interacting with the extracellular domains of various cell surface proteins (27, 40-42).

Two of the most important challenges of antibody-drug conjugates have been immunogenicity and purity. The body may recognize antibodies as foreign entity and initiate compensatory immunogenic reaction. And the conventional drug conjugation techniques often lead to heterogeneous product mixtures having different conjugation sites, antibody-drug molar ratios, and pharmacokinetic and safety profiles (27).

1.3.3 Targeting with protein domains. Targeting with antibody molecules have some intrinsic challenges as compared to small molecule targeting ligands. Antibody molecules contain multiple light and heavy chains which are linked via disulfide bonds. This sophisticated structure makes them difficult to express and the site-specific conjugation of the drug or drug carrier is a very complicated process. In case of drug carriers, it is also very difficult to accommodate multiple antibody targeting ligands on the carrier surface due to the large size of the antibody molecules. Additionally, it is a very time consuming and complicated task to engineer the full length antibody molecule to optimize its targeting efficiency (27).

In general, an ideal protein targeting moiety should have: (a) sufficient solubility with minimal aggregation and high stability, (b) expression in bacterial system in high quantity and lower production costs, and (c) possess functional units that allow site specific conjugation (27).

Numerous efforts have been made to reduce the size of the antibody molecule and create smaller binding units having affinity and specificity like an antibody. Various protein scaffolds have been explored in order to find such compliant ligands, such as, antibody fragments,

knottins, avimers, affibodies, centyrins, Kunitz domains, adnectins, anticalins, darpins, affilins, etc. (31, 43, 44).

1.3.4 Targeting with aptamers. Aptamers are small single stranded nucleic acids, RNA or DNA. They can display diverse structures and possess the potential to bind to many biochemical targets including small molecules and large proteins. Since first developmental work, they have existed as a distinct class of targeting molecules. Aptamer's binding ability derives from its sequence; a 5' and 3' consensus region ranging from 12-20 nucleotide long which flanks a central part of entirely or partially randomized nucleotide sequence. Aptamer's advantages as the targeting moiety include: (a) aptamers can be synthesized with specific functional moieties like amino, sulfhydryl, carboxylate or aldehyde, at one end which allows simple site specific conjugation and prevents heterogeneous product mixtures, (b) they are generally non-immunogenic, (c) they are non-toxic, and (d) they can be modified for stability in circulation. Aptamers can be synthesized chemically with low batch to batch variability. Because of their smaller size as compared to antibodies, they can form compact structures and bind to clefts, and enzymatic active sites more efficiently. One major limitation of aptamer based targeted drug delivery in vivo has been the degradation of aptamers by nucleases in the biological system. Attempts have been made to develop nuclease resistant aptamers by replacing 2'-hydroxyl RNAs. Aptamers resistant to nuclease activity which can bind to different cancer biomarkers (HER2, MUC1, HER3, EGF receptor, PSMA, VEGF receptor) have been successfully applied for various tumor targeting (27, 45-48).

1.3.5 Targeting with peptides. Short chains of amino acids linked by amide bonds are called peptides. Peptides (except the cyclic ones) contain an N-terminal (amine end) and a C-terminal (carboxyl end) (Figure 1.5). Amino acid units in the peptide sequence are called

"residues" because either a proton (H^+) from the amine side or a hydroxyl ion (OH^-) from the carboxyl side, or both, are released as a water molecule during each amide bond formation. Peptides differ from proteins (also chains of amino acids) on the number of residues, and conventionally they contain less than 50 amino acids, while the larger ones are regarded as proteins. Peptides consisting of 2-20 amino acids are referred to as oligopeptides and those having 20-50 residues are called polypeptides (49, 50).

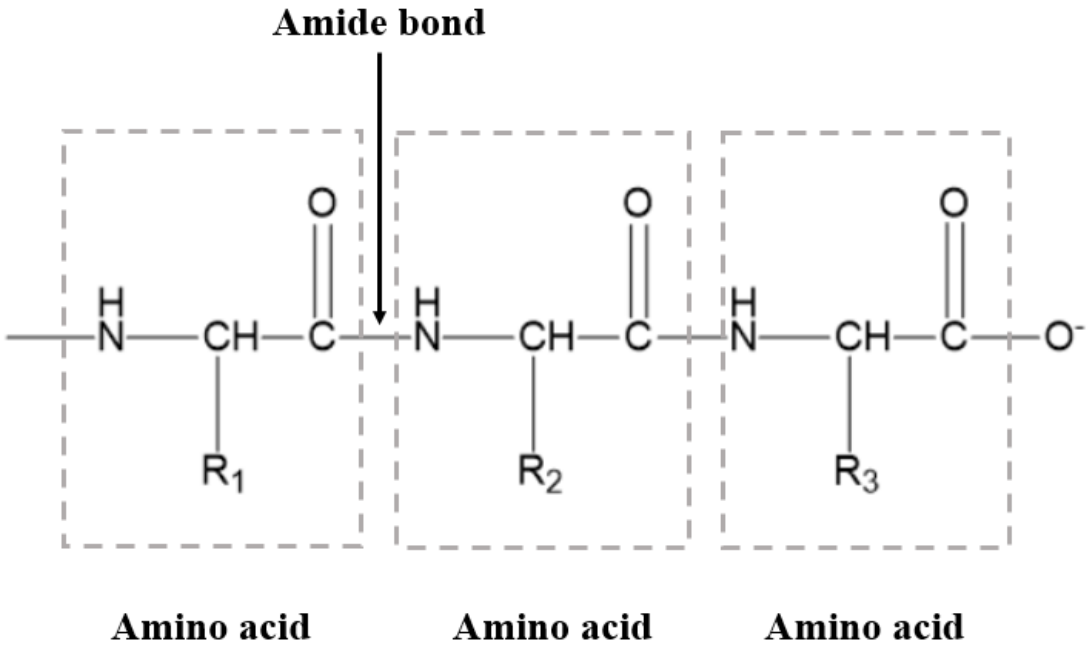

Figure 1.5: General schematic of peptide

Peptides offer one of the most attractive active targeting options. Peptides are usually larger than small molecules but much smaller than antibodies. It might be very challenging to design a small molecule ligand which will fit into a hydrophobic and shallow binding pocket. As

a junction of the antibody and small molecule, peptides provide smaller size, as well as selectivity and high affinity (27).

1.3.5.1 Advantages of peptide targeting ligands. Since cellular targeting peptides have smaller size (on an average < 30 amino acid long) and defined chemical structure, they have distinct advantages over antibodies, protein domains and oligosaccharides. Few notable advantages are (51-57):

- Easy to manufacture by simple chemical synthesis
- Easily scalable and relatively inexpensive manufacturing procedure
- Peptides generally show good biocompatibility
- Peptides can be easily manipulated for conjugation with chemical drugs, therapeutic genes or cytokines
- Some peptides have found to assist deep penetration inside tumor

1.3.5.2 Tumor targeting peptides. Cancer cells and the surrounding tumor microenvironment differ characteristically in terms expressing certain biomarkers. These biomarkers make the tumor cells and the tumor vasculature susceptible for ligand mediated delivery of therapeutics or diagnostics (51). Some of the recent tumor targeting approaches that uses peptide ligands are summarized below:

1.3.5.2.1 Peptides targeting tumor vasculature. Tumor vasculatures are significantly different than the normal blood vessels both morphologically and structurally (51, 58). Numerous peptides have been identified having tumor vasculature homing property (Table 1.1).

Table 1.1

List (non-exhaustive) of tumor vasculature targeting peptides

Sequence	Name	Receptor	Target cell	Target tumor
CDCRGDCFC	RGD-4C	αvβ3/αvβ5	Angiogenic blood vasculature	Several tumor types
CNGRCVSGCAGRC	NGR	Aminopeptidase N (CD13)	Angiogenic blood vasculature	Several tumor types
CRGDKGPDC	iRGD	αvβ3 αvβ5 integrins	Blood vessels and tumor cells	Several tumor models
KDEPQRRSARLSAKPAPPKPEPKPKK APAKK	F3	Nucleolin	Blood vessels and tumor cells	MDA-MB-435 cells, breast carcinoma cells
DITWDQLWDLMK	Esbp	E-selectin	Activated EC	Human umbilical vein EC (HUVEC), human immortalized vascular EC (IVECs)
IELLQAR		E-selectin		Mouse B16 melanoma and human lung adenocarcinoma HAL-8Luc cells
WHSDMEWWYLLG	F56	VEGFR-1	Angiogenic blood vasculature, stromal cells, TAMs and tumor cells	MGC-803 human gastric cancer, BICR-H1 human breast cancer
HTMYYHHYQHHL	K237	VEGFR -2 KDR/Flk-1	Angiogenic blood vasculature	BICR-H1 human breast cancer

(continued)

Table 1.1 (continued)

Sequence	Name	Receptor	Target cell	Target tumor
ATWLPPR	A7R	VEGFR -2 KDR/Flk-1	Angiogenic blood vasculature	HUVEC non-cancerous human EC
CSCKNTDSRC KARQLELNER TCRC		Neuropilin-1	Angiogenic blood vessels, breast, prostate, melanoma and other cancer cells	MDA-MB-231 human breast adenocarcinoma, 4 T1 mouse mammary cancer, HUVEC non-cancerous human ECs
KDEPQRRSAR LSAKPAPPKPE PKPKK APAKK	F3	Nucleolin	Blood vessels and tumor cells	MDA-MB-435 cells, breast carcinoma cells
CREKA	CREK A	Fibrin-fibronectin complexes deposited as a result of subtle clotting	Tumor blood vessels and the tumor stroma	MMTV-PyMT transgenic breast cancer mice
CTPSPFSHC	TCP-1	Not determined	Blood vessels of orthotopic colorectal cancer (colon 26)	Orthotopic colorectal cancer model
TAASGVRSMH , LTLRWVGLMS		Chondroitin sulfate proteoglyca n, NG2	Blood-vessels and associated pericytes	B16F10 mouse melanoma
CKAAKNK	KAA	Pre-malignant vessels	Pancreatic tumor cells	Mouse Tg model of pancreatic islet carcinogenesis

(continued)

Table 1.1 (continued)

Sequence	Name	Receptor	Target cell	Target tumor
CRSRKG	RSR	Angiogenic vasculature	Angiogenic islet vessels	Mouse Tg model of pancreatic islet carcinogenesis
CRGRRST	RGR	Angiogenic and pre-malignant, as well as tumorigenic blood vessels	Angiogenic islet vessels and pancreatic tumor cells	Mouse Tg model of pancreatic islet carcinogenesis
CGNKRTRGC	LyP-1	Cell surface P32	Tumor cells, lymphatic endothelium, hypoxic areas inside tumor cells	MDA-MB-435, spontaneous prostate and breast cancer mouse models, KRIB osteosarcoma
CNRRTKAGC	LyP-2	Lymphatic endothelium	Lymphatic vessels	Pre-malignant and malignant lesions of the cervix and dysplasias and squamous cell carcinomas of the skin

1.3.5.2.2 Peptides targeting tumor cells. Due to the better accessibility of peptides to blood vessel, targeting the tumor vasculature is far easier than the tumor cell targeting, several peptides targeting the tumor cell have been identified and tested (51) (Table 1.2).

Table 1.2

List (non-exhaustive) of tumor cell surface targeting peptides

Sequence	Name	Receptor	Target cell	Target model
YHWYGYTPQNVI	GE11	EGFR	Tumor cells	SMMC-7721 human hepatoma cells
D(CVRAC)		EGFR	Tumor cells	HN5 cells, GEO cells and EF43.fgf-4 cells
WHSDMEWWYLLG	F56	VEGFR-1	Tumor blood vessels, stromal cells, TAMs, and tumor cells	Several tumor models
CSDSWHYWC	P1	VEGFR-3	Tumor cells	HT29 human colon cancer, Y79 human retinoblastoma cancer
CRTIGPSVC		Tf-R	Tumor cells	Human glioblastoma
SPRPRHTLRLSL	B18	Tf-R	Tumor cells	Tf-R1-positive tumor cells and tissue
LTVSPWY		Her2	Tumor cells	Her2-positive breast cancer SKBR3 cells
SWELYYPLRANL		E- and N-cadherin	Tumor cells	MCF-7 human breast carcinom, MDA-MB-435 human breast carcinoma
YCAREPPTRTFAYWG	EPPT1	uMUC-1	Tumor cells	
WHPWSYLWTQQA (RP-1)		CD44	Tumor cells	Gastric cancer
RLVSYNGIIFFLK	A5G27	CD44v3 and CD44v6	Tumor cells	Various types of malignancies
VLWLKNR	FP16	FGF3	Tumor cells	Breast cancer

(continued)

Table 1.2 (continued)

Sequence	Name	Receptor	Target cell	Target model
ANTPCGPYTH DCPVKR	G3–C12	Galectin-3	Tumor cells	MDA-MB-435 breast carcinoma cells
PQNSKIPGPTF LDPH	G3–A9			
CTVALPGGYV RVC	pep42	glucose-regulated protein 78 (GRP78)	Tumor cells	Melanoma Me6652/4 cells
CSNRDARRC		Not determined	Tumor cells	HT-1376 human bladder transitional cell carcinoma
CSSRTMHHC		Not determined	Tumor cells	B16F10-Nex2 mouse melanoma
LLADTTHHRP WT		Not determined		Human glioma
c-dGHCitGPQ-c	OA02	α3-integrin	Ovarian adenocarcin oma	ES-2, SKOV-3
VRPMPLQ		Not determined	Dysplastic colonocytes	Human colon adenomas
YEQDPWGVK WWY	M2pep	CD11b+ F4/8 0highM2-like TAMs	TAMs	TAMs harvested from CT-26 syngeneic tumors in BALB/c mice
LSLERFLRCW SDAPA	PP1	Scavenger receptor-A (SR-A) on macrophages	Macrophage s found within atherosclero tic plaques	Atherosclerotic plaque
FYPSYHSTPQR P	DC3	Not determined	DCs	CD11c + BMDDCs
VTLTYEFAAG PRD	P-D2	CD11c/CD18	DCs	CD11c + DCs

1.4 Peptide Discovery/Design Methods

Peptide discovery/design methods can be broadly classified in to two categories: (a) structure free design methods, and (b) structure based methods (59).

1.4.1 Structure free peptide design methods. Cell surface binding peptides can be identified by creating and screening a combinatorial peptide library against a specific target molecule. Combinatorial libraries can be subdivided into three major classes: (a) focused libraries of antibody, (b) one-bead one-compound peptide libraries (OBOC), (c) phage display libraries. Although less commonly used, other biological approaches are bacterial, yeast, mRNA or ribosomal peptide display libraries (51, 60-63).

1.4.1.1 Focused libraries of antibody. Antibodies or their fragments have been used traditionally as targeting agents to deliver drugs or diagnostic molecules to the target organ or tissue. Antibodies exhibit high binding affinity and selectivity towards the molecular target (antigen). In fact, the hyper variable loops of the antibody's variable domain, referred to as the complementarity determining regions (CDRs), are conventionally acknowledged to be responsible for antigen recognition (64). A number of peptides having selective binding affinity towards the target antigen have been derived from the amino acid sequences of the CDRs (65). There are some major limitations of this technique. (a) In many cases, it is difficult to prepare the crystals suitable for structural characterization of antibody fragment complexed with proteins/peptides. (b) Recent studies suggest that the whole CDR sequence is not important for antigen binding, and residues outside of CDRs can contribute significantly in binding (66). (c) Due to the lack of a universal CDR identification method, CDRs are not well defined and thus may not act as a very good surrogate of binding site (64). Because of these limitations, one-

bead–one-compound and phage display libraries are more commonly used techniques for identifying new peptide ligands.

1.4.1.2 One-bead–one-compound libraries (OBOC). This library screening method is based on a chemical technique first reported by Kit Lam and colleagues in 1991 to identify new peptide ligands for delivering therapeutics, imaging agents and protein inhibitors (67-69). OBOC libraries consist of resin beads (90 μm in size), each containing a distinct sequence of peptides that can be synthesized chemically using the standard solid phase peptide synthesis method. In this method, beads are first divided into several equal amount portions. A specific amino acid is coupled to each portion. Then the amino acid loaded resin bead portions are combined, mixed thoroughly and again divided equally, followed by second amino acid coupling. This is called split and pool steps. These split and pool steps can be repeated sequentially to obtain a library of random peptide sequences (up to 10^7 sequences). The beads are then screened in parallel by incubating with live fluorescent cells or pre-labeled target protein. The beads which interact strongly with the cells are isolated by sorting. And the beads having only a few cells bound to them are discarded. Finally, the peptide on these positive beads is sequenced using Edman sequencing technique or by mass spectrometry (MS) after removing the coding tag from the bead.

The advantages of OBOC technique are (60, 70, 71):

- Allows the incorporation of non-natural amino acids, turned, cyclic or branched molecules
- Allows the identification of proteolytic degradation resistant peptides
- Screening can be performed with live cells which increases the possibility of identifying peptide ligands able to bind the native conformation of the target protein

- Binding affinity can be optimized by creating a secondary library from the first OBOC library

A major limitation of this technique is the use of pre-labeled target protein for screening step. Since the protein needs to be coupled with a fluorescent or chemical probe and purified before screening, there is a possibility that the protein might assume a non-native conformation which in turn would mislead the whole ligand identification process (51).

1.4.1.3 Phage display libraries. Phage display technique a biological approach that creates a random combinatorial peptide library (~ 10^8 peptides) (59). It was first introduced in 1985 by George Smith when bacteriophages containing filamentous DNA were engineered genetically to express foreign peptides (72). In this technique, fragment of a foreign DNA is incorporated into the genome of the bacteriophage. The foreign DNA fragment is placed in between the signal peptide coding sequences and the portion of the coat protein. So, the incorporated exogenous peptide is displayed on the surface of the phage as a fusion with the coat protein. The phage library is then incubated with the target protein, generally immobilized on solid support, followed by washing steps. The washing steps remove the unbound phage particles. Then the bound phage particles are collected using desired elution method. The collected phage is amplified, and bio-panning step is carried out multiple times. Finally, DNA sequencing is done for the encoding regions of the phage clones to identify the binding peptide sequences (Figure 1.6).

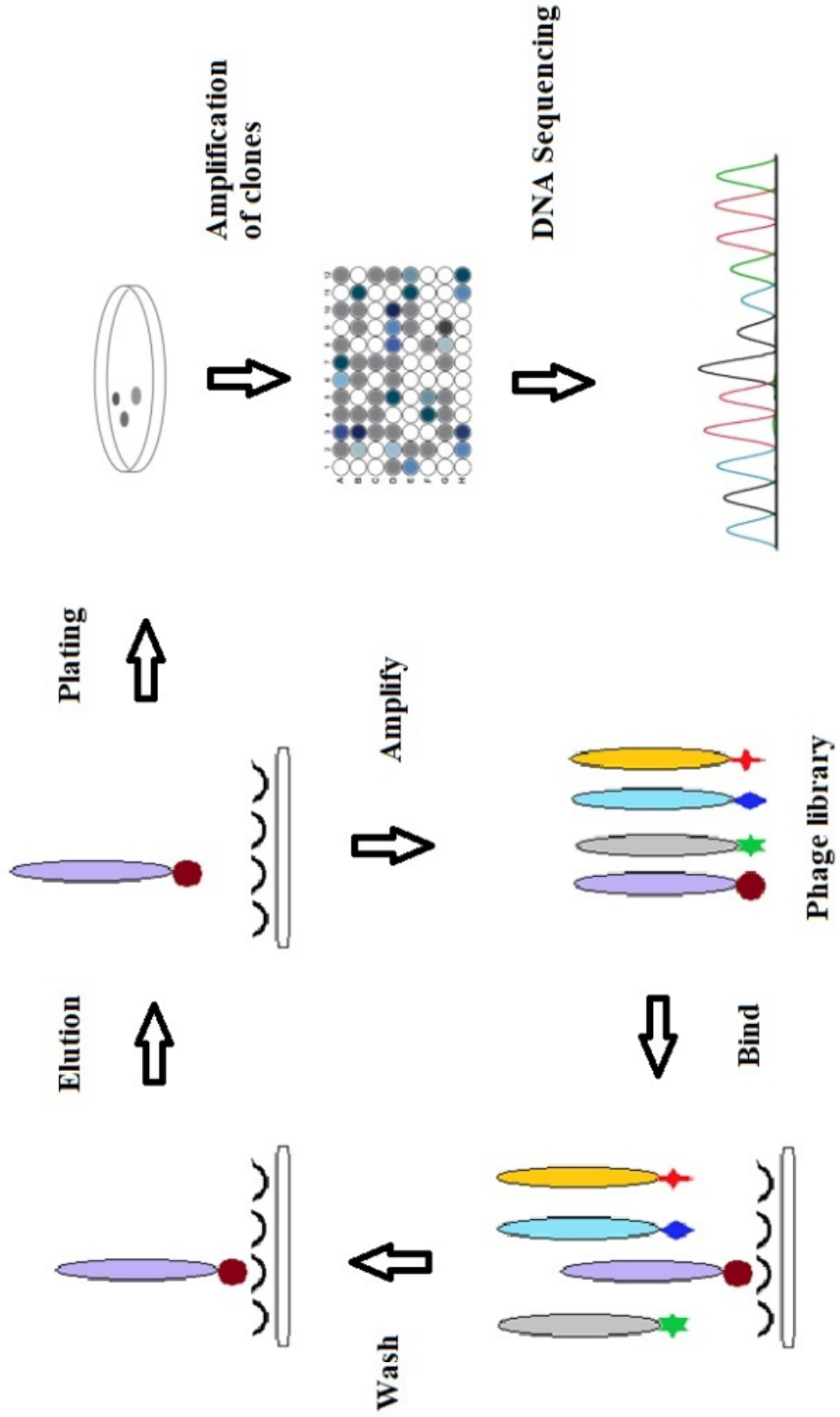

Figure 1.6: Typical steps of phage display technology

During past couple of decades, phage display technique had gone through many important changes and developments. In the early days, peptide library screening used to be done with soluble target protein immobilized on solid support. But later on live cells, tissue and live organisms have been utilized for selecting binding peptide candidates (54, 73, 74). These relatively new bio-panning methods allows the target protein to remain in its functional and native conformation.

Advantages of phage display technique are:

- Peptides with high binding affinity and selectivity have been identified by this method (original form and the modified bio-panning)
- Does not require prior knowledge of the structure or composition of the target protein

However, one of the limitations of phage display technique is that the peptides can only contain natural amino acid residues (51). Moreover, it is a trial-and-error based method which possess some degree of experimental complexity and can be relatively expensive.

1.4.2 Structure based peptide design methods. Structure based peptide design methods utilize the structural information obtained from the X-ray crystallographic structures of the target protein or even a related protein in some cases (59).

1.4.2.1 Peptide design based on protein-protein interaction. Peptide sequences identified by analyzing the protein-protein crystallographic interface constitute the primary source of structure-based peptide design (75). The first peptide identified by this technique was a 36-amino acid long peptide, enfuvirtide, which got US-FDA (US Food and Drug Administration) approval as anti-HIV therapy. It is considered as one of the most significant achievement in peptide therapeutics field (76).

Transcriptional factors generally have large protein-protein interfaces, making them very difficult to target by small molecules. But peptides are being used now to target these transcriptional factors. A breakthrough study reported the inhibition of downstream transcription of NOTCH signaling by directly inhibiting an important ternary complex (77).

An alpha-helical peptide was derived from a co-factor (BH3 helix, pro-apoptotic in nature), and a technique called 'peptide stapling' was used to stabilize the inhibitory peptide binding (78). Stapling stabilized the peptide binding to the anti-apoptotic protein, MCL-1. MCL-1 is a member of BCL-2 family proteins and has been found to be overexpressed in certain cancers (79).

1.4.2.2 Peptide design based on protein-peptide interaction. The structural information of the protein-peptide binding interface can be utilized to predict or model the interaction of a designed peptide with the protein. This technique had been employed by three main ways:

(1) A protein structure complexed with peptide ligand is used as the template and model a domain associated sequence by homology, followed by mutation in silico using a design (protein design) algorithm to change the amino acid side chains keeping the peptide backbone fixed (80, 81).

(2) A protein peptide complex structure to model the peptide sequence by homology keeping the peptide backbone flexible. This has been used to redesign the peptide structures from the PDZ domain for specificity (82). Another approach that permits backbone flexibility was validated using 89 peptide complexes (83).

(3) The protein structure is used while only the approximate binding site of the peptide ligand is known. The algorithm, PepSpec, is not dependent on the peptide structural model, rather it requires only a single residue anchoring in the binding pocket. It incorporates backbone movements in the target protein by ensemble modeling. This approach has been evaluated with different peptide binding domains, like SH2, SH3, and PDZ (84).

1.4.2.3 Peptide design using protein docking and fragment-based docking. This is the more typical method used to design peptides, combining the use of target protein structures (or homology model) with docking algorithms to derive peptide sequences for the selected site on the target. There are techniques to structurally distinguish the assumed binding sites, for example, the use of geometric amino acid reliant predilections resulting from a number of binding modes (85). A genetic algorithm in combination with Autodock, a popular docking algorithm, was used to design tetra-peptides for binding on a predefined hydrophobic pocket of the protein α-synuclein, which is implicated in aggregation diseases. Experimental evaluation confirmed multiple binding peptides with micro-molar affinities in terms of dissociation constant (86).

Another example uses the Gaussian Network Model for binding site identification, followed by docking a database of dipeptides pairwise using Autodock on the grid along a selected stretchy binding path. This derives an optimal peptide for the a target surface (87).

1.5 Aminopeptidase N (CD13)

Aminopeptidase N (APN), also known as CD13, is Zn^{+2} dependent cell surface ectopeptidase. CD13 consists of 967 amino acid residues. It has a short N-terminal intracellular domain, a single transmembrane region, and a large extracellular domain which contains the active site (Figure 1.7). CD13 can be found as monomer and dimers on the cell surface. The PI of CD13 is approximately 5 and its molecular weight is 140-150 kDa. CD13 is heavily glycosylated with carbohydrates that is at least 20% of the protein mass. CD13 has at least five different isoforms with differential O-glycosylation sites (88-90).

Although, CD13 is widely expressed in different mammalian cells, such as myeloid cells, mast cells, antigen presenting cells, keratinocytes, epithelial cells of the small intestine, prostate, renal proximal tubules and bile duct canaliculi, it has been reported to be linked to the development of both normal and malignant cells. In terms of normal physiological functions, CD13 plays crucial role in processing of peptide hormones, such as, neuropeptides, angiogenesis and inflammation associated chemokines, and angiotensin III and IV. It preferentially degrades the peptide hormones or proteins having neutral N-terminal amino acids. CD13 is also involved in cell adhesion and endocytosis. CD13 also act as a viral receptor and may be associated in cholesterol turnover (88-96).

While there is very little or no CD13 expression in normal vessels, it is overexpressed in angiogenic vessels of the neoplastic tissues. CD13 has been found to be upregulated in other angiogenesis involved pathological conditions. For example, it was shown that CD13 is overexpressed in cardiac angiogenesis in mouse model. Different tumor cells also express or overexpress CD13 receptor. In terms of malignant cell growth, CD13 is implicated in tumor cell invasion, differentiation, proliferation and apoptosis, motility and angiogenesis (91, 94, 97-102).

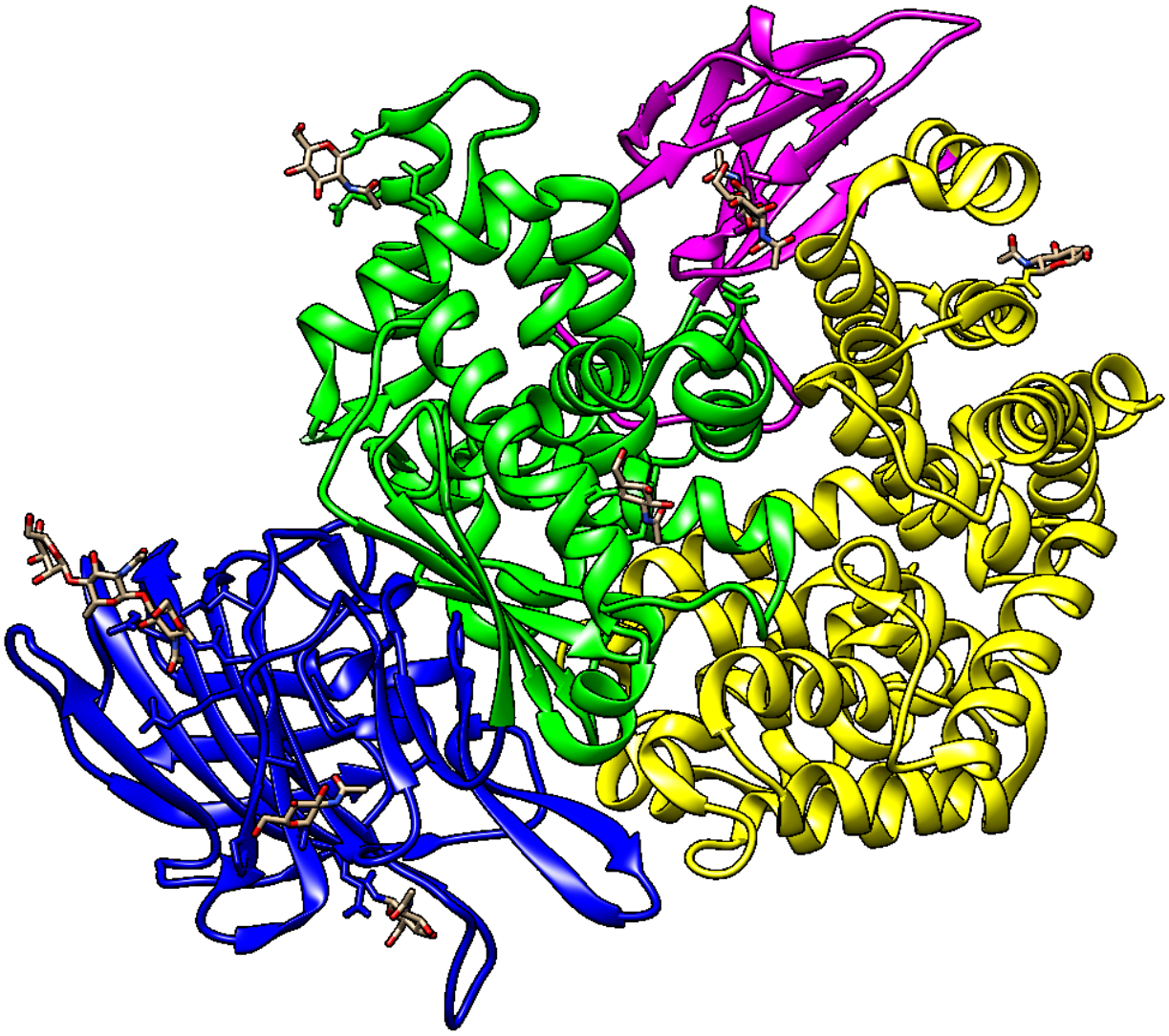

Figure 1.7: Structure of the human CD13 ectodomain. Domain I, II, III, and IV are blue, green, magenta, and yellow, respectively. Numbers designate the domain limits. N-Linked oligosaccharides are displayed in stick representation.

1.5.1 CD13 as a target for cancer therapy and CD13 targeting ligand. CD13 is overexpressed in many cancers like breast, kidney, prostate, ovarian, colon, gastric, pancreatic and thyroid cancer (91, 95). A phage display study in mouse model identified that Asn-Gly-Arg (NGR) peptide sequence flanked by at least one amino acid at each end (NGR motif) can specifically interact with CD13 (98, 103). Among the 5 identified isoforms of CD13, NGR motif can only bind to the CD13 isoform expressed exclusively on the tumor vasculature, but not normal CD13-rich tissues (97). Some of the NGR motifs that have been identified to target tumor vasculature CD13 are cyclic CNGRC [CNGRC (C1-C5)] (disulfide linked), GNGRG, NGRAHA, cyclic KNGRE (head to tail), triazole linked cyclic NGR, and CVLNGRMEC (104, 105). CD13 targeted NGR peptide-based drugs which were under clinical trial are summarized in table 1.3 (104).

Table 1.3

Clinical trials of CD13 targeted NGR peptide based drugs

Clinical trial number	Drug(s)	Target(s)	Status
NCT00483080	NGR-hTNF	Colorectal cancer	Phase II
NCT00484211	NGR-hTNF	Hepatocellular carcinoma	Phase II
NCT00098943	NGR-hTNF	Colorectal cancer/ Head and neck cancer/ Kidney cancer/ Unspecified adult solid tumor	Phase I
NCT00484276	NGR-hTNF	Malignant pleural mesothelioma	Phase II
NCT00419328	NGR-hTNF	Advanced solid tumors	Phase I

(continued)

Table 1.3 (continued)

Clinical trial number	Drug(s)	Target(s)	Status
NCT00878111	NGR-hTNF	Solid tumors	Phase I
NCT01358084	NGR-hTNF / Placebo	Advanced malignant pleural mesothelioma	Phase II
NCT01098266	NGR-hTNF / Placebo	Malignant pleural mesothelioma	Phase III
NCT00483509	NGR-hTNF/ Doxorubicin	Small cell lung cancer	Phase II
NCT00484341	NGR-hTNF/ Doxorubicin	Locally advanced or metastatic soft tissue sarcoma	Phase II
NCT00484432	NGR-hTNF/ Doxorubicin	Advanced or metastatic ovarian cancer	Phase II
NCT00305084	NGR-hTNF/ Doxorubicin	Cancer	Phase I
NCT01358071	NGR-hTNF/ PEGylated liposomal doxorubicin	Ovarian cancer	Phase II
NCT00483093	NGR-hTNF/ Cisplatin	Solid tumors	Phase I
NCT00994097	NGR-hTNF/ Cisplatin / Gemcitabine / Pemetrexed	Non-small cell lung cancer	Phase II
NCT00675012	NGR-hTNF/ Oxaliplatin/ Capecitabine	Colon cancer	Phase II

1.6 Statement of Problem

Proteins, peptides, antibodies, carbohydrates, aptamers, and vitamins are the most commonly used ligands for drug. Among them, peptides possess several advantages such as smaller size compared to antibodies, ease of large-scale synthesis by chemical methods and high target specificity. Recent advances in robust chemical conjugation techniques are expected to increase their use in cancer diagnosis, imaging and therapy. The most widely used strategy to identify a peptide ligand against a target is to screen peptide libraries created by phage display method. Even though, several peptide ligands have been identified using phage display technology, this trial-and-error based technique is inherently time consuming and expensive. On the other hand, the structure based computational peptide design methods utilize structural information obtained from crystallographic protein-protein interfaces. The computational design method combines homology models or structural information with docking to develop new targeting peptides. Various computational methods have been utilized to date for developing a number of peptide targeting ligands. However, currently there is no rational approach to design peptide ligands based on the packing of the ligand amino acid residues at the target protein binding site.

Therefore, a rational peptide design technique based on the clear mapping of amino acid side-chain packing arrangements between ligand and target proteins has distinct advantages. In this study, a rational peptide design method was developed that clearly defines the packing of the ligand at the binding site of the receptor protein. The method is based on a novel description of protein-packing known as Knob-Socket model that provides a simplified yet accurate representation of residue packing between two molecules. In this study, tumor vasculature biomarker, CD13, was used as a model target receptor.

1.7 Hypothesis

Peptide ligands can be designed using a rational method based on protein-protein interactions defined by Knob-Socket protein packing model for selective binding to target protein.

1.8 Specific Aims

The purpose of this dissertation research is to develop a rational method to design peptide ligands. The peptides with specific binding ability to CD13 will be designed, synthesized and characterized. The peptide ligands will be used as a binding moiety to design peptide-drug conjugate. The research objectives will be achieved through the following specific aims:

(1) To design peptides based on knob-socket analysis of the crystal structure. Peptide ligands which can specifically bind to the CD13 are designed.

(2) To perform molecular modeling studies, to determine the binding energy and binding site by Molecular Operating Environment (MOE) and AutoDock Vina software, respectively. These parameters are used to select peptide ligand candidates for further in vitro evaluation.

(3) To synthesize and characterize the peptides. Peptides with and without FITC conjugation are synthesized for this purpose.

(4) To demonstrate that the designed peptides exhibit specific binding affinity towards CD13 similar to the conventional peptide ligand, CNGRC (C1-C5). These properties were tested by performing in-vitro binding affinity determination and cellular binding/uptake studies.

(5) To show the applicability of the designed peptide drug conjugate, it's in vitro and in vivo evaluations are performed. Peptide drug conjugate with a cleavable linker to a model drug, MMAE, are prepared. The in vitro cytotoxicity and in vivo tumor efficacy of the peptide drug conjugates are evaluated for this purpose.

Chapter 2: Design and Screening of Peptide Ligands

2.1 Introduction

The world of medicine is moving fast towards precision and personalized care where drugs are being tailored according to individual variability, and delivered specifically to the diseased tissue (106). One of the most popular strategies to enhance the therapeutic efficacy while minimizing the systemic toxicities has been the active drug targeting with the aid of specially designed ligand moieties (107-109).

Antibodies, peptides and aptamers are some of the commonly used targeting molecules. Among these, peptides possess several attractive features such as, high target specificity, reduced likelihood of unintended immunogenic interactions, and smaller size leading to better tissue penetration and favorable pharmacokinetic properties (110, 111). There are more than 60 peptide drug products approved by US Food and Drug Administration, with additional 140 peptide drugs in clinical trials and more than 500 therapeutic peptides in preclinical stage (112). Recent advances in robust chemical synthesis and conjugation techniques are expected to further increase the use of peptide-based molecules in diagnosis, imaging and therapy.

Efficient design of high-affinity peptide ligands via rational methods has been a major obstacle to the development of this potential drug class (59). The most widely adopted strategy to identify a new peptide ligand is phage display, where a large library of peptides is screened against a predetermined target (54, 113, 114). This high throughput technique has been a powerful and versatile approach for peptide ligand identification, but it is inherently time consuming and resource demanding. One relatively new peptide design methodology, the computational design method combines structural information with docking, to develop new

peptides (59). Campa et al. reported the design of a novel type III Epidermal Growth Factor Receptor (EGFRvIII) binding peptide through hydropathic complementarity approach (115). Using the program ANIMOMAT, the peptide sequences were designed to bind EGFRvIII. In 2000, Park et al. published a study on the design of a peptidomimetic having comparable biological properties to those of an antibody (116). This peptidomimetic was developed based on an analysis of the human epidermal growth factor receptor 2 (HER2/neu) - antibody (anti-HER2/neu) co-crystal structure. In another computer assisted in silico screening of a large virtual library of peptides by Song et al., selected a peptide ligand for EGFR binding (117). Generally, peptides derived from an analysis of the protein interface structure constitute the primary source of these designs (59). However, none of them identify peptide ligands using a model that exactly defines the specific packing of the ligand residues within a structure's binding interface. Therefore, a rational peptide design technique based on the clear mapping of amino acid side-chain packing arrangements between ligand and target proteins has distinct advantages. In this regard, the Knob-Socket based approach (118-120) could help to reduce the development time by allowing rational and expeditious in-process optimization and provides plausible alternatives to the experimental high-resolution receptor protein-peptide complex structures.

In this study, a rational peptide design method is investigated that clearly defines the packing of the ligand at the binding site of the receptor protein. The method is based on a novel description of protein-packing known as Knob-Socket (KS) that provides a simplified yet accurate representation of residue packing between two molecules (118-120). The KS model uses the precision of Voronoi Polyhedra/Delauney Tessellations to identify contacts (121, 122) and is described as a 4-residue tetrahedral motif, where a one-residue knob belonging to a secondary structure packs into a three-residue socket on another secondary structure (Figure 2.1).

The KS model also provides information about the propensities of the knobs that most likely can pack into a respective socket (Figure 2.2).

We employed this rational method to design peptide ligands for a prototype target- tumor vascular endothelial CD13 (Cluster of Differentiation 13) receptor. CD13 is a good prototype target for the present study since it has an established peptide ligand CNGRC (C1-C5), identified through a phage display study, which can serve as a direct comparison for the evaluation of designed peptides. Additionally, this target allows a clean in vivo evaluation of the designed peptides as the endothelial cells of the tumor vasculature are readily accessible to the ligands, and the vascular endothelial cells are genetically more stable than the tumor cells in developing drug resistance (123, 124).

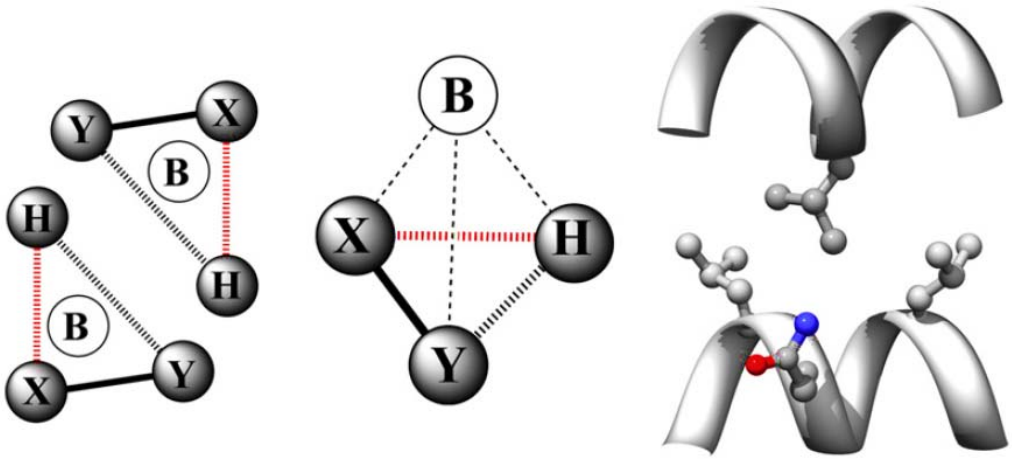

(1) (2) (3)

Figure 2.1: Two-dimensional representation of Knob-Socket model (118).

(1) Two-dimensional representation of the knob–socket motif shows the three residues X, Y, and H in the socket are all packed against a knob residue B from the other helix. While the residues side chains all pack against each other, the hydrogen bond (broken red line) connects X and H. Consecutive residues X and Y share a peptide bond (continuous black line). Residues Y and H only pack with their side chains (broken black line).

(2) The tetrahedral arrangement of the four-residue knob–socket motif. The knob residue B contacts all the three socket residues only through side-chain.

(3) The knob–socket motif shown between two α-helices.

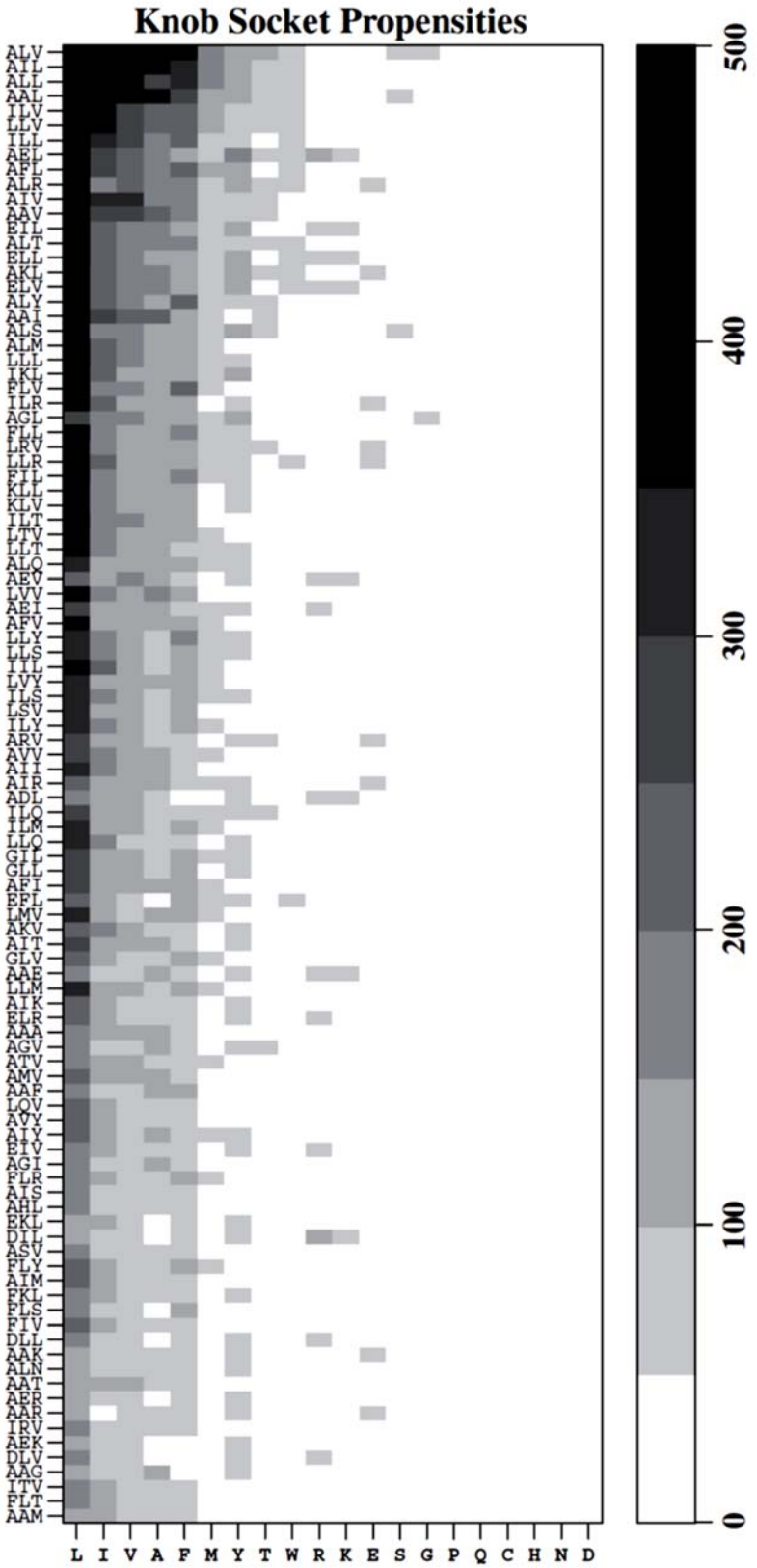

Figure 2.2: Knob-Socket frequency map (118).

2.2 Methods

2.2.1 Peptide design.

2.2.1.1 Confirming the peptide binding site on human CD13 (hCD13). The crystal structure of porcine CD13 (pCD13) is available in complex with a peptide targeting ligand CNGRCG (C1-C5) [Protein Data Bank (PDB) ID: 4OU3] (125). However, the crystal structure of human CD13 (hCD13) is only available in complex with the endogenous ligand ANG IV (PDB ID: 4FYS) (88). To confirm the target site for the peptide ligand, PDB ID: 4FYS and PDB ID: 4OU3 were loaded in Molecular Operating Environment (MOE) software (Version 2013.08, Chemical Computing Group, Montreal, QC, Canada) with a solution phase AMBER10:EHT forcefield and R-field solvation model. Non-binding portions of the protein structures were then deleted keeping only the binding site residues. For hCD13, the amino acids are A191-A215, K340-L487 and R855-R908, and for pCD13, they are A186-T210, K335-L482 and R852-R905. The homology between the hCD13 and pCD13 binding sites were analyzed using the Align and Superpose functions in the MOE.

2.2.1.2 Mapping the hCD13 – ANG IV binding interface. The PDB file of hCD13 – ANG IV complex (PDB ID: 4FYS) was loaded in the UCSF (University of California, San Francisco) Chimera program package (126). The program connected the sequences of hCD13 and ANG IV together and renumbered all the amino acids for the whole complex. DSSP (Dictionary of Secondary Structure of Proteins) program (127) was used to assign the secondary structure definition to the hCD13. An in-house program named relative packing clique (RPC) was used to precisely define a set of all residues that contact each other and classify them based on contact order (128). Contacts were calculated from a Voronoi polyhedra analysis (121) which

included side-chain-to-side-chain contacts and side-chain-to-main-chain contacts for all the residues. In addition, contacts were considered for main-chain-to-main-chain contacts for all non-neighboring residues. The resulting Delaunay tessellation defines a contact graph between residues (122). Based on the calculated two-dimensional contact graph, all sockets and knobs formed on the binding interface were identified.

2.2.1.3 Designing peptide ligands. The sockets on the protein that took part in ligand binding along with some other free sockets were selected as the target site for the peptide ligands. Peptides were then designed by selecting the amino acid residues having highest (or second highest) propensities towards the selected sockets on the target site (Table 2.1). When the distance between two knob residues was far because of the physical separation between the two CD13 surface sockets, flanking amino acids were inserted to fill the gap. A database of five amino acid (5-mer) long peptides was created using different combinations of amino acids from the list of highest (or second highest) propensity knobs. A second database of eight amino acid (8-mer) long peptides was also created using the same method to cover larger binding surface.

Table 2.1

Knob-Socket propensity data. For each amino acid knobs (columns) higher the number, higher is its' propensity for the respective sockets (rows) (118-120) (http://tsailab.chem.pacific.edu/helix-socket-prediction.html).

Sockets	Knobs																				
	W	**P**	**G**	**Y**	**F**	**V**	**I**	**L**	**A**	**E**	**K**	**R**	**Q**	**D**	**S**	**T**	**N**	**M**	**H**	**C**	**Total**
HE:H	0.00	0.00	0.03	0.14	0.03	0.00	0.10	0.00	0.00	0.10	0.00	0.00	0.31	0.03	0.00	0.03	0.00	0.00	0.07	0.14	**0.98**
V:HE	0.17	0.00	0.08	0.33	0.17	0.00	0.08	0.00	0.00	0.00	0.00	0.08	0.00	0.00	0.08	0.00	0.00	0.00	0.00	0.00	**0.99**
TV:H	0.03	0.03	0.00	0.12	0.24	0.09	0.26	0.09	0.03	0.00	0.03	0.00	0.00	0.00	0.03	0.00	0.00	0.06	0.00	0.00	**1.01**
R:TV	0.00	0.09	0.00	0.15	0.06	0.12	0.09	0.27	0.03	0.03	0.06	0.00	0.03	0.00	0.00	0.03	0.00	0.03	0.00	0.00	**0.99**
S:ER	0.08	0.00	0.00	0.00	0.08	0.00	0.08	0.00	0.00	0.17	0.00	0.00	0.00	0.00	0.25	0.25	0.00	0.08	0.00	0.00	**0.99**
SR:T	0.05	0.05	0.10	0.00	0.05	0.10	0.10	0.20	0.00	0.00	0.15	0.10	0.00	0.00	0.05	0.00	0.00	0.00	0.05	0.00	**1.00**
LN:Y	0.04	0.00	0.00	0.09	0.27	0.09	0.09	0.11	0.00	0.00	0.09	0.04	0.00	0.00	0.07	0.02	0.00	0.04	0.02	0.02	**0.99**
ND:R	0.00	0.00	0.00	0.22	0.00	0.11	0.11	0.00	0.00	0.00	0.00	0.22	0.00	0.11	0.00	0.11	0.00	0.00	0.00	0.11	**0.99**
N:YR	0.00	0.06	0.00	0.06	0.00	0.06	0.12	0.31	0.00	0.00	0.00	0.12	0.06	0.06	0.00	0.00	0.06	0.00	0.00	0.06	**0.97**
SN:Q	0.00	0.00	0.00	0.00	0.33	0.00	0.33	0.00	0.00	0.00	0.00	0.00	0.00	0.00	0.00	0.00	0.33	0.00	0.00	0.00	**0.99**
N:QA	0.05	0.00	0.03	0.16	0.08	0.13	0.00	0.21	0.05	0.00	0.00	0.05	0.00	0.00	0.05	0.08	0.05	0.03	0.00	0.03	**1.00**
TS:I	0.00	0.00	0.02	0.07	0.16	0.14	0.11	0.16	0.05	0.00	0.05	0.02	0.02	0.05	0.00	0.07	0.02	0.02	0.02	0.02	**1.00**
QA:R	0.01	0.03	0.01	0.07	0.07	0.10	0.12	0.14	0.04	0.18	0.00	0.01	0.03	0.00	0.01	0.00	0.01	0.06	0.01	0.08	**0.98**
YR:A	0.05	0.03	0.03	0.11	0.11	0.16	0.06	0.08	0.13	0.05	0.02	0.00	0.00	0.02	0.02	0.03	0.00	0.05	0.06	0.00	**1.01**
S:IS	0.02	0.02	0.00	0.04	0.08	0.12	0.12	0.18	0.04	0.02	0.02	0.02	0.06	0.00	0.04	0.00	0.08	0.10	0.00	0.02	**0.98**
IS:N	0.05	0.00	0.00	0.10	0.10	0.05	0.10	0.25	0.00	0.10	0.00	0.00	0.10	0.00	0.00	0.05	0.05	0.05	0.00	0.00	**1.00**
AGA	0.01	0.04	0.03	0.01	0.05	0.09	0.06	0.09	0.18	0.03	0.03	0.05	0.02	0.03	0.06	0.04	0.06	0.06	0.01	0.05	**1.00**
FAA	0.00	0.00	0.13	0.13	0.13	0.07	0.13	0.07	0.00	0.07	0.07	0.07	0.00	0.07	0.00	0.07	0.00	0.00	0.00	0.00	**1.00**

2.2.2 Screening of the peptide ligands. Peptide sequences were first screened from the initial database using the following predetermined criteria. Peptides that have Glutamine at the N-terminal can easily condense to form pyroglutamate degradation products (129). Peptides with Xaa-Proline residues at the N-terminal may lead to diketopiperazine formation (130). And oxidation of Methionine produces sulfoxide amino acids (131). Consequently, peptides with Glutamine or Xaa-Proline on the N-terminal, or Methionine in the sequence were discarded. Additionally, peptides containing same amino acids consecutively were also removed from the initial database. The remaining peptides were constructed in MOE using the Molecule Builder tool, and energy minimization was performed using the AMBER10:EHT forcefield and R-field solvation model. After loading the hCD13 – ANG IV complex (PDB ID: 4FYS) in MOE, the protein structure was prepared using the LigX function with the default setting except the receptor strength of 5000. The glycan, solvent and buffer molecules as well as the endogenous ligand ANG IV were removed from the docking simulation. Docking of the peptides was performed on the hCD13's peptide binding site using Dock function with rigid receptor protocol. Timeout (seconds) and No. of Return Poses in the default Triangle Matcher Placement option of the docking window were configured to 500 and 2,000, respectively. At the end of docking, MOE produced 100 possible conformations for each peptide and respective docking score for the complex of peptides and hCD13. Potential peptide candidates were selected using the docking score from MOE. The docking score function estimates the free energy of binding of the ligand from a given binding pose. A low (negative) docking score indicates a stable system and thus a likely interaction between the receptor and ligand. Further docking studies were performed using a second molecular modeling software – AutoDock Vina (132). The hCD13 structure (PDB ID: 4FYS) was prepared using Dock Prep in UCSF Chimera. The endogenous ligand

ANG IV, glycans, buffer and water molecules were removed. The designed peptide structures along with the positive control CNGRC (C1-C5) peptide were generated in Chimera using Build Structure function with default settings. The peptide structures were then prepared using Dock Prep and Minimize Structure functions. AutoDockTools within MGLTools (version 1.5.6) were used to generate the PDBQT format files of the peptides and receptor. The docking was performed using the methods described by Hauser and Windshügel (133) and in AutoDock Vina manual (http://vina.scripps.edu/manual.html). The position of the grid box center was set at (x, y, z) = (101.98, 20.068, 18.861), and the xyz dimensions of the grid box were 80 Å, 62 Å and 62 Å, respectively. The exhaustiveness of the docking run was set at 100. A small set of peptides were selected for further experimental evaluation based on the AutoDock Vina predicted binding sites.

2.3 Results and Discussions

2.3.1 Peptide design. Porcine CD13 (pCD12) and human CD13 (hCD13) have high similarity of sequence (80% overall, 100% in the active site, 94% in the peptide-binding region) (134). When the peptide-binding regions of hCD13 and pCD13 were aligned and superposed using MOE, the overall root-mean-square deviation (RMSD) was 0.833 Å, indicative of significant similarity in their binding site conformation (Figure 2.3). The endogenous ligand ANG IV and the peptide ligand CNGRCG (C1-C5) were also observed to reside very close to each other (Figure 2.3). This suggested that the location where ANG IV binds on hCD13 could be used as the target site for designing novel peptide ligands.

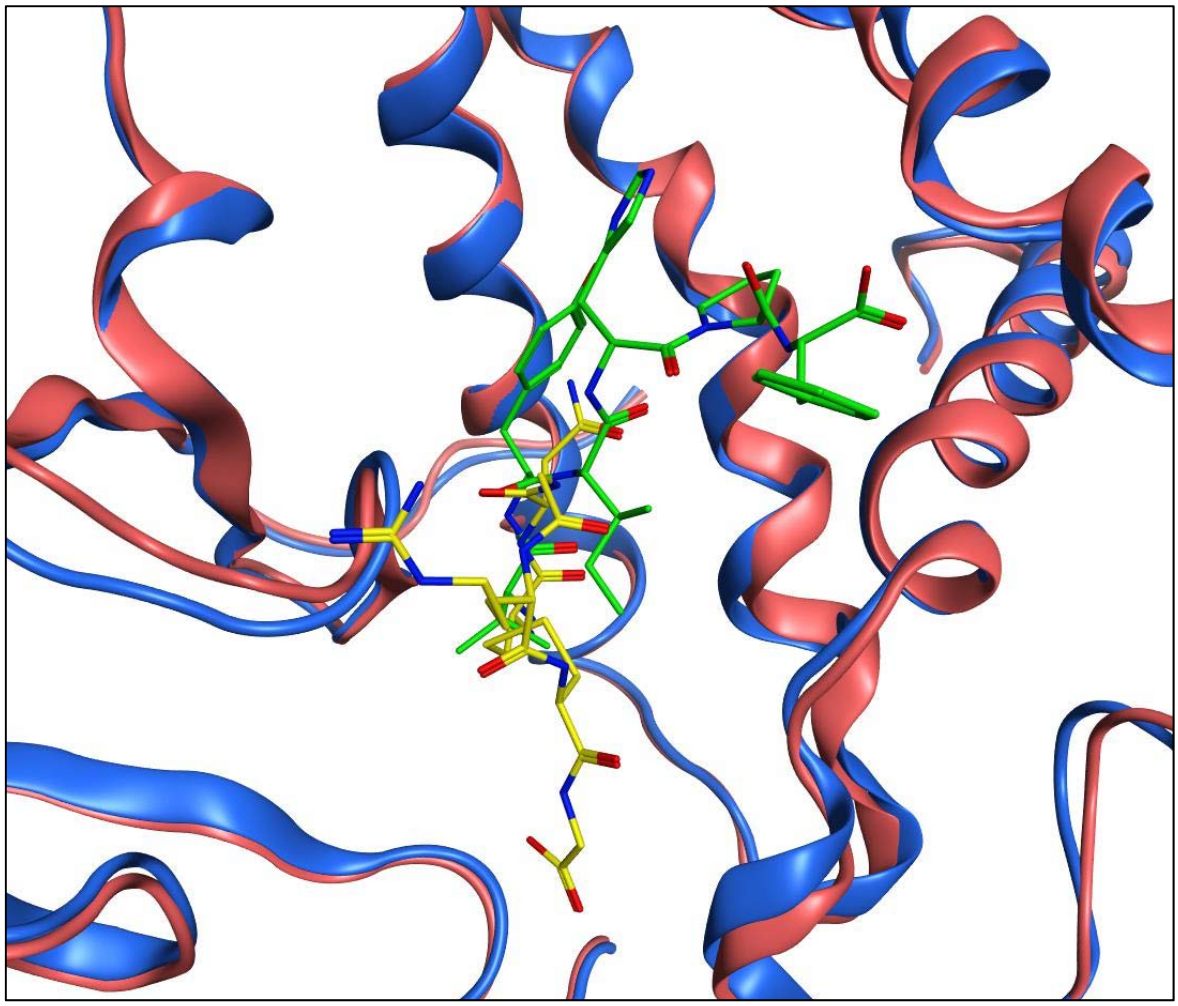

Figure 2.3: The binding sites of hCD13 & pCD13 aligned and superposed [Blue structure – hCD13, green coil – ANG IV, magenta structure – pCD13, yellow coil – CNGRCG (C1-C5)]

Using the Knob-Socket model, the complicated CD13 ligand binding interface (Figure 2.4) can be simplified and made more intelligible by the two-dimensional map of quaternary packing interactions shown in Figure 2.5. A clear picture of the peptide residues knobs from ANG IV packing into sockets on the hCD13 surface is represented. There are nine sockets on hCD13 filled by the knob residues coming from ANG IV. ANG IV also forms five sockets, which pack knobs from hCD13. For the 5-mer peptide design, six out of the nine sockets and one additional free socket formed by residues Y441, R442, and A445 were selected as the target site surface for the designed peptides (Figure 2.6). For the designed peptide ligand, positions 1, 2 and 5 were chosen as knobs to pack into the binding sockets. At position 1, knobs were chosen for 2 binding sites: one consisting of two sockets in the helix and another consisting of a socket from a coil region. Position 2's knob only comes from the helix, while position 5's knob is a single socket, but at 2 possible positions. Knobs with high propensities to interact with these sockets were chosen as the basis for the peptide sequences. Because these sockets span between 2 types of secondary structure that are 12 Å apart at closest approach, two residues (positions 3 and 4 on the peptide) were necessary to bridge between the binding sites. All possible combinations of the highest propensity knobs (Figure 2.6 inset table) produced thirty-two (32) 5-mer peptide sequences (Table 2.2).

For the 8-mer peptide design, all sockets from 5-mer design and two additional free socket formed by residues T860, S861 & I864, and S861, I864 & S865, respectively, were selected as the target site surface for the designed peptides (Figure 2.7). In case of 8-mer peptide design, a total of 384 peptides (Table 2.3) were obtained using all possible combinations of the highest propensity knobs (Figure 2.7 inset table).

Figure 2.4: Binding site of hCD13 with the endogenous ligand ANG IV (magenta coil)

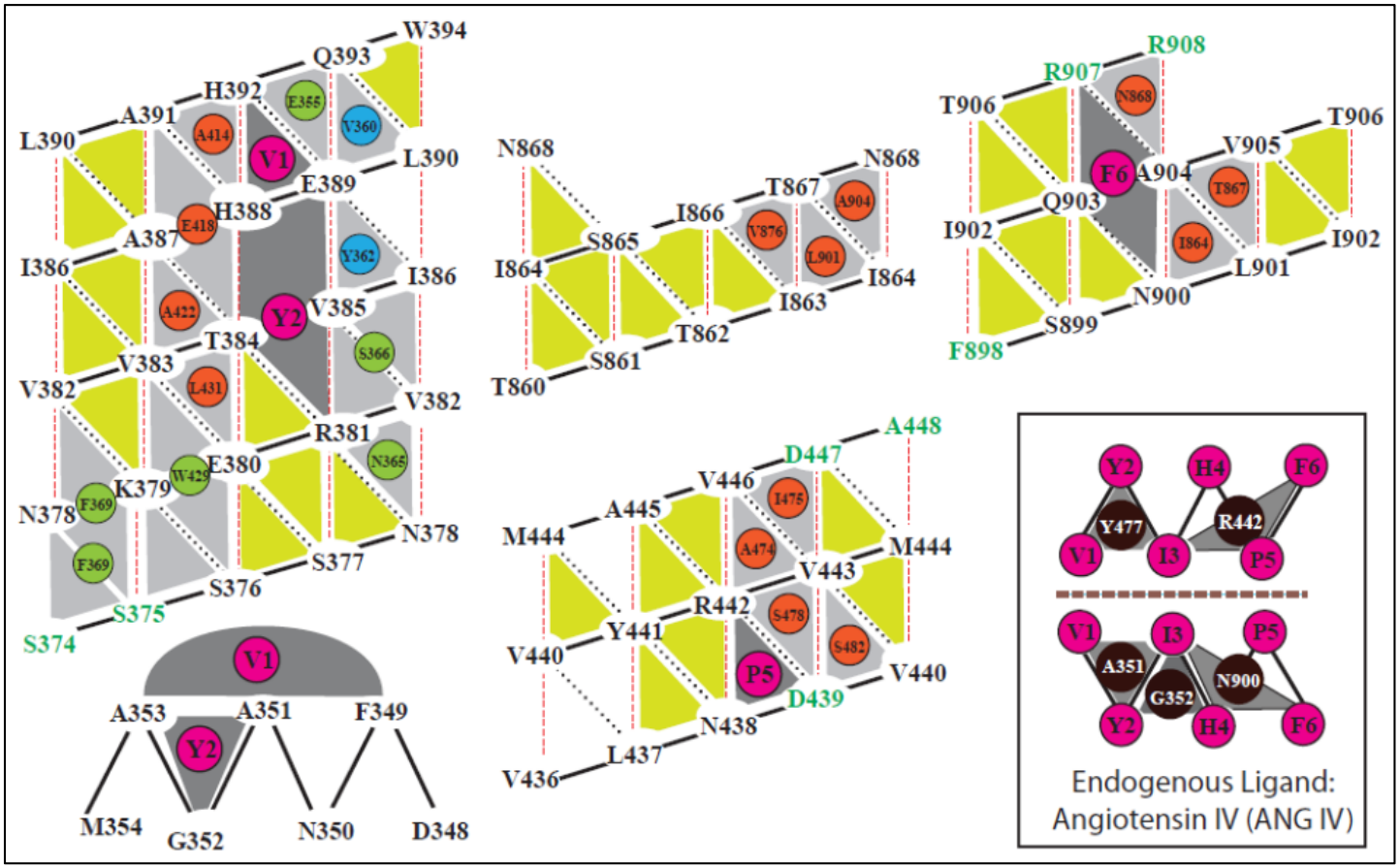

Figure 2.5: 2D lattice diagram of the binding interface between hCD13 and ANG IV. Sockets are represented by triangles or half elipses, while residues knobs are shown as circles. Gray and yellow shaded sockets are the filled and empty sockets on hCD13, respectively. Knobs are colored based on their origin. Knobs involved in tertiary structure packing within hCD13 are colored green from coil, red from helix, and blue from sheet. Knobs involved in quaternary binding of the peptide ligand are colored magenta. Black circles represent the knobs coming from receptor which pack against sockets formed by endogenous ligand.

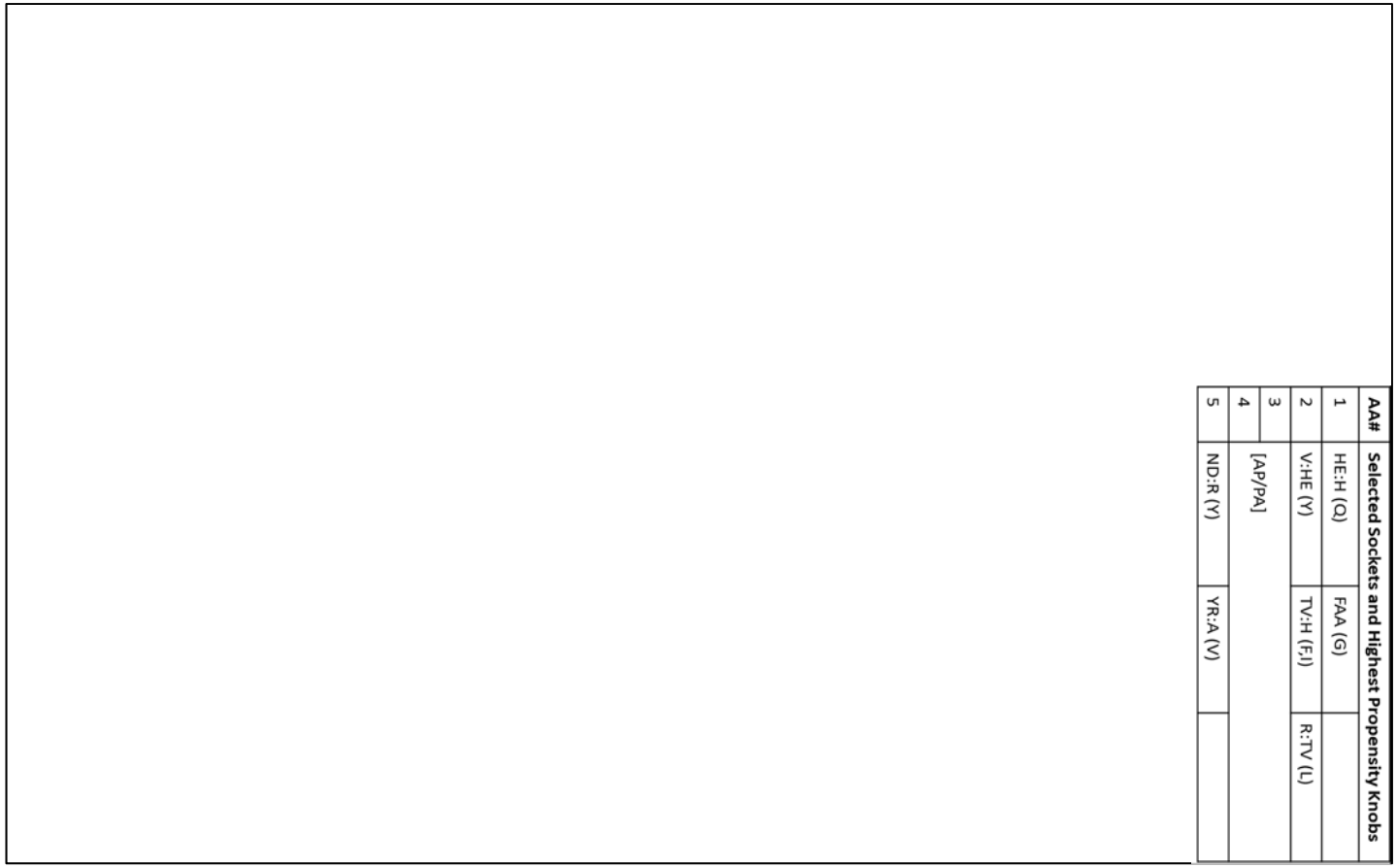

AA#	Selected Sockets and Highest Propensity Knobs		
1	HE:H (Q)	FAA (G)	
2	V:HE (Y)	TV:H (F,I)	R:TV (L)
3	[AP/PA]		
4			
5	ND:R (Y)	YR:A (V)	

Figure 2.6: Peptide design for the 5-mer molecules. Blue shades sockets are the hCD13 sockets used to select high propensity knobs for peptide design. The knobs used in peptide design are also colored magenta. Receptor knobs were omitted, and the inset table lists the high propensity knobs at each position.

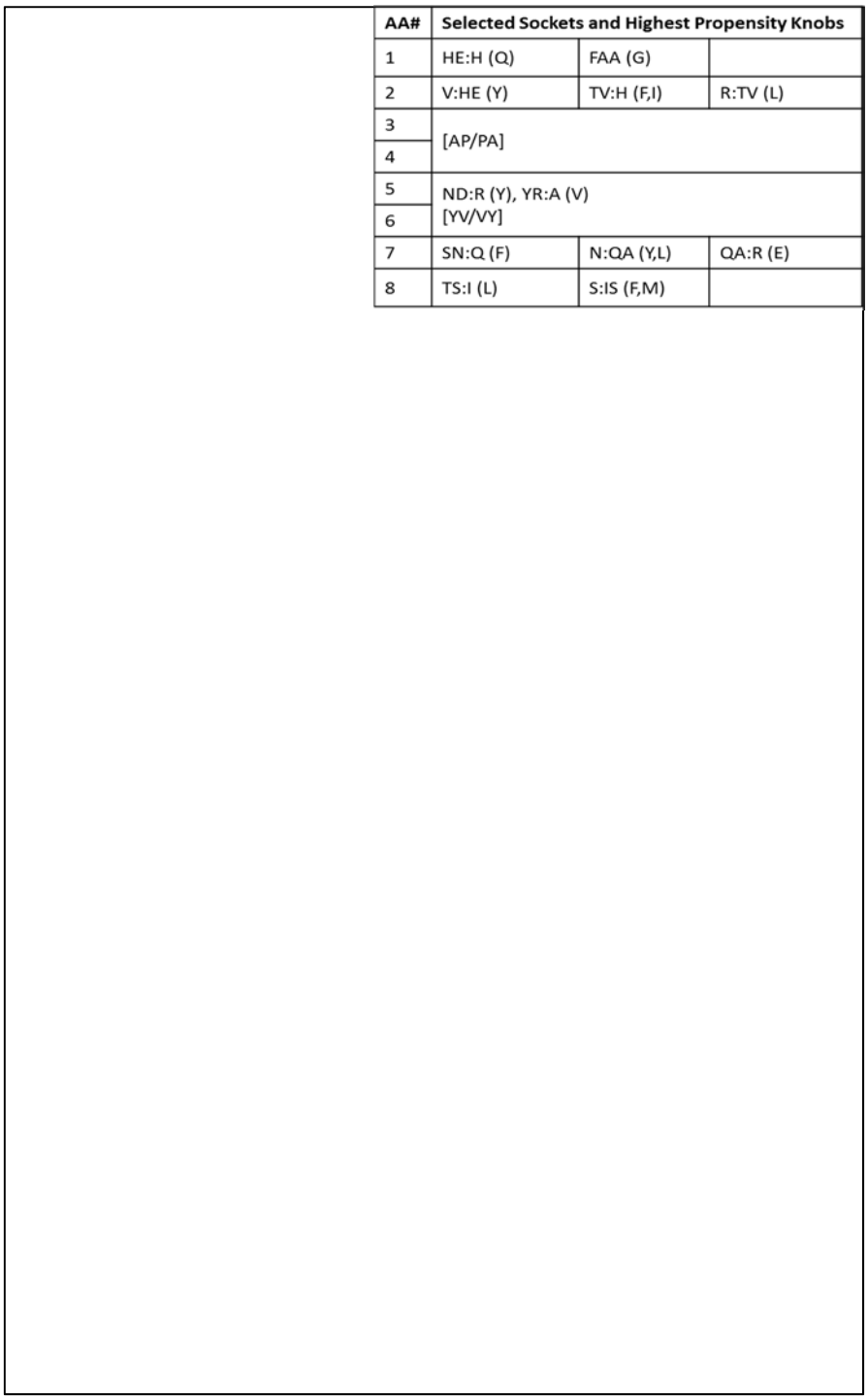

AA#	Selected Sockets and Highest Propensity Knobs		
1	HE:H (Q)	FAA (G)	
2	V:HE (Y)	TV:H (F,I)	R:TV (L)
3	[AP/PA]		
4			
5	ND:R (Y), YR:A (V) [YV/VY]		
6			
7	SN:Q (F)	N:QA (Y,L)	QA:R (E)
8	TS:I (L)	S:IS (F,M)	

Figure 2.7: Peptide design for the 8-mer molecules. Blue shades sockets are the hCD13 sockets used to select high propensity knobs for peptide design. The knobs used in peptide design are also colored magenta. Receptor knobs were omitted, and the inset table lists the high propensity knobs at each position.

Table 2.2

5-mer peptide sequences

AA# → Peptide#↓	**1**	**2**	**3**	**4**	**5**
1	Q	Y	A	P	V
2	Q	Y	A	P	Y
3	Q	Y	P	A	V
4	Q	Y	P	A	Y
5	Q	F	A	P	V
6	Q	F	A	P	Y
7	Q	F	P	A	V
8	Q	F	P	A	Y
9	Q	I	A	P	V
10	Q	I	A	P	Y
11	Q	I	P	A	V
12	Q	I	P	A	Y
13	Q	L	A	P	V
14	Q	L	A	P	Y
15	Q	L	P	A	V
16	Q	L	P	A	Y
17	G	Y	A	P	V
18	G	Y	A	P	Y
19	G	Y	P	A	V
20	G	Y	P	A	Y
21	G	F	A	P	V
22	G	F	A	P	Y
23	G	F	P	A	V
24	G	F	P	A	Y
25	G	I	A	P	V
26	G	I	A	P	Y
27	G	I	P	A	V
28	G	I	P	A	Y
29	G	L	A	P	V
30	G	L	A	P	Y
31	G	L	P	A	V
32	G	L	P	A	Y

Table 2.3

8-mer peptide sequences

AA# → Peptide#↓	**1**	**2**	**3**	**4**	**5**	**6**	**7**	**8**
33	Q	Y	A	P	V	Y	Y	L
34	Q	Y	A	P	V	Y	Y	M
35	Q	Y	A	P	V	Y	Y	F
36	Q	Y	A	P	V	Y	L	L
37	Q	Y	A	P	V	Y	L	M
38	Q	Y	A	P	V	Y	L	F
39	Q	Y	A	P	V	Y	F	L
40	Q	Y	A	P	V	Y	F	M
41	Q	Y	A	P	V	Y	F	F
42	Q	Y	A	P	Y	V	Y	L
43	Q	Y	A	P	Y	V	Y	M
44	Q	Y	A	P	Y	V	Y	F
45	Q	Y	A	P	Y	V	L	L
46	Q	Y	A	P	Y	V	L	M
47	Q	Y	A	P	Y	V	L	F
48	Q	Y	A	P	Y	V	F	L
49	Q	Y	A	P	Y	V	F	M
50	Q	Y	A	P	Y	V	F	F
51	Q	Y	P	A	Y	V	Y	L
52	Q	Y	P	A	Y	V	Y	M
53	Q	Y	P	A	Y	V	Y	F
54	Q	Y	P	A	Y	V	L	L
55	Q	Y	P	A	Y	V	L	M
56	Q	Y	P	A	Y	V	L	F
57	Q	Y	P	A	Y	V	F	L
58	Q	Y	P	A	Y	V	F	M
59	Q	Y	P	A	Y	V	F	F
60	Q	Y	P	A	V	Y	Y	L
61	Q	Y	P	A	V	Y	Y	M
62	Q	Y	P	A	V	Y	Y	F
63	Q	Y	P	A	V	Y	L	L
64	Q	Y	P	A	V	Y	L	M
65	Q	Y	P	A	V	Y	L	F
66	Q	Y	P	A	V	Y	F	L
67	Q	Y	P	A	V	Y	F	M
68	Q	Y	P	A	V	Y	F	F
69	Q	F	A	P	V	Y	Y	L
70	Q	F	A	P	V	Y	Y	M

(continued)

Table 2.3 (continued)

AA# → Peptide#↓	**1**	**2**	**3**	**4**	**5**	**6**	**7**	**8**
71	Q	F	A	P	V	Y	Y	F
72	Q	F	A	P	V	Y	L	L
73	Q	F	A	P	V	Y	L	M
74	Q	F	A	P	V	Y	L	F
75	Q	F	A	P	V	Y	F	L
76	Q	F	A	P	V	Y	F	M
77	Q	F	A	P	V	Y	F	F
78	Q	F	A	P	Y	V	Y	L
79	Q	F	A	P	Y	V	Y	M
80	Q	F	A	P	Y	V	Y	F
81	Q	F	A	P	Y	V	L	L
82	Q	F	A	P	Y	V	L	M
83	Q	F	A	P	Y	V	L	F
84	Q	F	A	P	Y	V	F	L
85	Q	F	A	P	Y	V	F	M
86	Q	F	A	P	Y	V	F	F
87	Q	F	P	A	Y	V	Y	L
88	Q	F	P	A	Y	V	Y	M
89	Q	F	P	A	Y	V	Y	F
90	Q	F	P	A	Y	V	L	L
91	Q	F	P	A	Y	V	L	M
92	Q	F	P	A	Y	V	L	F
93	Q	F	P	A	Y	V	F	L
94	Q	F	P	A	Y	V	F	M
95	Q	F	P	A	Y	V	F	F
96	Q	F	P	A	V	Y	Y	L
97	Q	F	P	A	V	Y	Y	M
98	Q	F	P	A	V	Y	Y	F
99	Q	F	P	A	V	Y	L	L
100	Q	F	P	A	V	Y	L	M
101	Q	F	P	A	V	Y	L	F
102	Q	F	P	A	V	Y	F	L
103	Q	F	P	A	V	Y	F	M
104	Q	F	P	A	V	Y	F	F
105	Q	I	A	P	V	Y	Y	L
106	Q	I	A	P	V	Y	Y	M
107	Q	I	A	P	V	Y	Y	F
108	Q	I	A	P	V	Y	L	L

(continued)

Table 2.3 (continued)

AA# → Peptide#↓	1	2	3	4	5	6	7	8
109	Q	I	A	P	V	Y	L	M
110	Q	I	A	P	V	Y	L	F
111	Q	I	A	P	V	Y	F	L
112	Q	I	A	P	V	Y	F	M
113	Q	I	A	P	V	Y	F	F
114	Q	I	A	P	Y	V	Y	L
115	Q	I	A	P	Y	V	Y	M
116	Q	I	A	P	Y	V	Y	F
117	Q	I	A	P	Y	V	L	L
118	Q	I	A	P	Y	V	L	M
119	Q	I	A	P	Y	V	L	F
120	Q	I	A	P	Y	V	F	L
121	Q	I	A	P	Y	V	F	M
122	Q	I	A	P	Y	V	F	F
123	Q	I	P	A	Y	V	Y	L
124	Q	I	P	A	Y	V	Y	M
125	Q	I	P	A	Y	V	Y	F
126	Q	I	P	A	Y	V	L	L
127	Q	I	P	A	Y	V	L	M
128	Q	I	P	A	Y	V	L	F
129	Q	I	P	A	Y	V	F	L
130	Q	I	P	A	Y	V	F	M
131	Q	I	P	A	Y	V	F	F
132	Q	I	P	A	V	Y	Y	L
133	Q	I	P	A	V	Y	Y	M
134	Q	I	P	A	V	Y	Y	F
135	Q	I	P	A	V	Y	L	L
136	Q	I	P	A	V	Y	L	M
137	Q	I	P	A	V	Y	L	F
138	Q	I	P	A	V	Y	F	L
139	Q	I	P	A	V	Y	F	M
140	Q	I	P	A	V	Y	F	F
141	G	Y	A	P	V	Y	Y	L
142	G	Y	A	P	V	Y	Y	M
143	G	Y	A	P	V	Y	Y	F
144	G	Y	A	P	V	Y	L	L
145	G	Y	A	P	V	Y	L	M
146	G	Y	A	P	V	Y	L	F
147	G	Y	A	P	V	Y	F	L

(continued)

Table 2.3 (continued)

AA# → Peptide#↓	1	2	3	4	5	6	7	8
148	G	Y	A	P	V	Y	F	M
149	G	Y	A	P	V	Y	F	F
150	G	Y	A	P	Y	V	Y	L
151	G	Y	A	P	Y	V	Y	M
152	G	Y	A	P	Y	V	Y	F
153	G	Y	A	P	Y	V	L	L
154	G	Y	A	P	Y	V	L	M
155	G	Y	A	P	Y	V	L	F
156	G	Y	A	P	Y	V	F	L
157	G	Y	A	P	Y	V	F	M
158	G	Y	A	P	Y	V	F	F
159	G	Y	P	A	Y	V	Y	L
160	G	Y	P	A	Y	V	Y	M
161	G	Y	P	A	Y	V	Y	F
162	G	Y	P	A	Y	V	L	L
163	G	Y	P	A	Y	V	L	M
164	G	Y	P	A	Y	V	L	F
165	G	Y	P	A	Y	V	F	L
166	G	Y	P	A	Y	V	F	M
167	G	Y	P	A	Y	V	F	F
168	G	Y	P	A	V	Y	Y	L
169	G	Y	P	A	V	Y	Y	M
170	G	Y	P	A	V	Y	Y	F
171	G	Y	P	A	V	Y	L	L
172	G	Y	P	A	V	Y	L	M
173	G	Y	P	A	V	Y	L	F
174	G	Y	P	A	V	Y	F	L
175	G	Y	P	A	V	Y	F	M
176	G	Y	P	A	V	Y	F	F
177	G	F	A	P	V	Y	Y	L
178	G	F	A	P	V	Y	Y	M
179	G	F	A	P	V	Y	Y	F
180	G	F	A	P	V	Y	L	L
181	G	F	A	P	V	Y	L	M
182	G	F	A	P	V	Y	L	F
183	G	F	A	P	V	Y	F	L
184	G	F	A	P	V	Y	F	M
185	G	F	A	P	V	Y	F	F
186	G	F	A	P	Y	V	Y	L

(continued)

Table 2.3 (continued)

AA# → Peptide#↓	1	2	3	4	5	6	7	8
187	G	F	A	P	Y	V	Y	M
188	G	F	A	P	Y	V	Y	F
189	G	F	A	P	Y	V	L	L
190	G	F	A	P	Y	V	L	M
191	G	F	A	P	Y	V	L	F
192	G	F	A	P	Y	V	F	L
193	G	F	A	P	Y	V	F	M
194	G	F	A	P	Y	V	F	F
195	G	F	P	A	Y	V	Y	L
196	G	F	P	A	Y	V	Y	M
197	G	F	P	A	Y	V	Y	F
198	G	F	P	A	Y	V	L	L
199	G	F	P	A	Y	V	L	M
200	G	F	P	A	Y	V	L	F
201	G	F	P	A	Y	V	F	L
202	G	F	P	A	Y	V	F	M
203	G	F	P	A	Y	V	F	F
204	G	F	P	A	V	Y	Y	L
205	G	F	P	A	V	Y	Y	M
206	G	F	P	A	V	Y	Y	F
207	G	F	P	A	V	Y	L	L
208	G	F	P	A	V	Y	L	M
209	G	F	P	A	V	Y	L	F
210	G	F	P	A	V	Y	F	L
211	G	F	P	A	V	Y	F	M
212	G	F	P	A	V	Y	F	F
213	G	I	A	P	V	Y	Y	L
214	G	I	A	P	V	Y	Y	M
215	G	I	A	P	V	Y	Y	F
216	G	I	A	P	V	Y	L	L
217	G	I	A	P	V	Y	L	M
218	G	I	A	P	V	Y	L	F
219	G	I	A	P	V	Y	F	L
220	G	I	A	P	V	Y	F	M
221	G	I	A	P	V	Y	F	F
222	G	I	A	P	Y	V	Y	L
223	G	I	A	P	Y	V	Y	M
224	G	I	A	P	Y	V	Y	F
225	G	I	A	P	Y	V	L	L

(continued)

Table 2.3 (continued)

AA# → Peptide#↓	1	2	3	4	5	6	7	8
226	G	I	A	P	Y	V	L	M
227	G	I	A	P	Y	V	L	F
228	G	I	A	P	Y	V	F	L
229	G	I	A	P	Y	V	F	M
230	G	I	A	P	Y	V	F	F
231	G	I	P	A	Y	V	Y	L
232	G	I	P	A	Y	V	Y	M
233	G	I	P	A	Y	V	Y	F
234	G	I	P	A	Y	V	L	L
235	G	I	P	A	Y	V	L	M
236	G	I	P	A	Y	V	L	F
237	G	I	P	A	Y	V	F	L
238	G	I	P	A	Y	V	F	M
239	G	I	P	A	Y	V	F	F
240	G	I	P	A	V	Y	Y	L
241	G	I	P	A	V	Y	Y	M
242	G	I	P	A	V	Y	Y	F
243	G	I	P	A	V	Y	L	L
244	G	I	P	A	V	Y	L	M
245	G	I	P	A	V	Y	L	F
246	G	I	P	A	V	Y	F	L
247	G	I	P	A	V	Y	F	M
248	G	I	P	A	V	Y	F	F
249	Q	Y	A	P	V	Y	E	L
250	Q	Y	A	P	V	Y	E	M
251	Q	Y	A	P	V	Y	E	F
252	Q	Y	A	P	Y	V	E	L
253	Q	Y	A	P	Y	V	E	M
254	Q	Y	A	P	Y	V	E	F
255	Q	Y	P	A	Y	V	E	L
256	Q	Y	P	A	Y	V	E	M
257	Q	Y	P	A	Y	V	E	F
258	Q	Y	P	A	V	Y	E	L
259	Q	Y	P	A	V	Y	E	M
260	Q	Y	P	A	V	Y	E	F
261	Q	F	A	P	V	Y	E	L
262	Q	F	A	P	V	Y	E	M
263	Q	F	A	P	V	Y	E	F
264	Q	F	A	P	Y	V	E	L

(continued)

Table 2.3 (continued)

AA# → Peptide#↓	1	2	3	4	5	6	7	8
265	Q	F	A	P	Y	V	E	M
266	Q	F	A	P	Y	V	E	F
267	Q	F	P	A	Y	V	E	L
268	Q	F	P	A	Y	V	E	M
269	Q	F	P	A	Y	V	E	F
270	Q	F	P	A	V	Y	E	L
271	Q	F	P	A	V	Y	E	M
272	Q	F	P	A	V	Y	E	F
273	Q	I	A	P	V	Y	E	L
274	Q	I	A	P	V	Y	E	M
275	Q	I	A	P	V	Y	E	F
276	Q	I	A	P	Y	V	E	L
277	Q	I	A	P	Y	V	E	M
278	Q	I	A	P	Y	V	E	F
279	Q	I	P	A	Y	V	E	L
280	Q	I	P	A	Y	V	E	M
281	Q	I	P	A	Y	V	E	F
282	Q	I	P	A	V	Y	E	L
283	Q	I	P	A	V	Y	E	M
284	Q	I	P	A	V	Y	E	F
285	G	Y	A	P	V	Y	E	L
286	G	Y	A	P	V	Y	E	M
287	G	Y	A	P	V	Y	E	F
288	G	Y	A	P	Y	V	E	L
289	G	Y	A	P	Y	V	E	M
290	G	Y	A	P	Y	V	E	F
291	G	Y	P	A	Y	V	E	L
292	G	Y	P	A	Y	V	E	M
293	G	Y	P	A	Y	V	E	F
294	G	Y	P	A	V	Y	E	L
295	G	Y	P	A	V	Y	E	M
296	G	Y	P	A	V	Y	E	F
297	G	F	A	P	V	Y	E	L
298	G	F	A	P	V	Y	E	M
299	G	F	A	P	V	Y	E	F
300	G	F	A	P	Y	V	E	L
301	G	F	A	P	Y	V	E	M
302	G	F	A	P	Y	V	E	F
303	G	F	P	A	Y	V	E	L

(continued)

Table 2.3 (continued)

AA# → Peptide#↓	1	2	3	4	5	6	7	8
304	G	F	P	A	Y	V	E	M
305	G	F	P	A	Y	V	E	F
306	G	F	P	A	V	Y	E	L
307	G	F	P	A	V	Y	E	M
308	G	F	P	A	V	Y	E	F
309	G	I	A	P	V	Y	E	L
310	G	I	A	P	V	Y	E	M
311	G	I	A	P	V	Y	E	F
312	G	I	A	P	Y	V	E	L
313	G	I	A	P	Y	V	E	M
314	G	I	A	P	Y	V	E	F
315	G	I	P	A	Y	V	E	L
316	G	I	P	A	Y	V	E	M
317	G	I	P	A	Y	V	E	F
318	G	I	P	A	V	Y	E	L
319	G	I	P	A	V	Y	E	M
320	G	I	P	A	V	Y	E	F
321	Q	L	A	P	V	Y	Y	L
322	Q	L	A	P	V	Y	Y	M
323	Q	L	A	P	V	Y	Y	F
324	Q	L	A	P	V	Y	L	L
325	Q	L	A	P	V	Y	L	M
326	Q	L	A	P	V	Y	L	F
327	Q	L	A	P	V	Y	F	L
328	Q	L	A	P	V	Y	F	M
329	Q	L	A	P	V	Y	F	F
330	Q	L	A	P	Y	V	Y	L
331	Q	L	A	P	Y	V	Y	M
332	Q	L	A	P	Y	V	Y	F
333	Q	L	A	P	Y	V	L	L
334	Q	L	A	P	Y	V	L	M
335	Q	L	A	P	Y	V	L	F
336	Q	L	A	P	Y	V	F	L
337	Q	L	A	P	Y	V	F	M
338	Q	L	A	P	Y	V	F	F
339	Q	L	P	A	Y	V	Y	L
340	Q	L	P	A	Y	V	Y	M
341	Q	L	P	A	Y	V	Y	F
342	Q	L	P	A	Y	V	L	L

(continued)

Table 2.3 (continued)

AA# → Peptide#↓	1	2	3	4	5	6	7	8
343	Q	L	P	A	Y	V	L	M
344	Q	L	P	A	Y	V	L	F
345	Q	L	P	A	Y	V	F	L
346	Q	L	P	A	Y	V	F	M
347	Q	L	P	A	Y	V	F	F
348	Q	L	P	A	V	Y	Y	L
349	Q	L	P	A	V	Y	Y	M
350	Q	L	P	A	V	Y	Y	F
351	Q	L	P	A	V	Y	L	L
352	Q	L	P	A	V	Y	L	M
353	Q	L	P	A	V	Y	L	F
354	Q	L	P	A	V	Y	F	L
355	Q	L	P	A	V	Y	F	M
356	Q	L	P	A	V	Y	F	F
357	Q	L	A	P	V	Y	E	L
358	Q	L	A	P	V	Y	E	M
359	Q	L	A	P	V	Y	E	F
360	Q	L	A	P	Y	V	E	L
361	Q	L	A	P	Y	V	E	M
362	Q	L	A	P	Y	V	E	F
363	Q	L	P	A	Y	V	E	L
364	Q	L	P	A	Y	V	E	M
365	Q	L	P	A	Y	V	E	F
366	Q	L	P	A	V	Y	E	L
367	Q	L	P	A	V	Y	E	M
368	Q	L	P	A	V	Y	E	F
369	G	L	A	P	V	Y	Y	L
370	G	L	A	P	V	Y	Y	M
371	G	L	A	P	V	Y	Y	F
372	G	L	A	P	V	Y	L	L
373	G	L	A	P	V	Y	L	M
374	G	L	A	P	V	Y	L	F
375	G	L	A	P	V	Y	F	L
376	G	L	A	P	V	Y	F	M
377	G	L	A	P	V	Y	F	F
378	G	L	A	P	Y	V	Y	L
379	G	L	A	P	Y	V	Y	M
380	G	L	A	P	Y	V	Y	F
381	G	L	A	P	Y	V	L	L

(continued)

Table 2.3 (continued)

AA# → Peptide#↓	1	2	3	4	5	6	7	8
382	G	L	A	P	Y	V	L	M
383	G	L	A	P	Y	V	L	F
384	G	L	A	P	Y	V	F	L
385	G	L	A	P	Y	V	F	M
386	G	L	A	P	Y	V	F	F
387	G	L	P	A	Y	V	Y	L
388	G	L	P	A	Y	V	Y	M
389	G	L	P	A	Y	V	Y	F
390	G	L	P	A	Y	V	L	L
391	G	L	P	A	Y	V	L	M
392	G	L	P	A	Y	V	L	F
393	G	L	P	A	Y	V	F	L
394	G	L	P	A	Y	V	F	M
395	G	L	P	A	Y	V	F	F
396	G	L	P	A	V	Y	Y	L
397	G	L	P	A	V	Y	Y	M
398	G	L	P	A	V	Y	Y	F
399	G	L	P	A	V	Y	L	L
400	G	L	P	A	V	Y	L	M
401	G	L	P	A	V	Y	L	F
402	G	L	P	A	V	Y	F	L
403	G	L	P	A	V	Y	F	M
404	G	L	P	A	V	Y	F	F
405	G	L	A	P	V	Y	E	L
406	G	L	A	P	V	Y	E	M
407	G	L	A	P	V	Y	E	F
408	G	L	A	P	Y	V	E	L
409	G	L	A	P	Y	V	E	M
410	G	L	A	P	Y	V	E	F
411	G	L	P	A	Y	V	E	L
412	G	L	P	A	Y	V	E	M
413	G	L	P	A	Y	V	E	F
414	G	L	P	A	V	Y	E	L
415	G	L	P	A	V	Y	E	M
416	G	L	P	A	V	Y	E	F

2.3.2 Screening of the peptide ligands. Using the predetermined criteria (previously discussed in the Method section) eight (8) 5-mer peptides were selected from the initial sequences and subjected to MOE docking. These eight (8) 5-mer peptides were ranked according to their MOE docking scores (Table 2.4). In case of 8-mer peptide design, the predetermined criteria led to forty (40) 8-mer peptide sequences. These 40 peptides were subjected to MOE docking and the top ten ranking peptides (top 25% based on the MOE docking score) are listed in Table 2.4.

An additional docking studies with AutoDock Vina were performed for all eight (8) of the 5-mer peptides and top 25% (10) of the 8-mer peptides based on MOE docking score ranking. Of these, AutoDock Vina predicted that three designed peptides [two 5-mer (PEP20, GYPAY and PEP24, GFPAY), and one 8-mer (PEP173, GYPAVYLF)] could bind to the intended active site of hCD13 similar to the positive control CNGRC (C1-C5) peptide ligand (NGR-2C) (Figure 2.8 & Table 2.4). These three (3) peptides along with two (2) other nonspecific peptides (PEP293, GYPAYVEF and PEP308, GFPAVYEF; as negative controls) were selected for experimental evaluation.

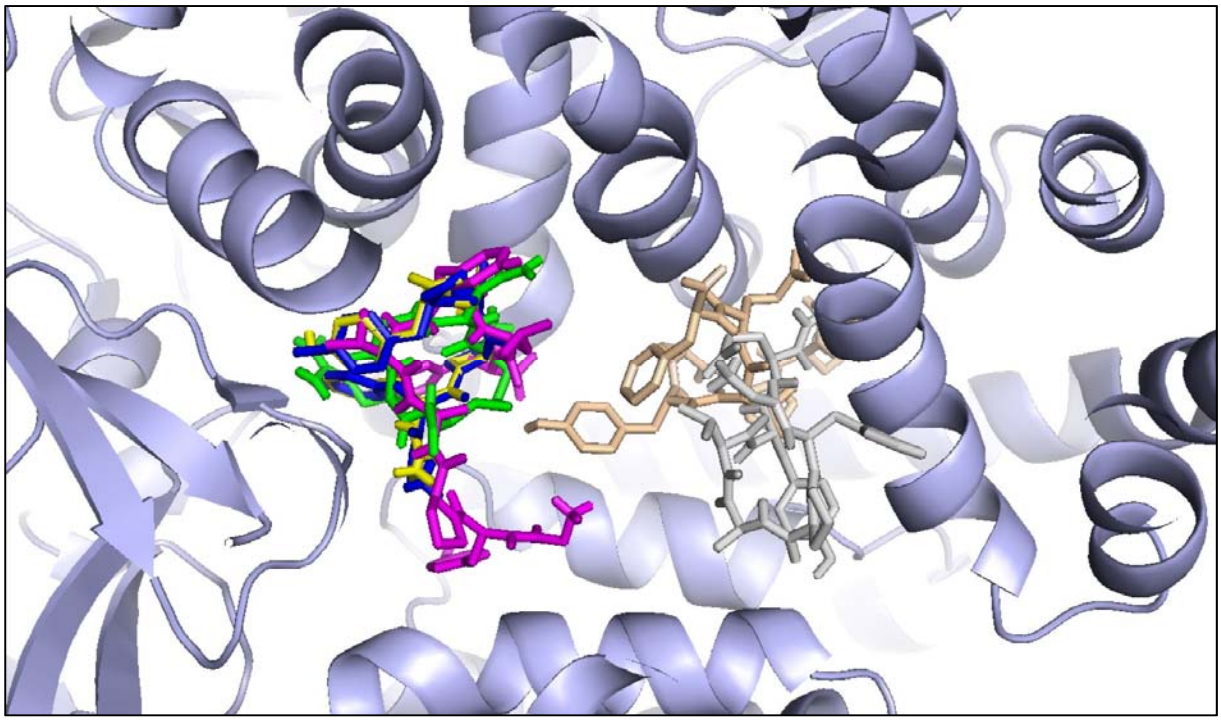

Figure 2.8: Peptides at hCD13 binding site after docking with AutoDock Vina. Green coil: CNGRC(C1-C5), Blue: PEP20, Yellow: PEP24, Magenta: PEP173, Wheat: PEP293, Grey: PEP308.

Table 2.4

Designed peptides with docking results

Ranking	Residue → Peptide↓	1	2	3	4	5	6	7	8	MOE Docking Score	AutoDock Vina Predicted Binding Site
						5-mer peptides					
1	20	G	Y	P	A	Y	-	-	-	-13.9095	On active site
2	24	G	F	P	A	Y	-	-	-	-11.9234	On active site
3	19	G	Y	P	A	V	-	-	-	-11.7211	Distant from active site
4	27	G	I	P	A	V	-	-	-	-11.6586	Distant from active site
5	32	G	L	P	A	Y	-	-	-	-11.5135	Distant from active site
6	28	G	I	P	A	Y	-	-	-	-11.3576	Distant from active site
7	31	G	L	P	A	V	-	-	-	-10.7643	Distant from active site
8	23	G	F	P	A	V	-	-	-	-10.7205	Distant from active site
-	NGR-2C	C	N	G	R	C(1-5)	-	-	-	-11.2815	On active site
						8-mer peptides					
1	296	G	Y	P	A	V	Y	E	F	-16.9475	Distant from active site
2	293	G	Y	P	A	Y	V	E	F	-16.6503	Distant from active site

(continued)

Table 2.4 (continued)

Ranking	Residue → Peptide↓	1	2	3	4	5	6	7	8	MOE Docking Score	AutoDock Vina Predicted Binding Site
3	317	G	I	P	A	Y	V	E	F	-16.6490	Distant from active site
4	389	G	L	P	A	Y	V	Y	F	-16.5394	Distant from active site
5	209	G	F	P	A	V	Y	L	F	-16.4622	Distant from active site
6	161	G	Y	P	A	Y	V	Y	F	-16.3548	Distant from active site
7	308	G	F	P	A	V	Y	E	F	-16.2962	Distant from active site
8	173	G	Y	P	A	V	Y	L	F	-16.2385	On active site
9	387	G	L	P	A	Y	V	Y	L	-16.0129	Distant from active site
10	245	G	I	P	A	V	Y	L	F	-15.8007	Distant from active site

Chapter 3: Synthesis and Characterization of Molecules

3.1 Introduction

Peptides are made by coupling the carboxyl group of one amino acid to the amino group of another. The classical peptide synthesis approach is the solution phase synthesis. However, most labs have replaced it by solid phase synthesis technique. The solid phase peptide synthesis (SPPS) was developed by Bruce Merrifield in 1963 and since then it has been widely used for peptide synthesis in academic labs and industry. The advantages of SPPS are: (a) can be used to synthesize peptides that cannot be made by bacteria, (b) it allows the incorporation of complicated moieties in peptide structure, (c) generally yields peptides with high purity. The limitations of SPPS are: (a) low yield as it carries many cycles of de-protection and coupling for each amino acid in the sequence, (b) sequence dependent synthetic difficulty (135).

In SPPS a peptide chain is created backwards starting from the C-terminal towards the N-terminal end on a solid resin support by creating amide bonds between amino acids (136). The SPPS can be carried out manually or with the aid of automatic synthesizer, especially if the sequence is relatively long (137).

In this study, Wang resin (typically preloaded with starting C-terminal amino acid) was selected as the solid support resin due to the compatibility with FITC-conjugation and straightforward method. Wang resin normally holds strong attachment to the peptides until cleaved by trifluoroacetic acid (TFA). In SPPS the solid resins and the synthesized peptides attached to them do not pass through the filter in the synthesis vessel.

Amino acid side chains contain different types of functional groups making them susceptible to side chain reactions during peptide synthesis. Consequently, protecting groups are required to obtain the desired peptide molecule. Benzyl (Bzl) or tert-butyl (tBu) groups are the most commonly used protecting groups (138). But various other protecting groups are also used during SPPS of a peptide depending on peptide sequence and N-terminal protecting moiety. Side chain protecting groups are permanent protecting groups. They tolerate multiple cycles of chemical reactions during the SPPS. They are removed at the end stage during cleavage of the peptide chain from the resin by treating with strong acids like TFA.

Peptide synthesis will be started with Wang resin (chlorotrityl resin in case of CNGRC (C1-C5) peptide) preloaded with the C-terminal amino acid having its N-terminal protected with Fmoc group. Fmoc stands for 9-Fluorenylmethoxycarbonyl which is the temporary N-terminal protecting group. The next steps involves creating the peptide chain by de-protecting the terminal amine and conjugation of next amino acid (Figure 3.1).

Fmoc can be removed by treating the resin with mild basic solution (20% piperidine in DMF) (Figure 3.2). The next amino acid is coupled to the peptide sequence by adding the amino acid together with carbodiimide, such as dicyclohexylcarbodiimide (DCC) or diisopropylcarbodiimide (DIC) which activates the C-terminal carboxylic group of that amino acid. Carbodiimide reacts with available carboxyl group and create a highly reactive O-acylisourea intermediate, which is immediately substituted by nucleophilic attack by the deprotected primary amine group on the N-terminal of the elongating peptide chain and forms amide bond (peptide bond) (Figure 3.3). However, reactive O-acylisourea intermediates may lead to racemization of the amino acids. Thus, racemic suppressors like 1-hydroxybenzotriazole (HOBt) that react with the O-acylisourea intermediate are generally added to eliminate

racemization (Figure 3.3). The newly formed N-terminal of the peptide is then deprotected again and coupled to the next amino acid. Kaiser test can be performed to monitor and confirm the completion of each deprotection and coupling steps (139) (Figure 3.4). This deprotection and coupling cycle is repeated until the full peptide sequence is created.

When all the amino acid couplings are complete, the peptide is cleaved from the solid resin. All sidechain protecting groups and the C-terminal attachment to the solid support are removed by acidic cleavage cocktail containing TFA. Peptide is normally isolated from the cocktail by using ice cold diethyl ether. Then the peptide is characterized by mass spectrophotometric techniques and high performance liquid chromatography (HPLC).

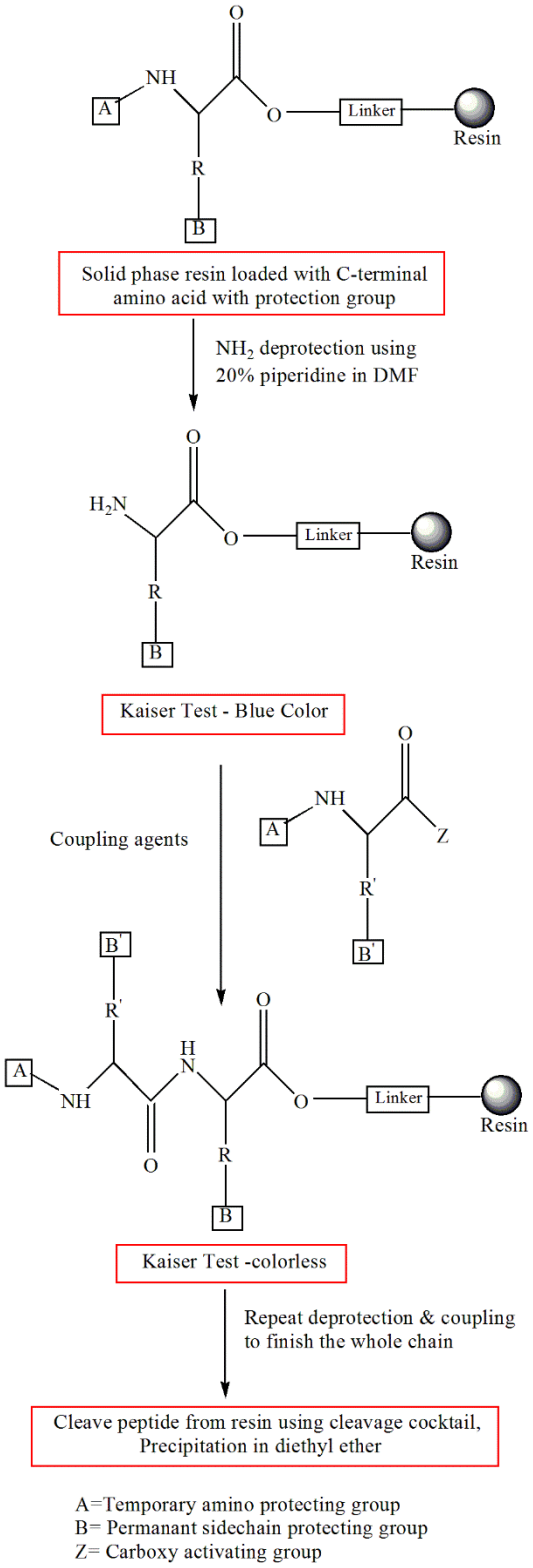

Figure 3.1: General solid phase peptide synthesis scheme using Fmoc chemistry

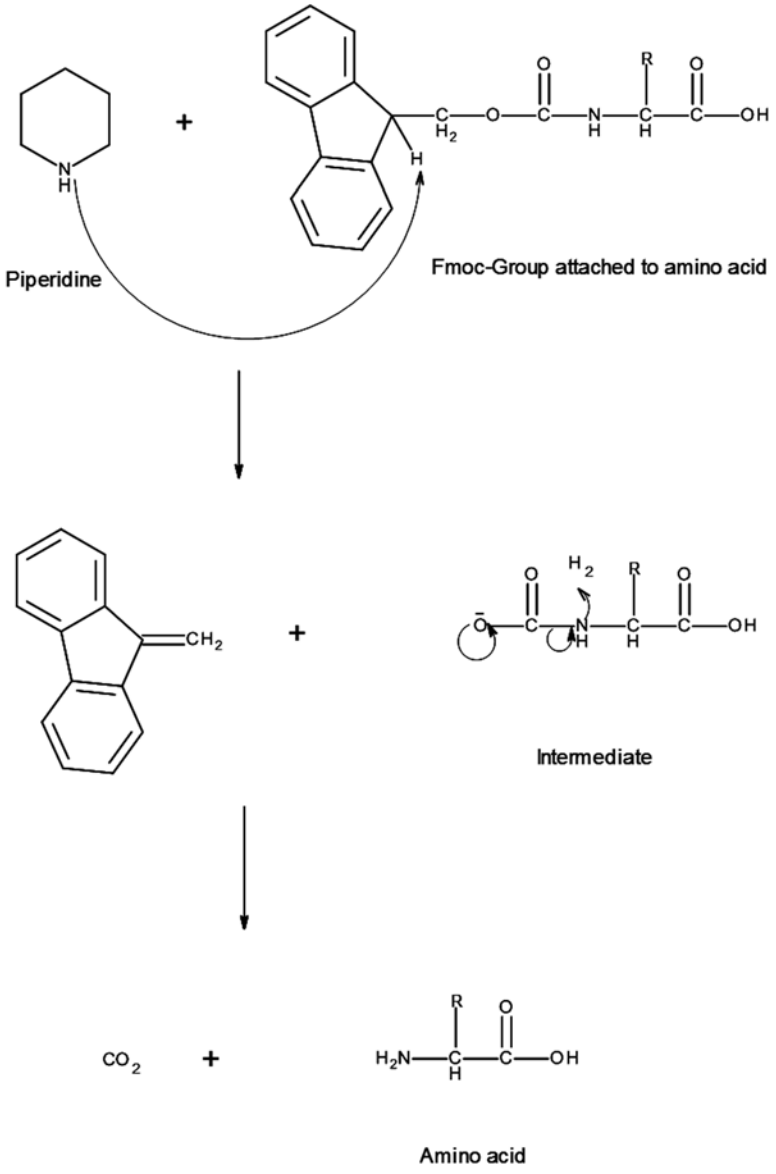

Figure 3.2: Fmoc-deprotection mechanism by piperadine

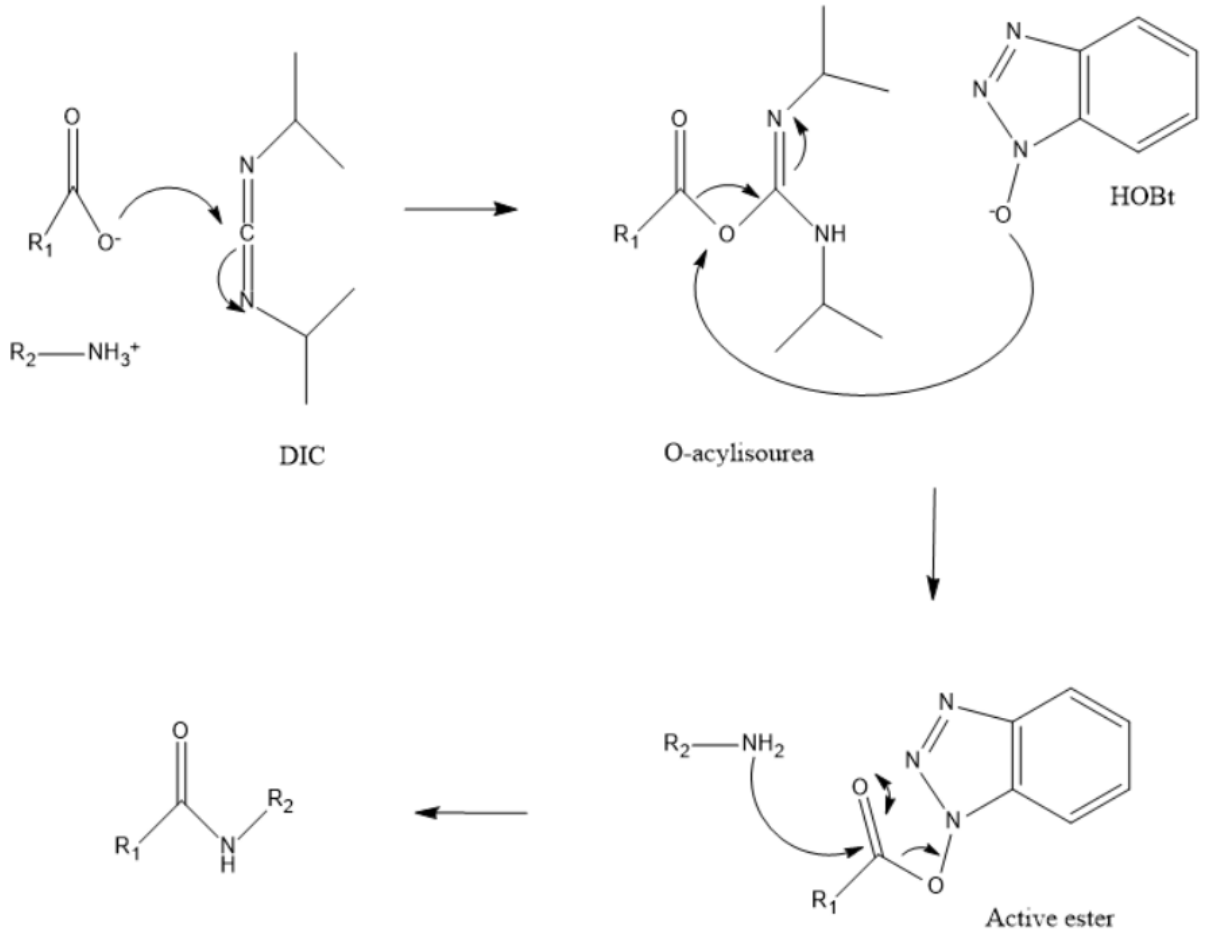

Figure 3.3: DIC/HOBt coupling mechanism

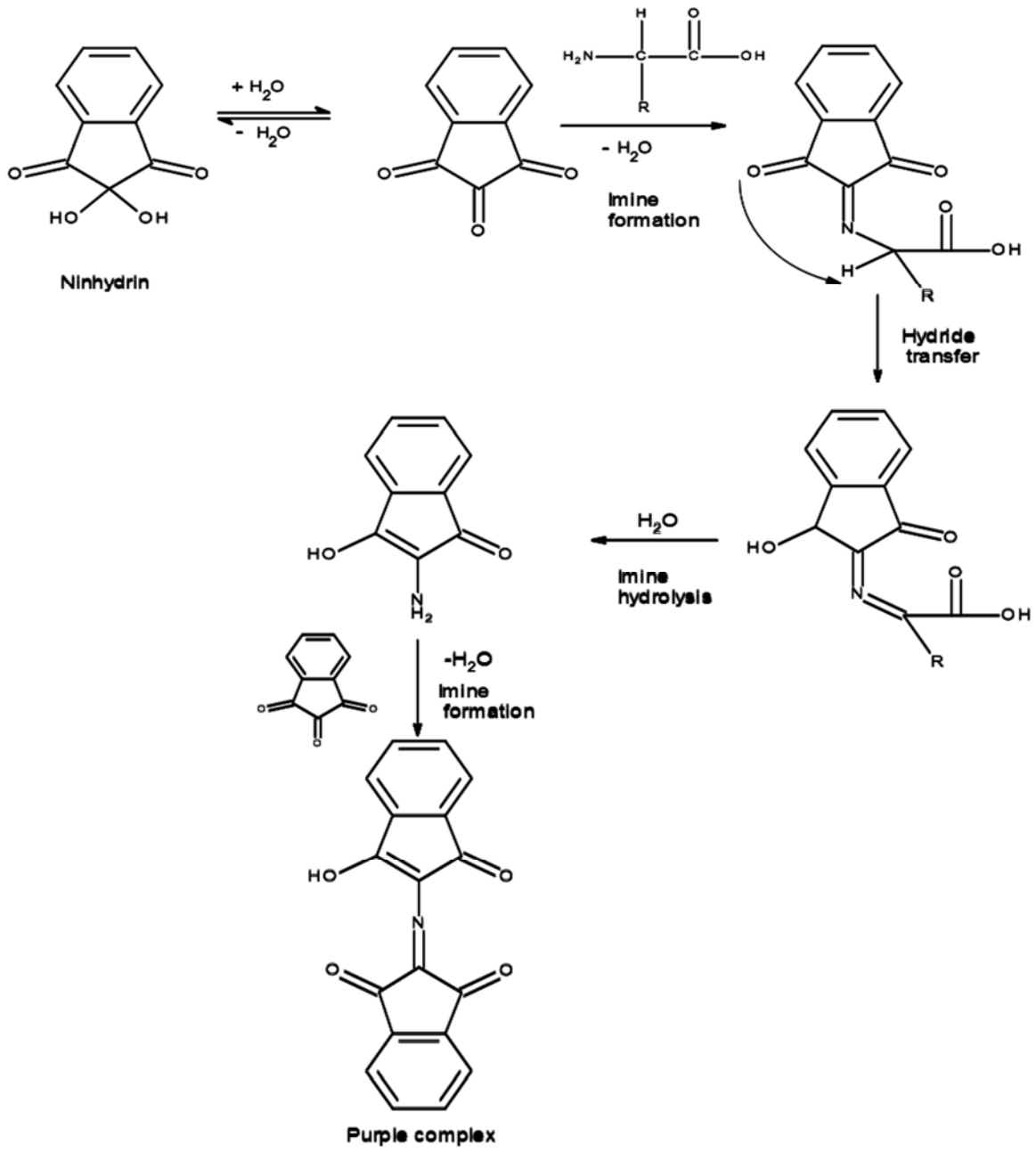

Figure 3.4: Mechanism of Kaiser test

3.2 Materials

Fmoc-amino acid-Wang resins, Fmoc-amino acid-2-chlorotrityl resins, Fmoc-amino acids, Boc-amino acids, Fmoc-aminohexanoic acid, N, N′-diisopropylcarbodiimide (DIC), diisopropylethylamine (DIPEA), triisopropylsilane (TIS), N-hydroxybenzotriazole (HOBT) were purchased from Chem-Impex International Ltd (Wood Dale, IL, USA). Trifluoro acetic acid (TFA) was obtained from Acros Organics (New Jersey, USA). Diethyl ether, N, N′-dimethylformamide (DMF) and dichloromethane (DCM) were purchased from Fisher Scientific (Pittsburgh, PA, USA). Fmoc-Lys(ivDde)-Wang resin was obtained from Peptides International (Louisville, KY, USA). FITC was obtained from AnaSpec (Fremont, CA, USA).

3.3 Methods

3.3.1 Synthesis of peptides. The selected designed peptides (PEP20, GYPAY; PEP24, GFPAY; and PEP173, GYPAVYLF), CNGRC (C1-C5) peptide (NGR-2C), and GARAG peptide (negative control) were synthesized by standard solid phase synthesis method (0.2 to 0.4 mmol scale). Coupling of subsequent amino acids was performed with 3 to 5 fold excess of 1-hydroxy-benzotriazole (HOBt) and diisopropyl-carbodiimide (DIC). Each coupling was done for 3 hours, followed by Kaiser test to confirm the completeness of reaction. Fmoc group was removed in each step by treating the resins was solution of 20% piperidine in DMF. Kaiser tests were also performed after each deprotection step. Boc protected amino acids were used only for the last N-terminal amino acids to eliminate the necessity of last Fmoc deprotection step. Cleavage of the peptides were done by treating the resins with trifluoroacetic acid – water – triisopropylsilane (95: 2.5: 2.5) cocktail for 3 hours. The obtained TFA-peptide solution was cooled and evaporated under nitrogen flow until it became thick viscous oily liquid. Ice cold

ether was added to the oily liquid to precipitate the peptide. The peptides are then freeze dried and stored in −20° C freeze until further use.

In case of CNGRC (C1-C5) peptide, the synthesis scheme started with Fmoc-L-Cys(Trt)-2-chlorotrityl resin and cyclization was achieved by the formation of 1-5 disulfide bond using iodine in dimethylformamide (DMF) at 0° C for 2 hours (140). The other steps were same as described above.

3.3.2 Synthesis of FITC conjugated peptides. The synthesis was started with Fmoc-Lys(ivDde)-Wang resin to maintain simple solid phase synthesis method and easily place the FITC probe towards C-terminal side (141) (Figure 3.5). A spacer (e.g. 6-aminohexanoic acid/ Ahx) was added between the peptide sequence and the lysine residue at the C-terminal using same DIC/HOBt coupling method. After coupling the last amino acid (Boc protected) at the N-terminal, the resins were treated with 2% hydrazine to remove the ivDde group from the C-terminal lysine. Then FITC was coupled to the exposed primary –NH2 group on the side chain of lysine (142). Finally, the FITC labelled peptides were cleaved from the resin using trifluoroacetic acid – water – triisopropylsilane (95 : 2.5 : 2.5) cocktail. After synthesis, the conjugated peptides were freeze-dried and stored in −20° C freeze until further use.

3.3.3 HPLC analysis of the synthesized molecules. The purity of the synthesized molecules was determined using high pressure liquid chromatography (HPLC) (Agilent 1100). The column used was Agilent Zorbax C18, 5 μ, 4.6×150 mm, and the wavelengths used for detection were 210, 254 and 280 nm. The samples were eluted with a mobile phase consisting of water with 0.1% TFA (A) and acetonitrile with 0.1% TFA (B) using a linear gradient from 10 to

90% B over 30 to 35 minutes, at 1.0 mL/min flow rate. The purified peptides were freeze dried and stored at -20° C.

3.3.4 Mass spectrometry analysis of the synthesized molecules. Formation of the synthesized molecules were confirmed by Electron Spray Ionization Mass Spectrometry (ESI-MS, API 3000 Mass Spectrometer). Samples were prepared in water/methanol or water/acetonitrile mixtures and were infused at 10μL/min.

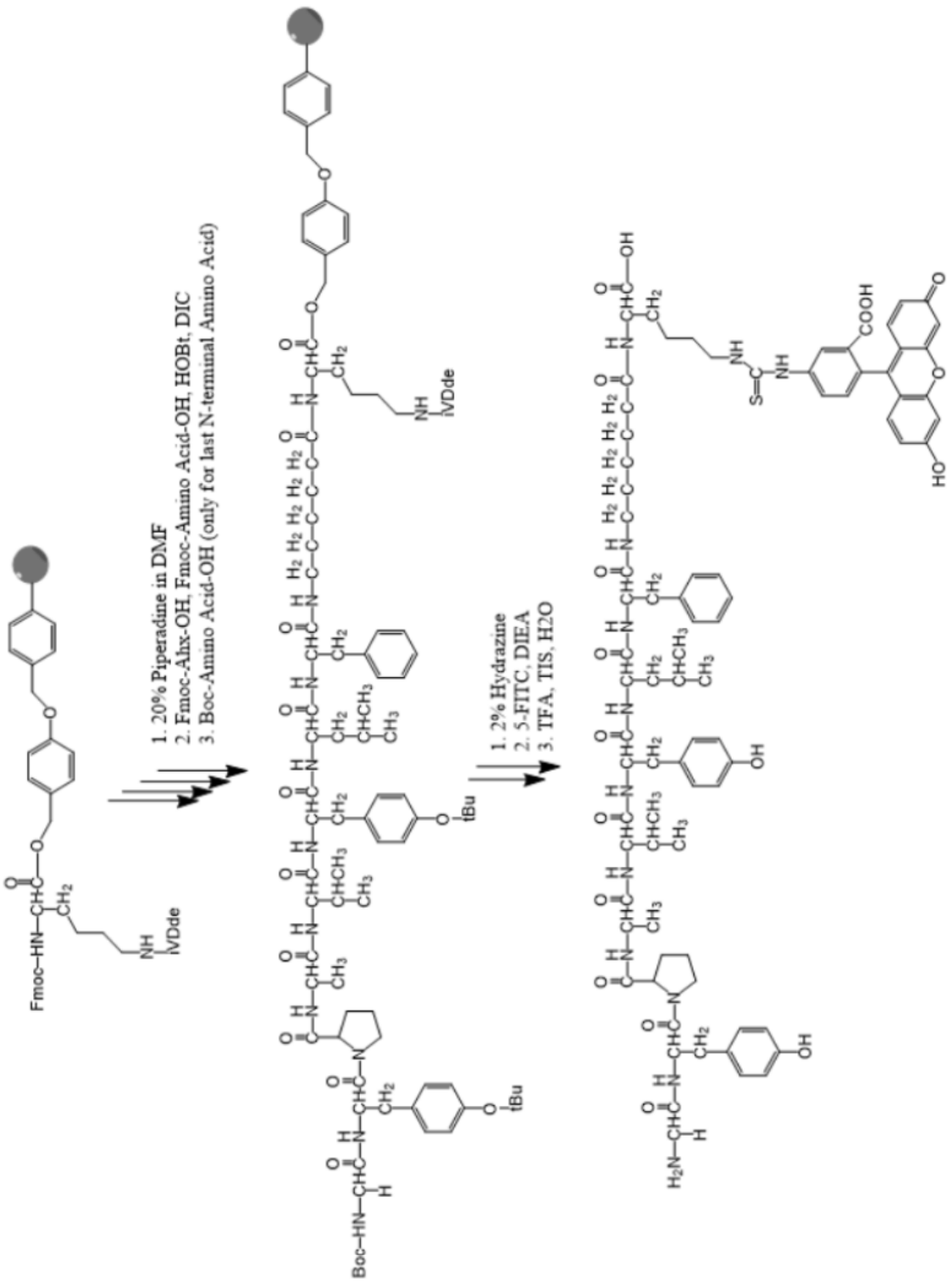

Figure 3.5: Synthesis scheme for the FITC conjugated peptides

3.4 Results and Discussion

All the peptides were successfully synthesized using standard solid phase synthesis method. These peptides were used for in vitro binding studies with CD13 protein by enzymatic activity inhibition studies. The fluorescent dye, FITC, was successfully conjugated with the peptides and used incell surface binding and confocal microscopy studies. The physicochemical properties of the peptides are shown in figures 3.6, 3.11, 3.16, 3.21, 3.26, 3.31, and 3.34.

All the molecules were characterized by ESI MS. The MS results showed the desired molecular weight of the synthesized molecules. The peptides were observed as singly charged species and the peptides with FITC were observed as doubly charged species. The MS confirmed the formation of all the molecules as shown in figures 3.7, 3.8, 3.12, 3.13, 3.17, 3.18, 3.22, 3.23, 3.27, 3.28, 3.32, and 3.35.

Reverse phase HPLC of the molecules was performed at 210 nm, 254 nm and/or 280 nm wavelength. Samples were eluted and collected to identify and confirm the molecular weight by MS. The desired peaks were finally separated and purified using a semi-preparative column. The purities of the synthesized molecules were in the range of 93% to 98% (Table 3.1). The HPLC chromatograms of the purified molecules are shown in figures 3.9, 3.10, 3.14, 3.15, 3.19, 3.20, 3.24, 3.25, 3.29, 3.30, 3.33, and 3.36.

Calculated and observed molecular weights along with the purity of the synthesized molecules are shown in table 3.1.

Table 3.1

Synthesized molecule sequences with MS and HPLC characterization data

Molecule	Calculated MS $(M+H^+)$ Ion	Observed MS $(M+H^+/2H)^+$ Ion	HPLC Purity (%)
PEP20 (GYPAY)	570.25	570.3	97.3
PEP20-FITC	1200.46	601.0	97.7
PEP24 (GFPAY)	554.25	554.3	97.4
PEP24-FITC	1184.47	592.9	97.8
PEP173 (GYPAVYLF)	929.47	929.8	93.0
PEP173-FITC	1569.68	780.6	96.2
NGR-2C [CNGRC(1-5)]	550.18	550.2	95.0
NGR-2C-FITC	1180.39	590.9	96.6
GARAG	431.23	431.3	95.0
GARAG-FITC	1061.44	531.4	96.4
PEP293 (GYPAYVEF)	945.42	945.7	98.0
PEP308 (GFPAVYEF)	929.43	929.7	98.0

PEP20

Analyzed sequence

G-Y-P-A-Y

Sequence length	5
Hydrophobicity	8.50
GRAVY	-0.56
MW average	569.6203 g/mol
MW monoisotopic	569.2486
Theoretical pI	5.9

Figure 3.6: Physicochemical properties of PEP20

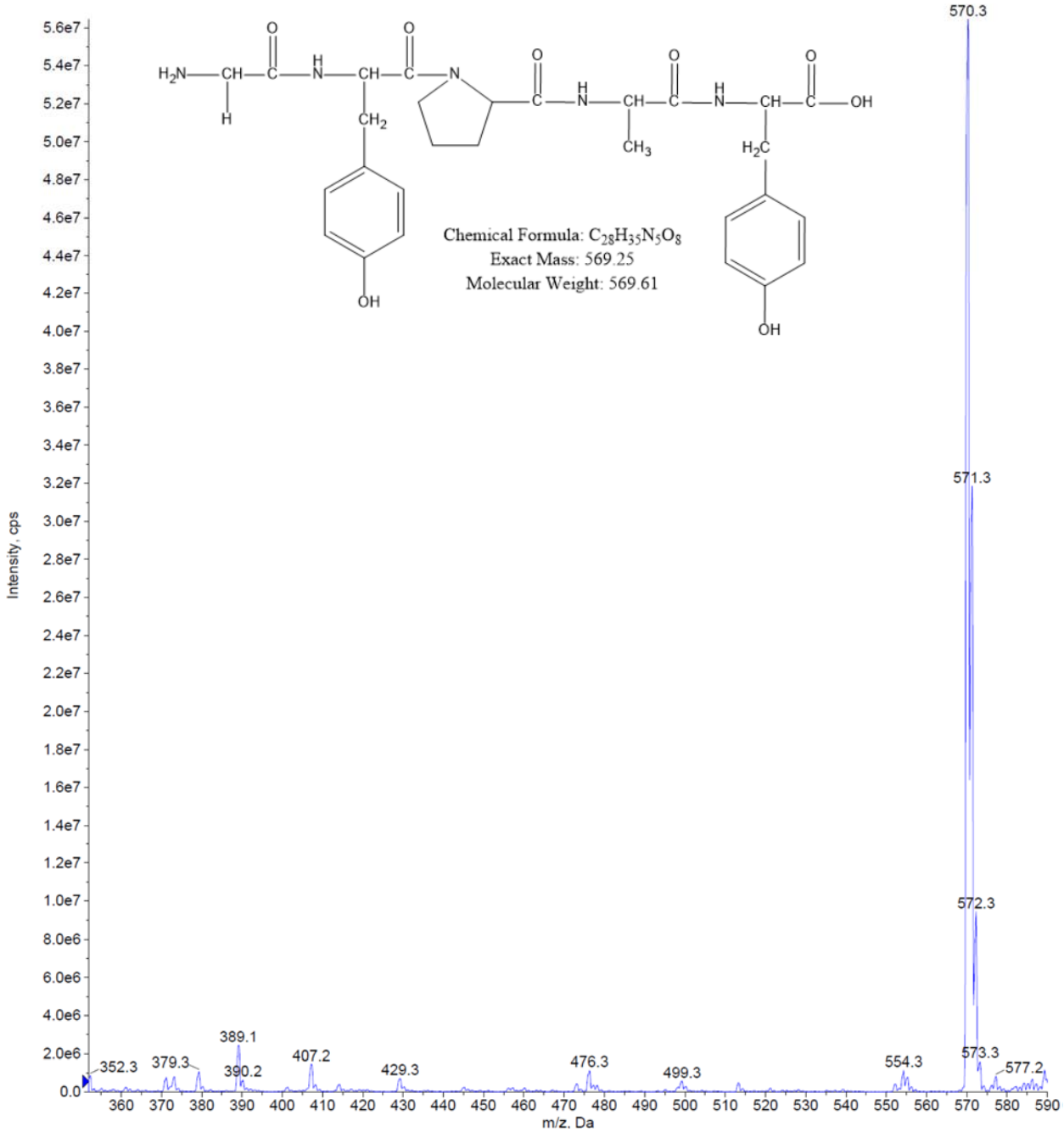

Figure 3.7: MS spectrum of PEP20

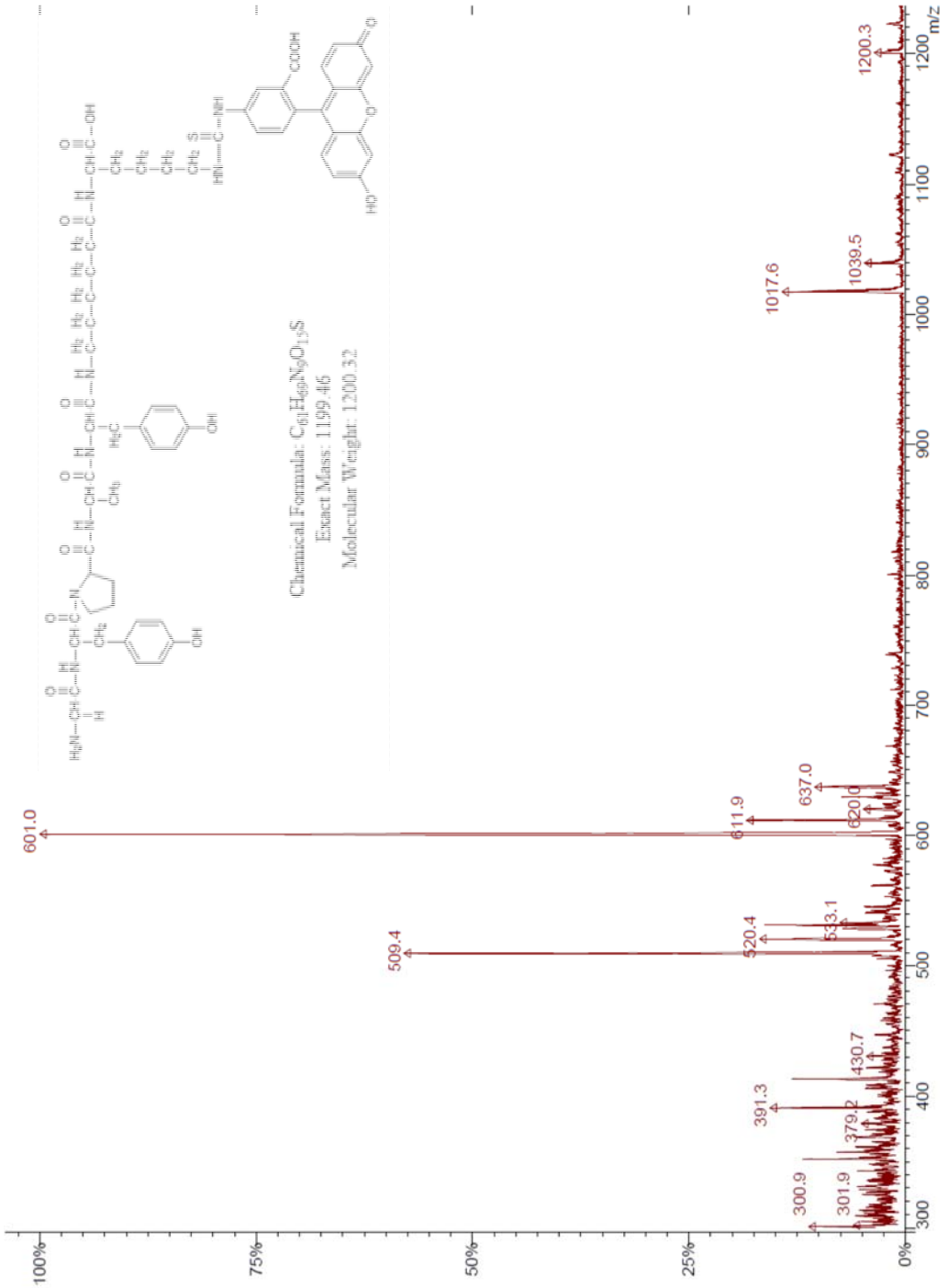

Figure 3.8: MS spectrum of PEP20-FITC

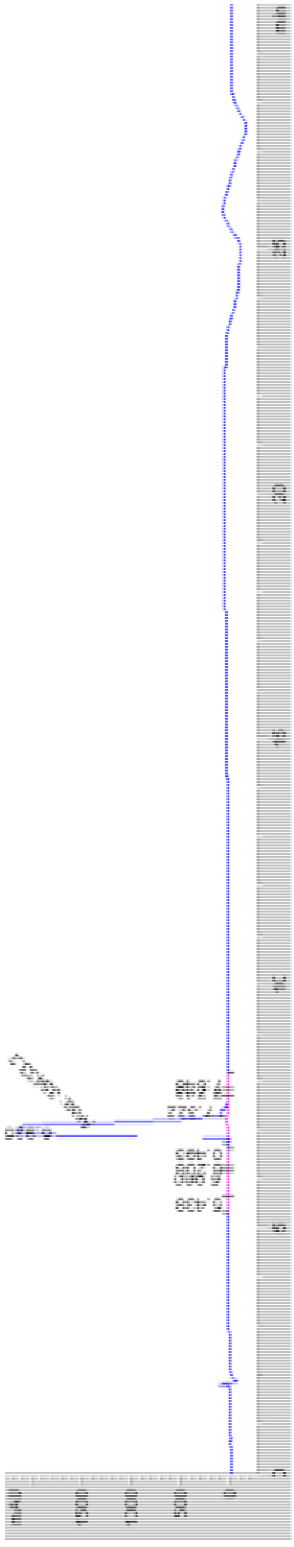

Figure 3.9: HPLC chromatogram of PEP20

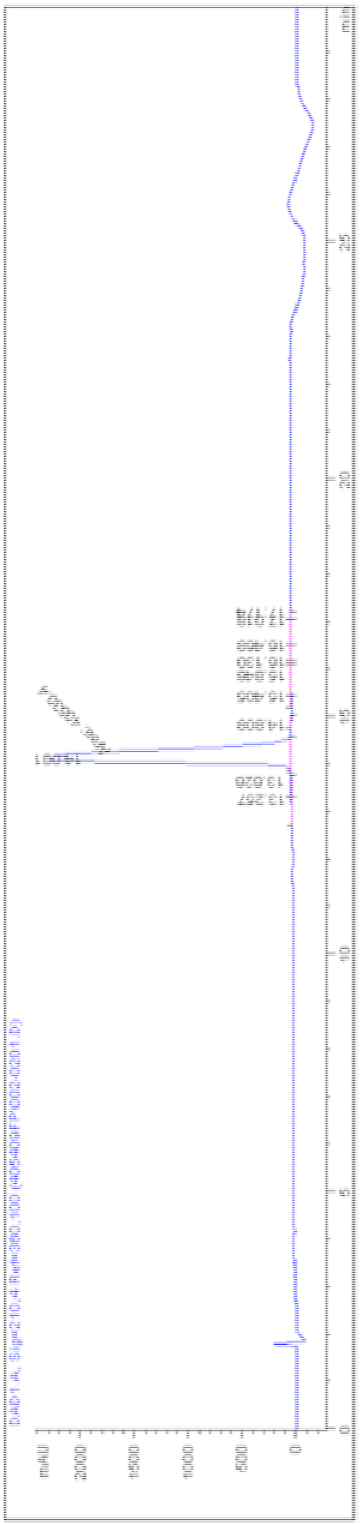

Figure 3.10: HPLC chromatogram of PEP20-FITC

PEP24

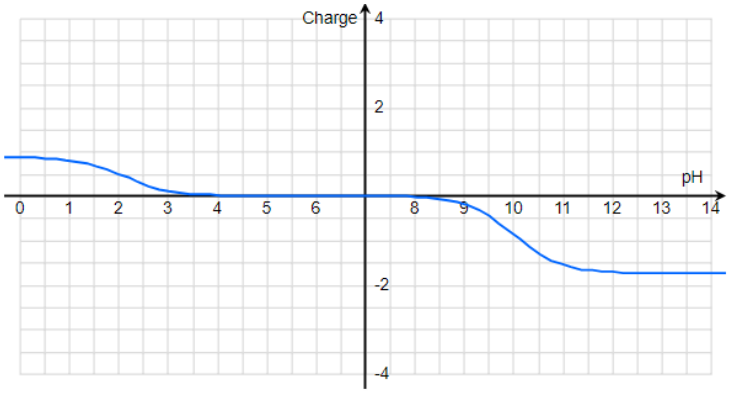

Analyzed sequence

G-F-P-A-Y

Sequence length	5
Hydrophobicity	13.81
GRAVY	0.26
MW average	553.6203 g/mol
MW monoisotopic	553.2537
Theoretical pI	5.9

Figure 3.11: Physicochemical properties of PEP24

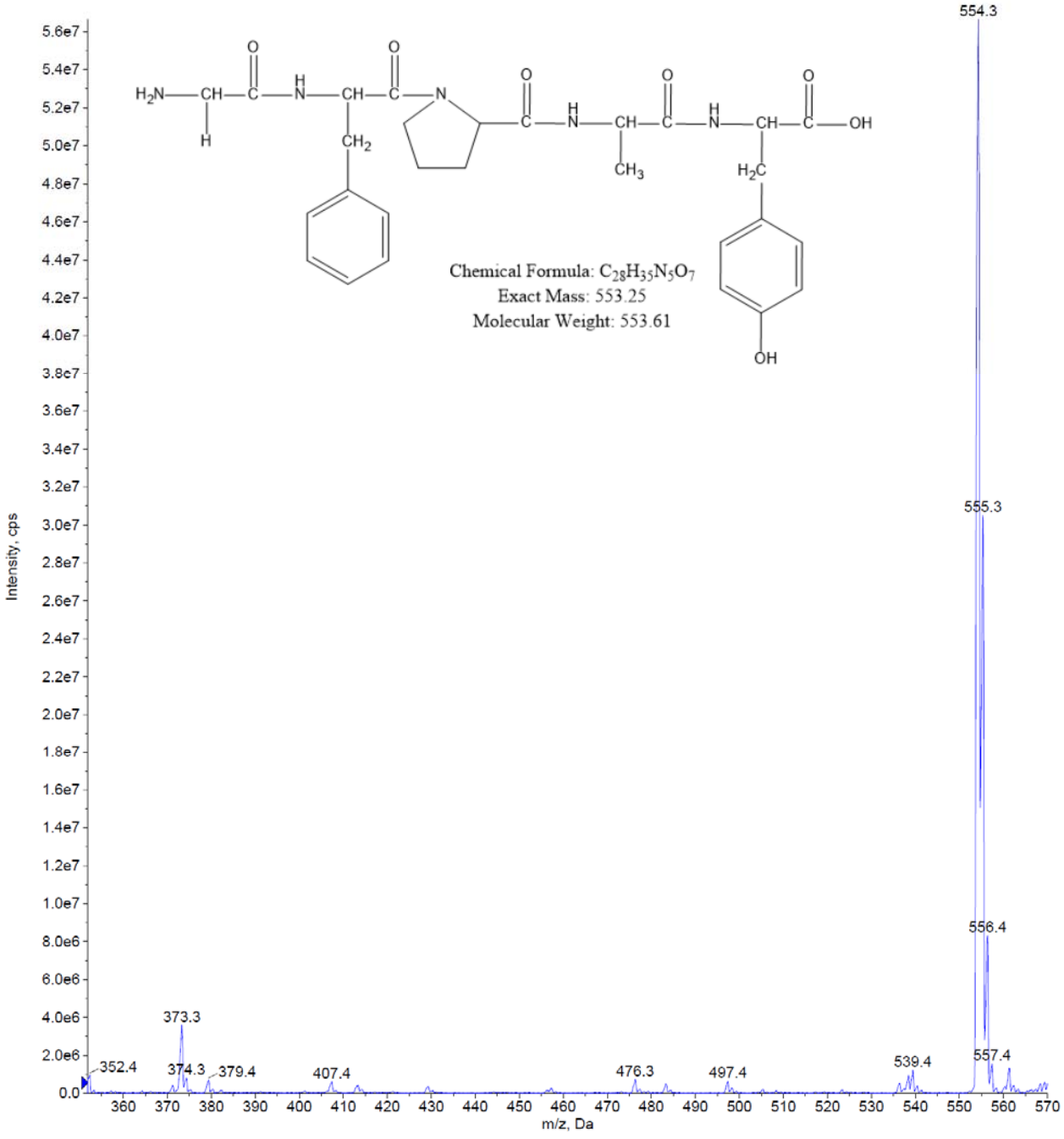

Figure 3.12: MS spectrum of PEP24

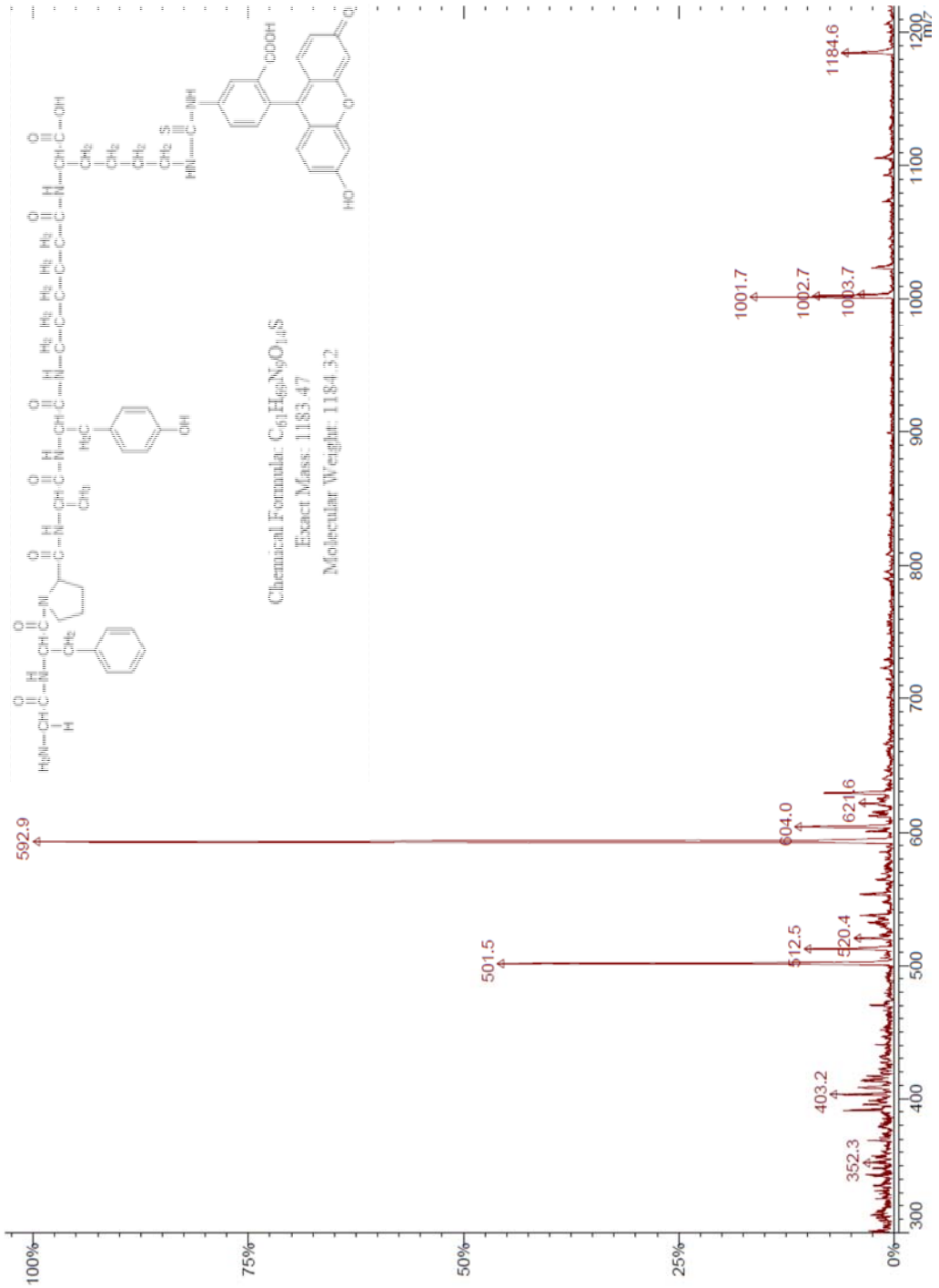

Figure 3.13: MS spectrum of PEP24-FITC

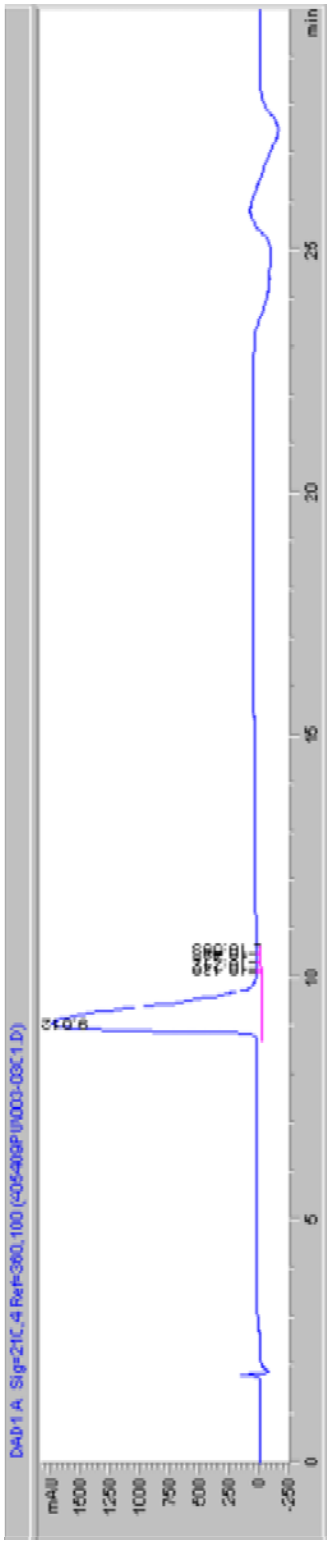

Figure 3.14: HPLC chromatogram of PEP24

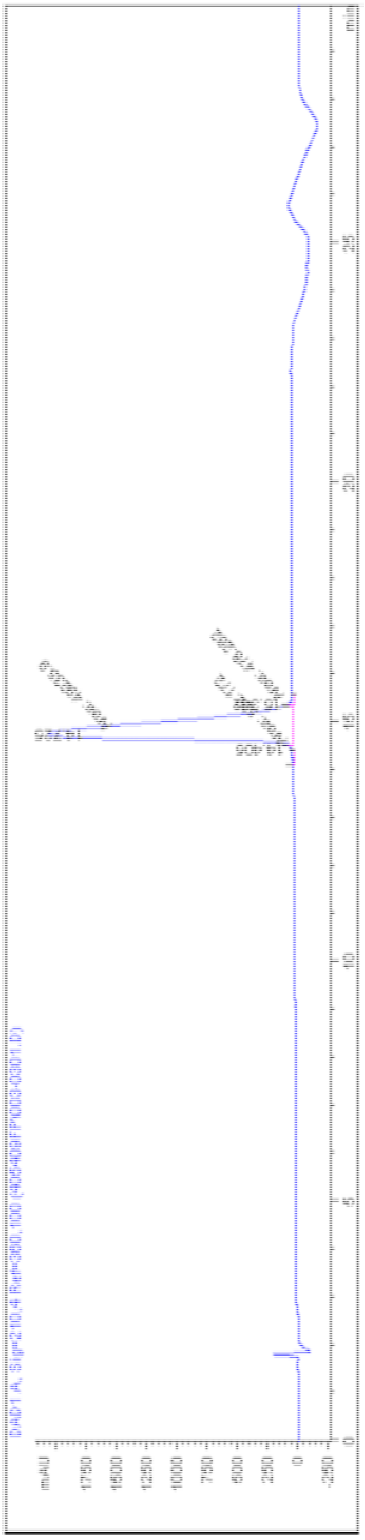

Figure 3.15: HPLC chromatogram of PEP24-FITC

PEP173

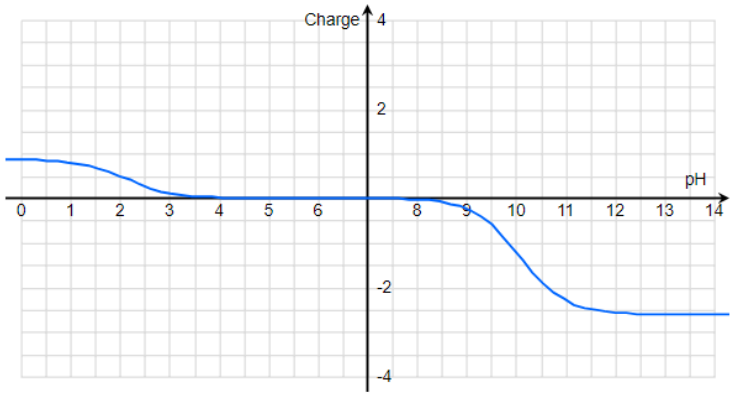

Analyzed sequence

G-Y-P-A-V-Y-L-F

Sequence length	8
Hydrophobicity	33.49
GRAVY	1.00
MW average	929.0933 g/mol
MW monoisotopic	928.4695
Theoretical pI	5.9

Figure 3.16: Physicochemical properties of PEP173

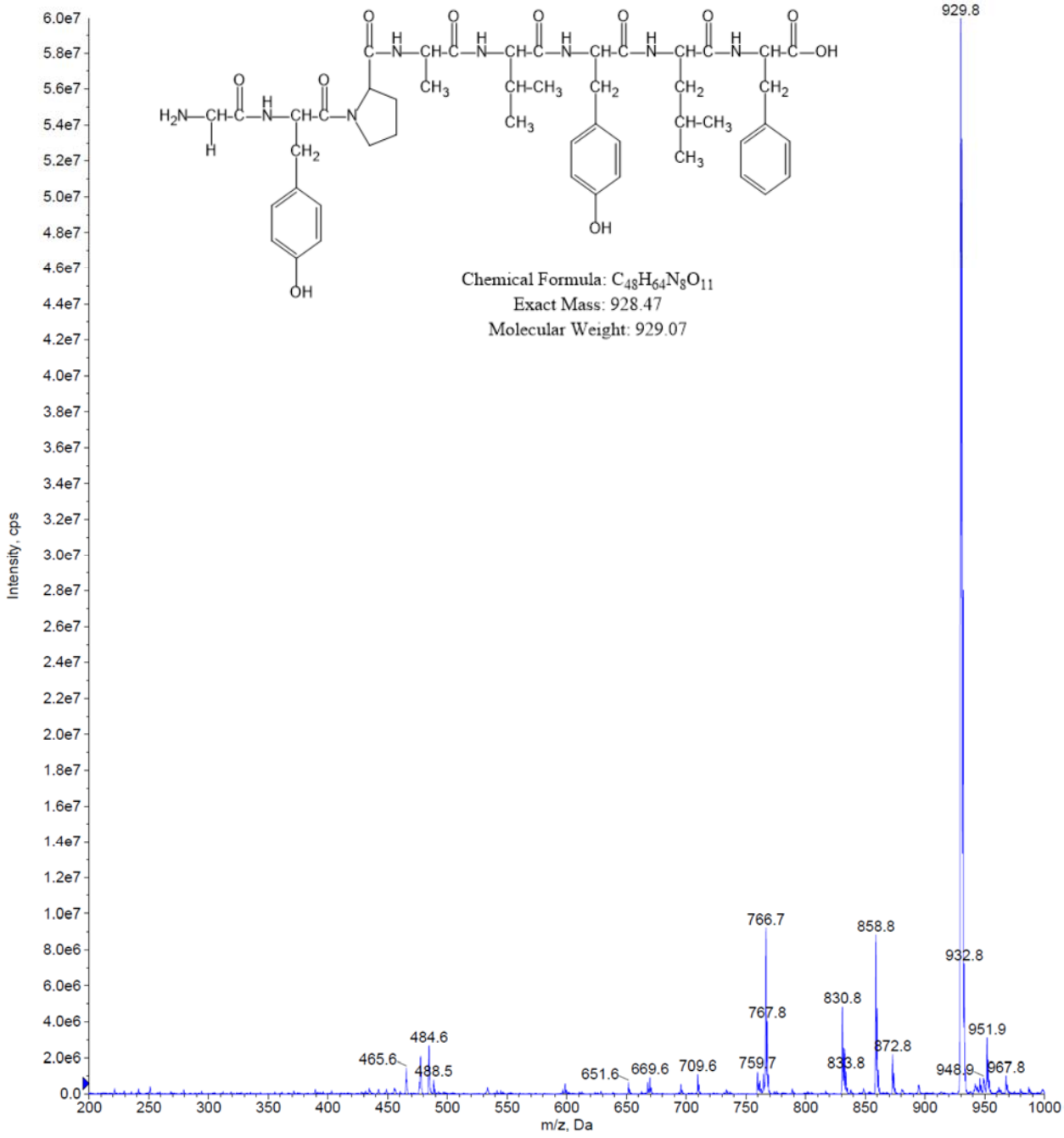

Figure 3.17: MS spectrum of PEP173

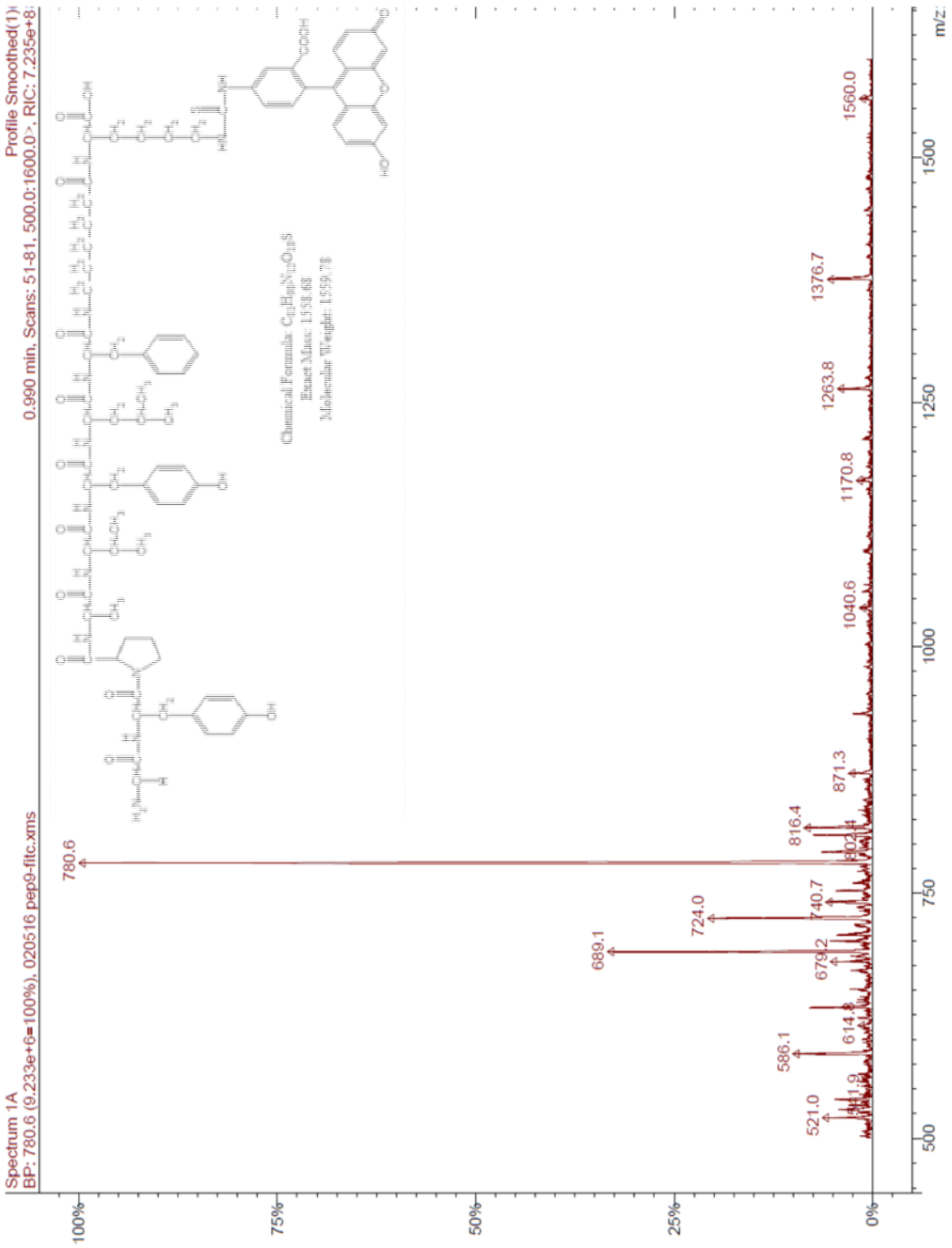

Figure 3.18: MS spectrum of PEP173-FITC

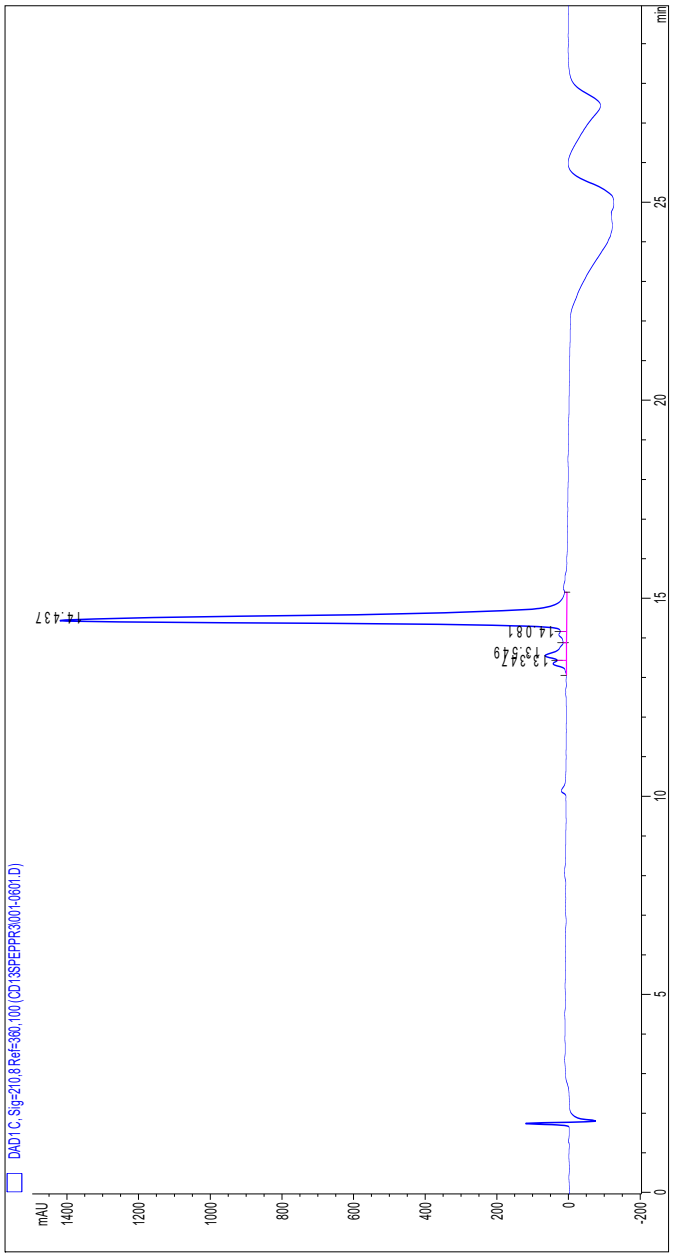

Figure 3.19: HPLC chromatogram of PEP173

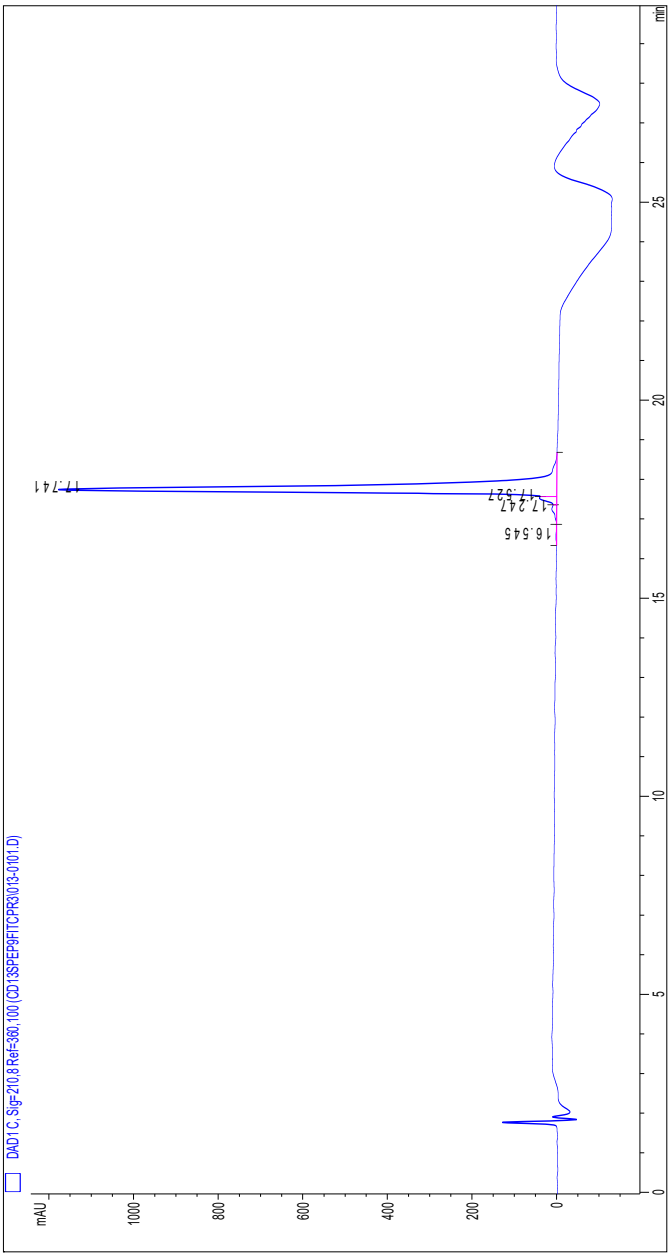

Figure 3.20: HPLC chromatogram of PEP173-FITC

NGR-2C

Sequence: CNGRC (C1-C5)

MW: 549.63

Theoretical PI: 8.23

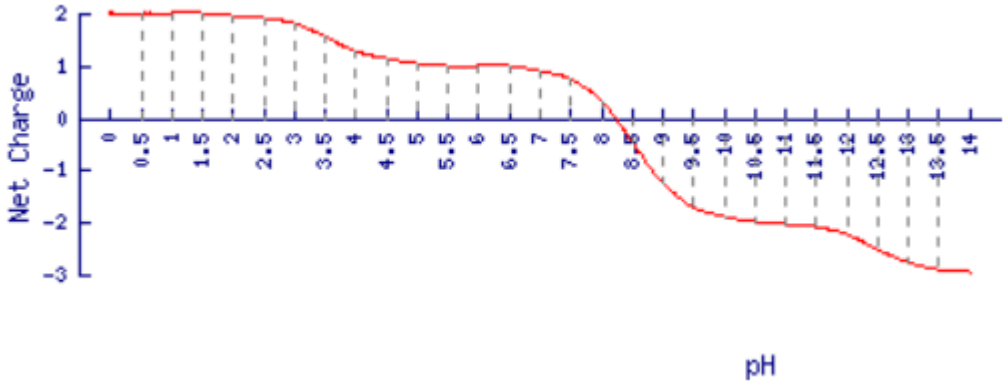

Figure 3.21: Physicochemical properties of NGR-2C

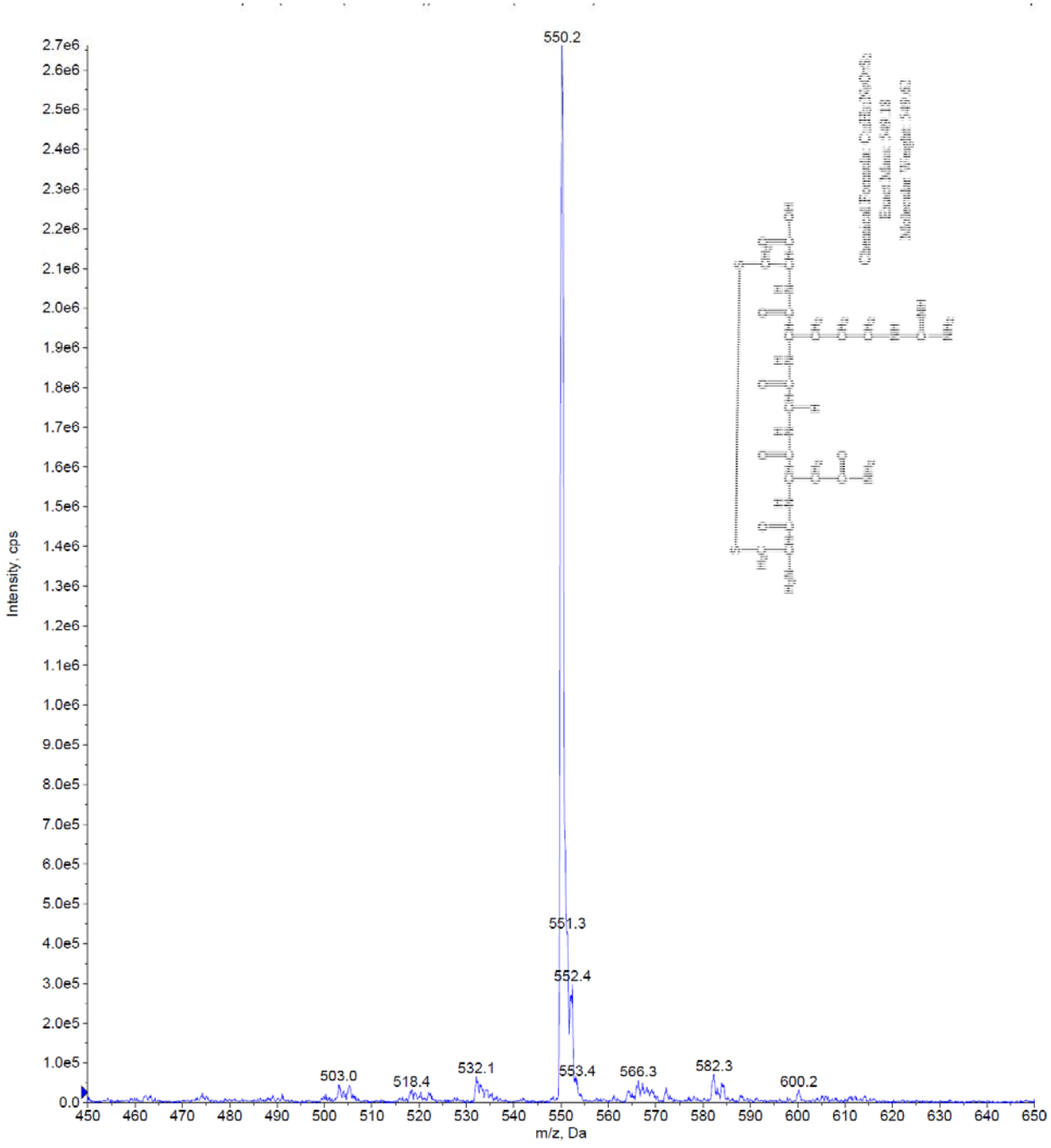

Figure 3.22: MS spectrum of NGR-2C

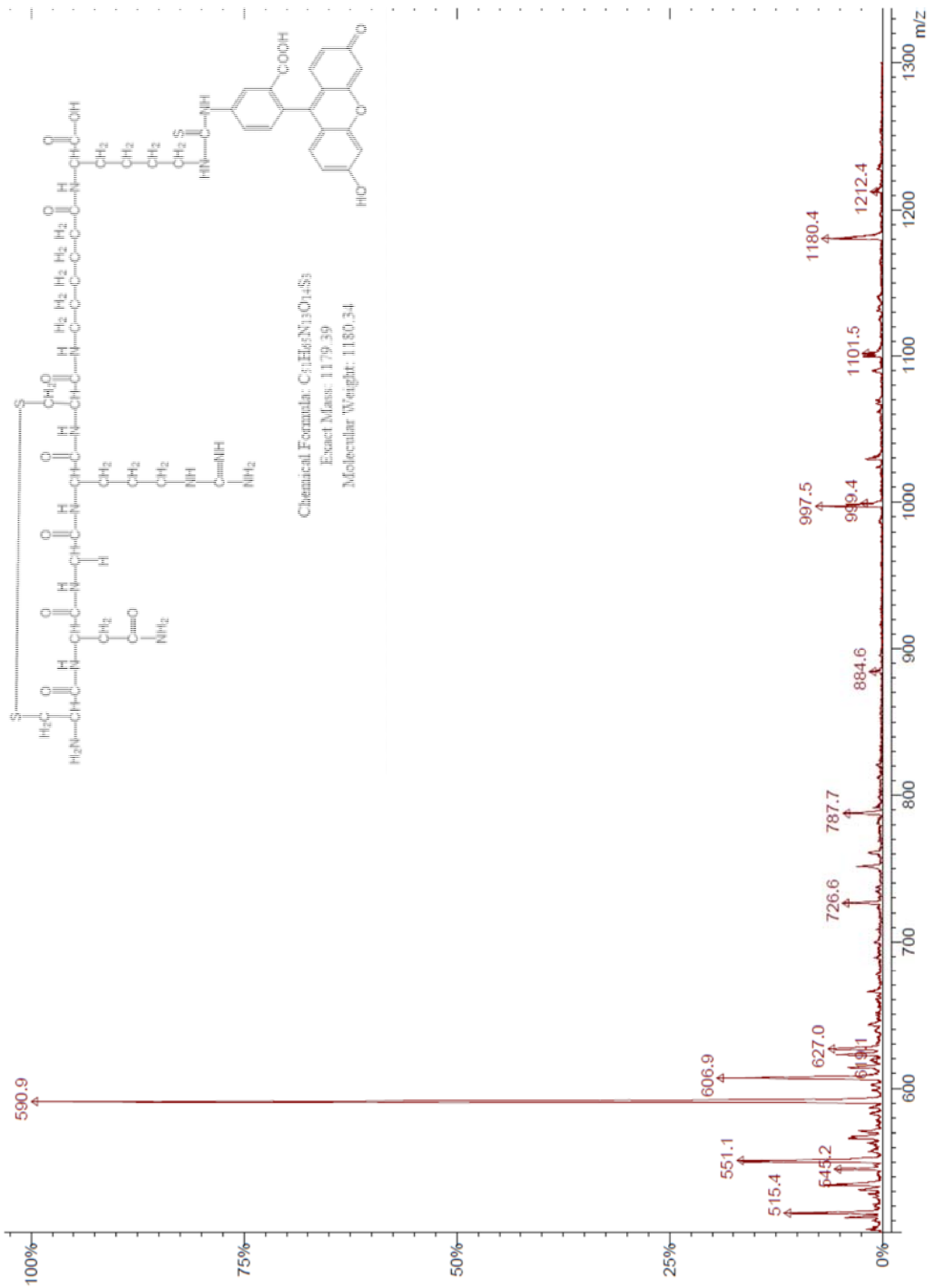

Figure 3.23: MS spectrum of NGR-2C-FITC

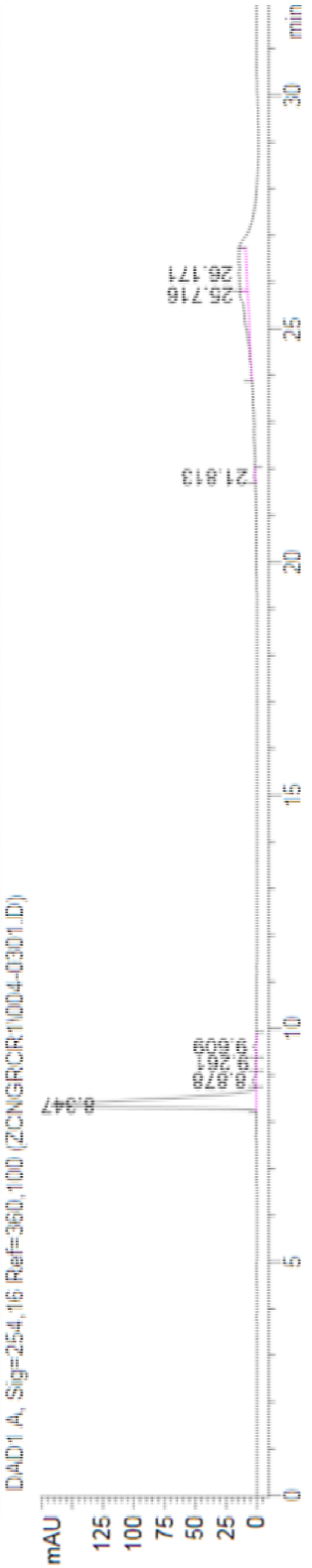

Figure 3.24: HPLC chromatogram of NGR-2C

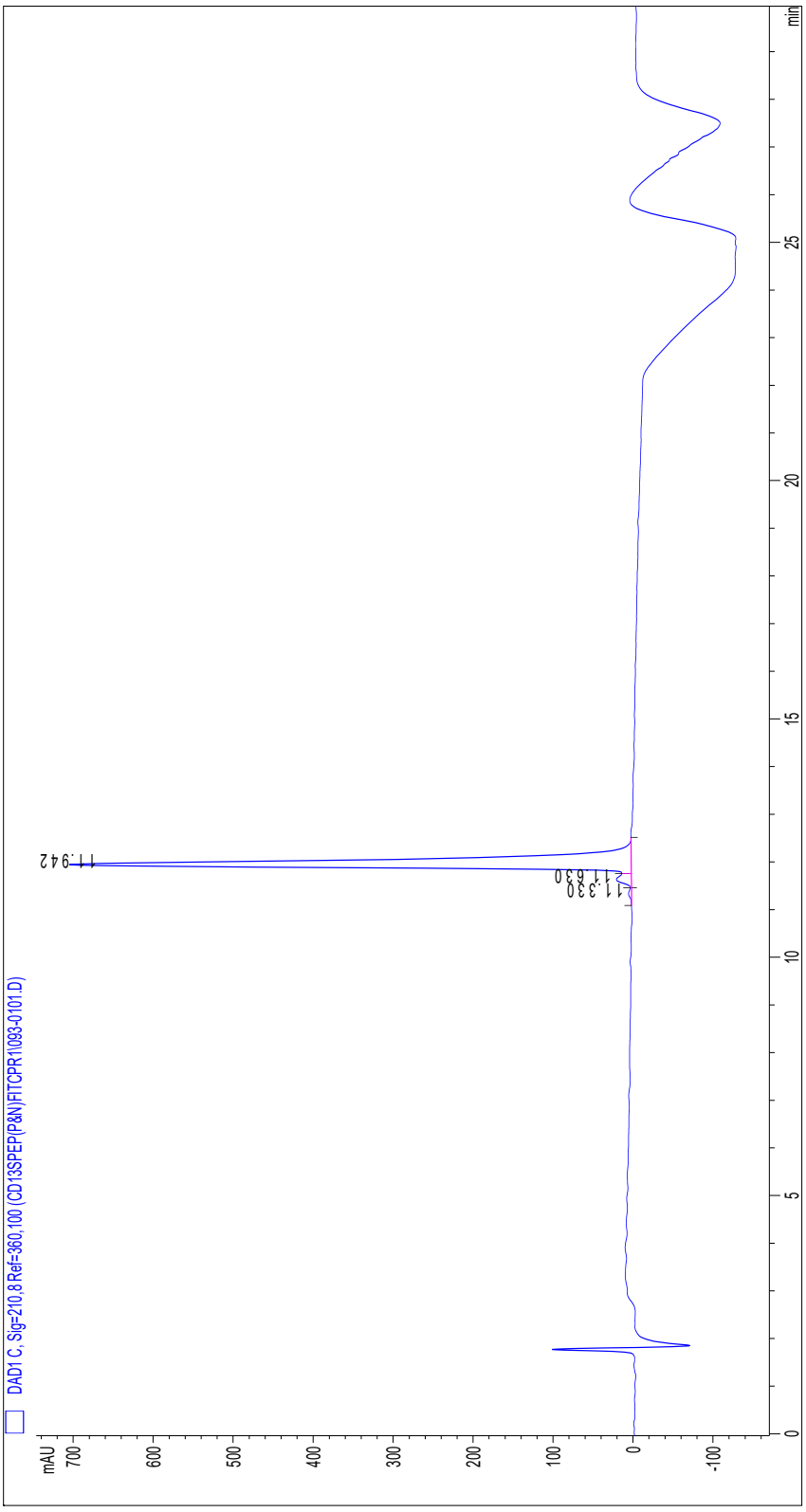

Figure 3.25: HPLC chromatogram of NGR-2C-FITC

GARAG

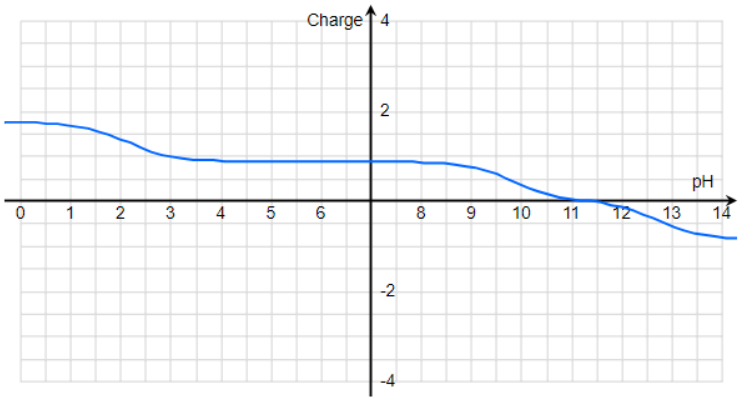

Analyzed sequence

G-A-R-A-G

Sequence length	5
Hydrophobicity	2.25
GRAVY	-0.34
MW average	430.4663 g/mol
MW monoisotopic	430.2289
Theoretical pI	11.1

Figure 3.26: Physicochemical properties of GARAG

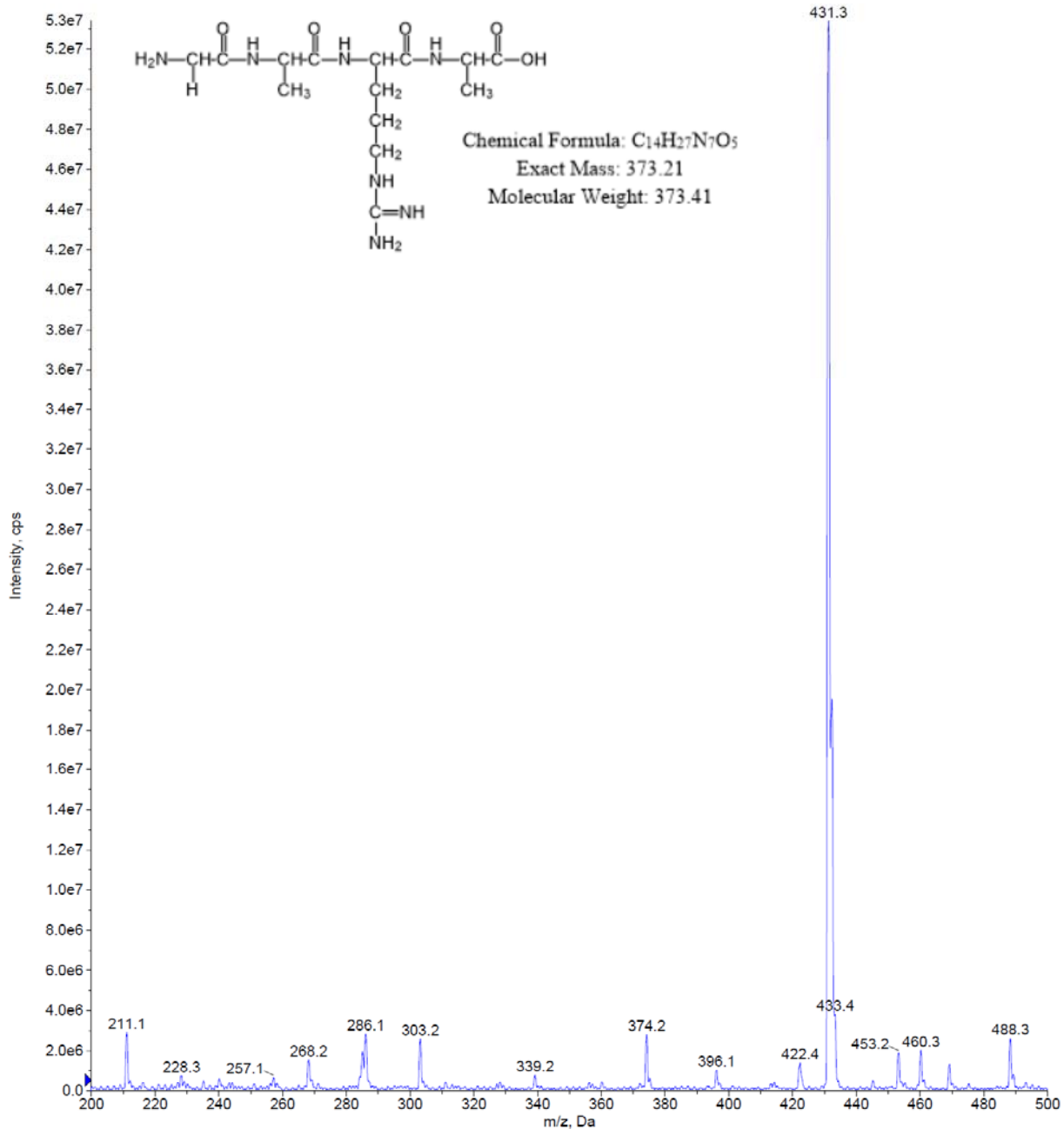

Figure 3.27: MS spectrum of GARAG

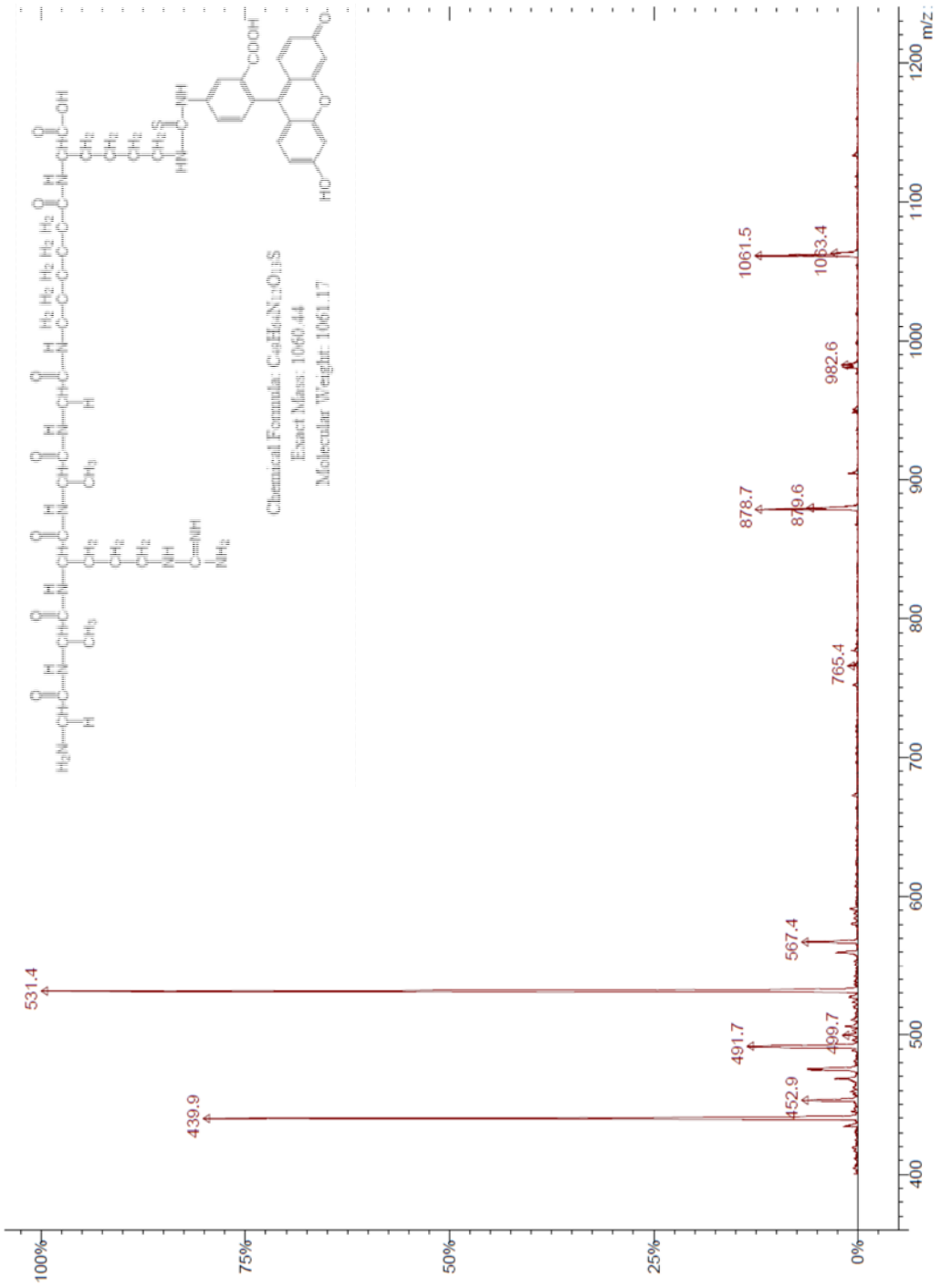

Figure 3.28: MS spectrum of GARAG-FITC

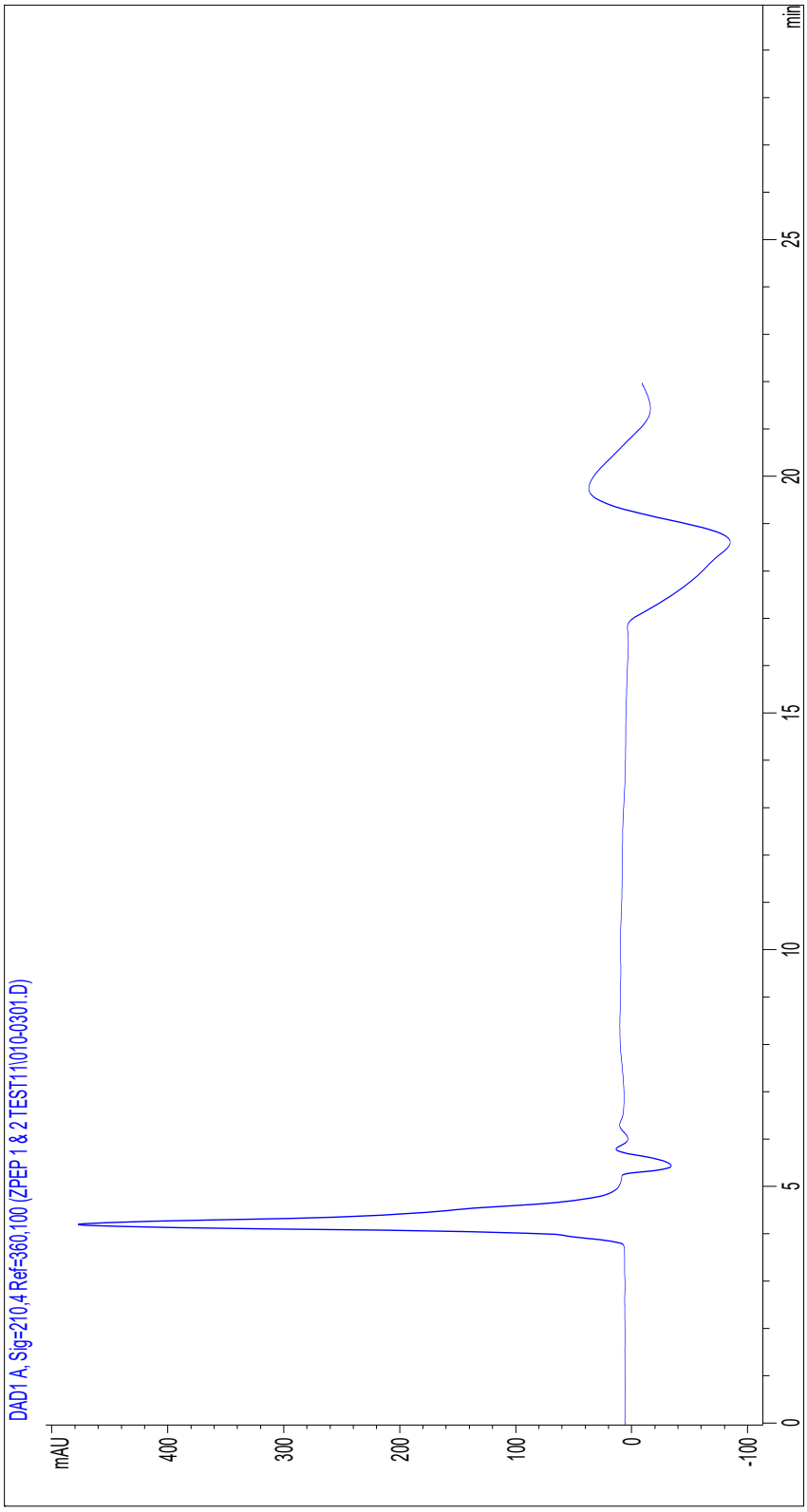

Figure 3.29: HPLC chromatogram of GARAG

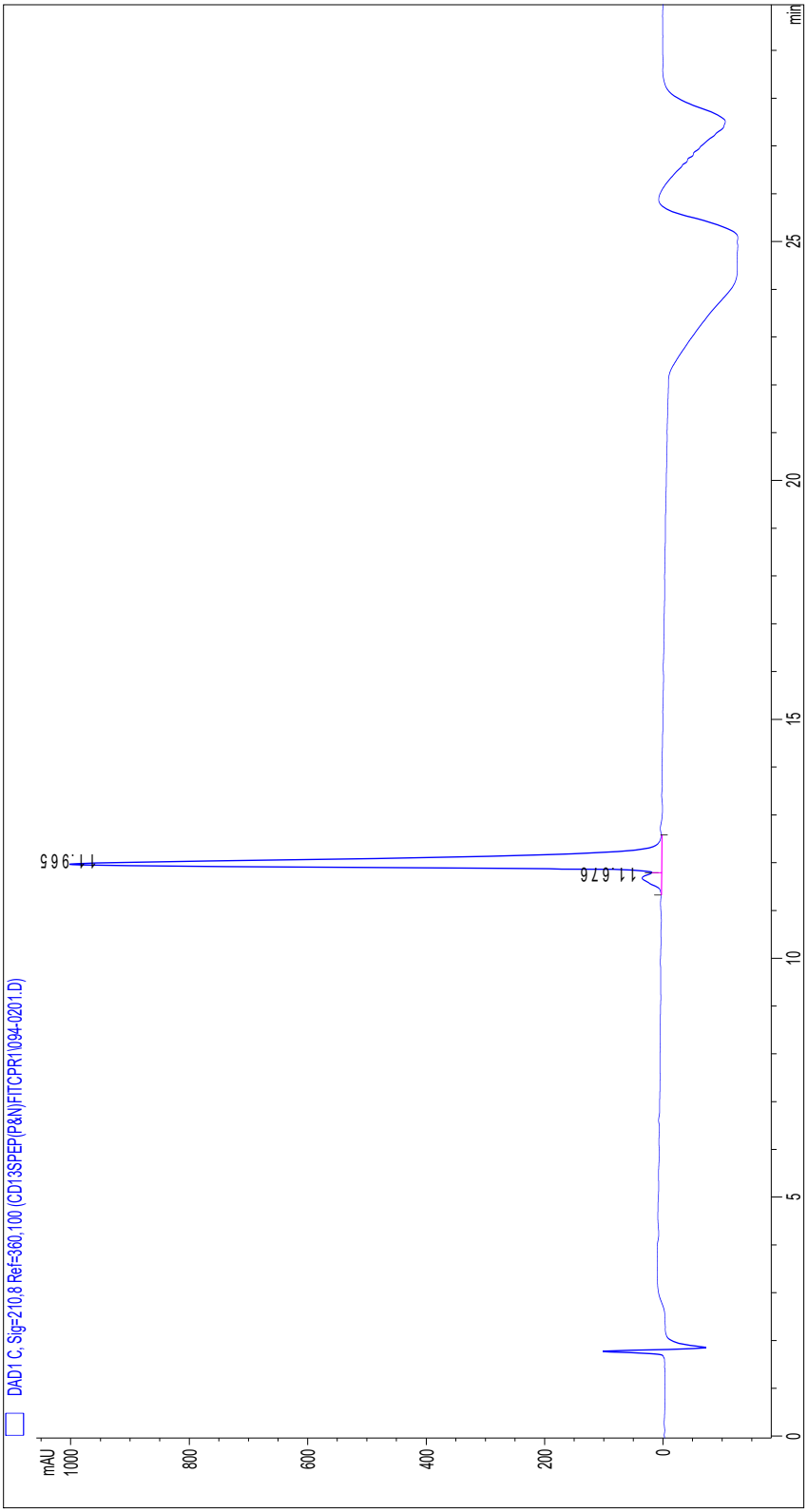

Figure 3.30: HPLC chromatogram of GARAG-FITC

PEP293

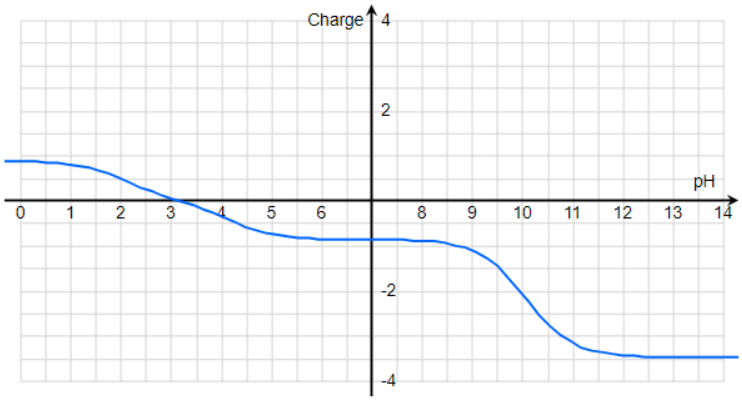

Analyzed sequence

G-Y-P-A-Y-V-E-F

Sequence length	8
Hydrophobicity	27.09
GRAVY	0.09
MW average	945.0483 g/mol
MW monoisotopic	944.4280
Theoretical pI	3.3

Figure 3.31: Physicochemical properties of PEP293

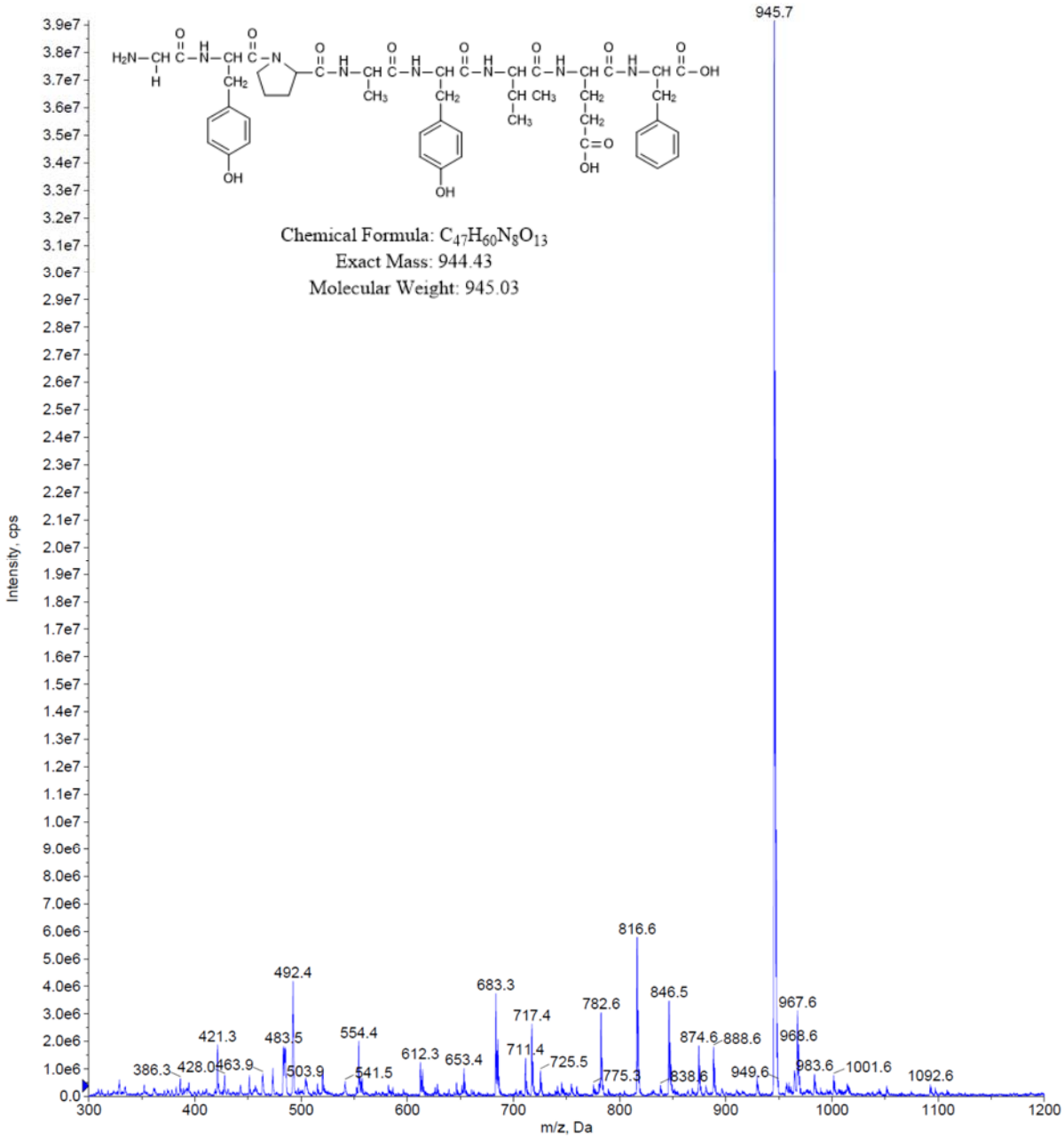

Figure 3.32: MS spectrum of PEP293

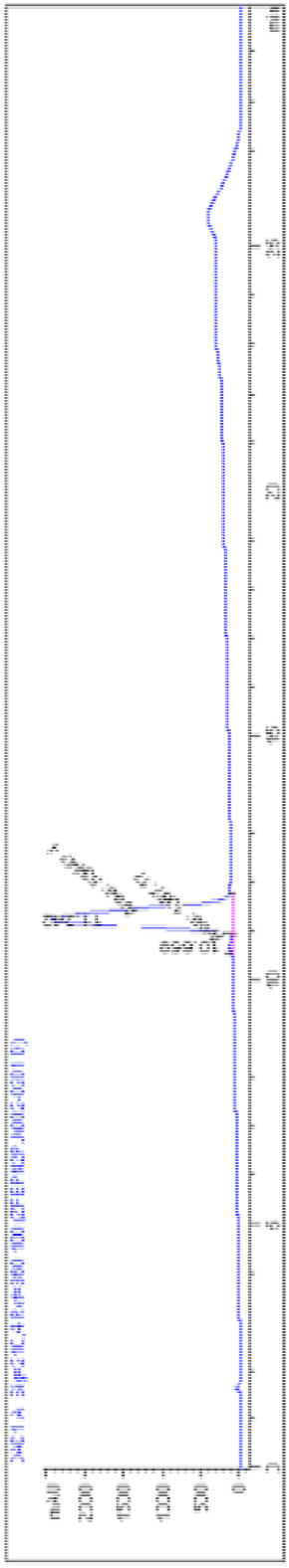

Figure 3.33: HPLC chromatogram of PEP293

PEP308

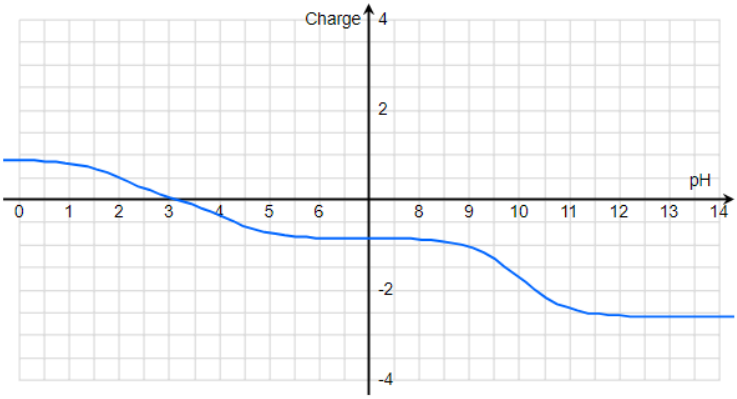

Analyzed sequence

G-F-P-A-V-Y-E-F

Sequence length	8
Hydrophobicity	31.84
GRAVY	0.60
MW average	929.0483 g/mol
MW monoisotopic	928.4331
Theoretical pI	3.3

Figure 3.34: Physicochemical properties of PEP308

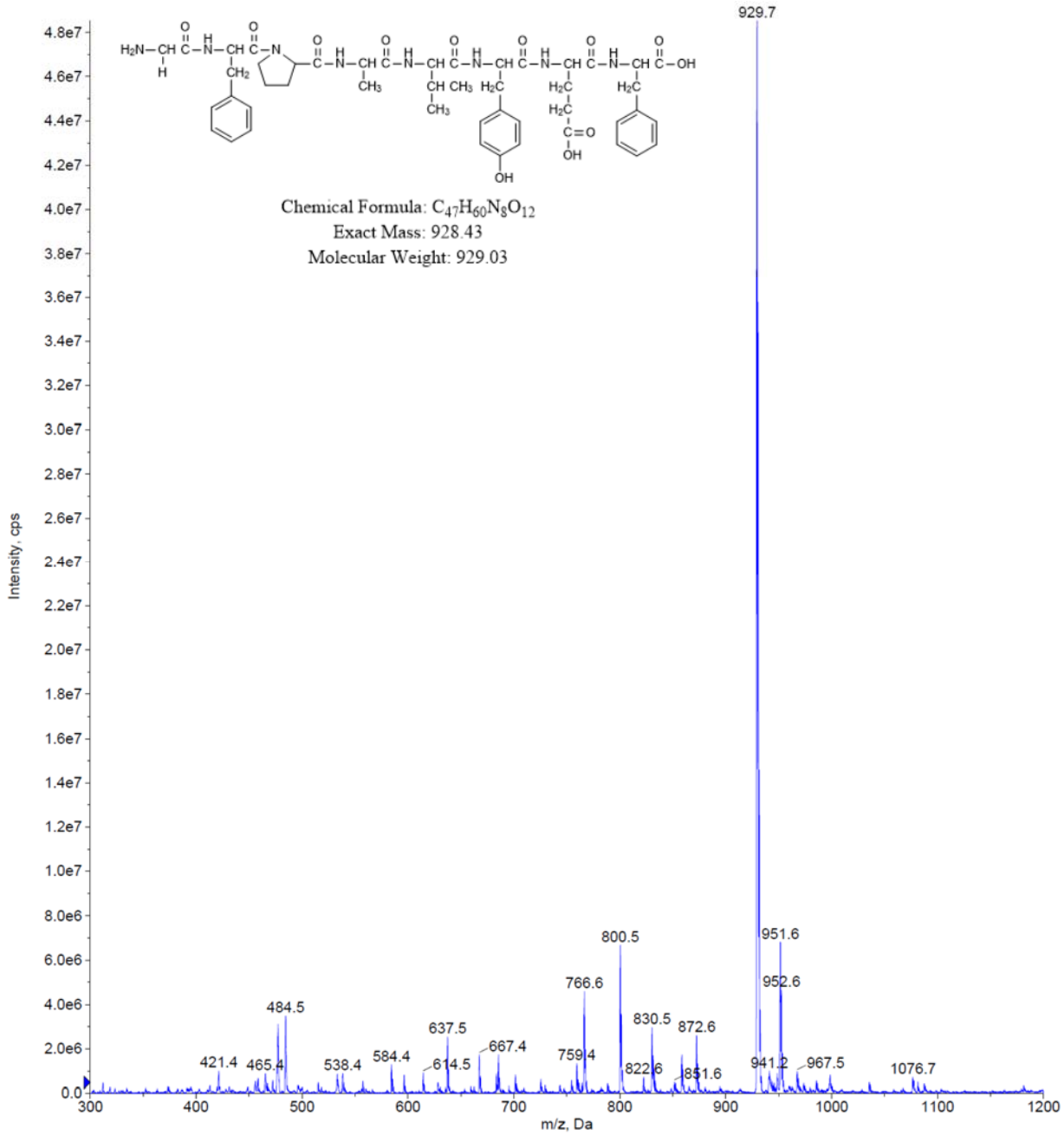

Figure 3.35: MS spectrum of PEP308

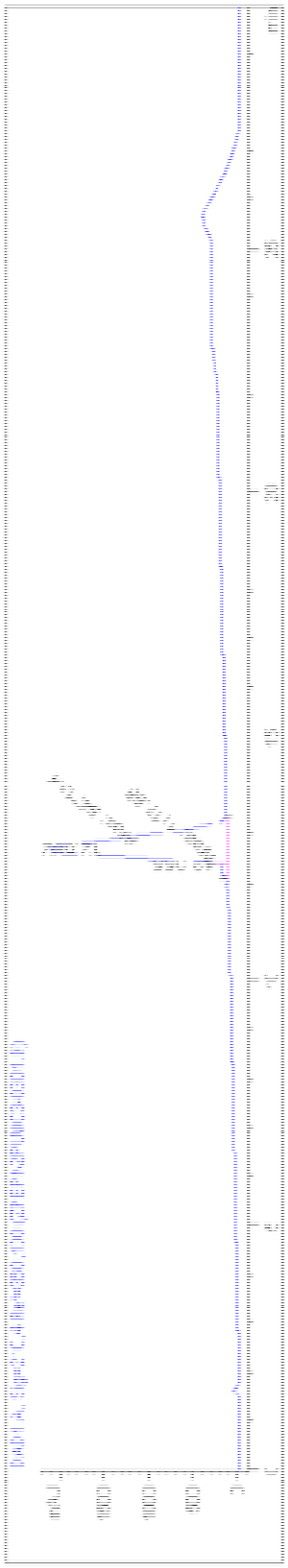

Figure 3.36: HPLC chromatogram of PEP308

Chapter 4: Characterization of CD13 Binding Properties of the Peptide Ligands

4.1 Introduction

An important concept of both theoretical studies and drug/ligand development is the quantification of ligand binding to the target receptor. The key aspects of ligand receptor interactions include binding affinity, binding specificity, binding site, target conformations, ligand efficiency, and binding thermodynamics. Every aspect of these ligand receptor interactions can be studied by different ligand binding assays. There are numerous ligand binding assays, such as labeled ligand, label free, structure based, thermodynamic, and whole cell ligand binding assays (143).

Labeled ligand binding assays use different types of probes like fluorescent, radioisotope or bioluminescent molecules attached to the ligand molecule. The major limitation of this type of assay is that the labeling of the ligand with a probe can lead to unwanted changes in binding properties of the ligand. The most widely used label free ligand binding assay, surface plasmon resonance (SPR), has low sensitivity to binding prompted conformational changes in receptor protein, and it does not generally provide any information about the binding site of the ligand. Structure based ligand binding assays like Nuclear magnetic resonance (NMR) or X-ray crystallography are typically very expensive and thus may not be used as routine binding assays. The thermodynamic binding assays, such as, Isothermal titration calorimetry (ITC), require large amount of sample. The whole cell ligand binding assays might not be suitable for relatively smaller ligand molecules like peptides (143).

The prototype target receptor of this study, CD13 (Aminopeptidase N), is an enzyme. The peptide ligand binding site overlaps with the enzymatic active site of CD13 (125, 134).

Therefore, binding of the peptide ligands at the intended binding site should inhibit the enzymatic activity of CD13 and the binding affinity can be quantified in terms of the equilibrium dissociation constant (K_i for enzyme inhibition) (125, 144-146). Importantly, this enzyme inhibition assay could also provide the information about the binding sites of the peptide ligands.

Enzymatic activity starts with the reversible binding of a substrate (S) to the free enzyme (E) to form ES complex leading to free enzyme and product (P).

$$E + S \leftrightarrow ES \rightarrow E + P$$

The rate or velocity (v) of an enzymatic reaction is measured either as the disappearance of the substrate or the formation of the product.

$$v = \frac{-d[S]}{dt} = \frac{d[P]}{dt}$$

Under steady state condition the reaction velocity (v) can be determined from the slope of a linear plot of [P] or [S] vs time.

Steady state enzyme velocity can be described as a saturable function of substrate concentration (Michaelis-Menten equation).

$$v = \frac{V_{max}[S]}{K_m + [S]}$$

V_{max} is the maximum velocity at infinite substrate concentration. K_m is the kinetic constant commonly referred to as Michaelis constant. K_m is the substrate concentration at which the reaction velocity is half of the maximum velocity.

A typical plot of reaction velocity vs substrate concentration at steady state is presented in figure 4.1.

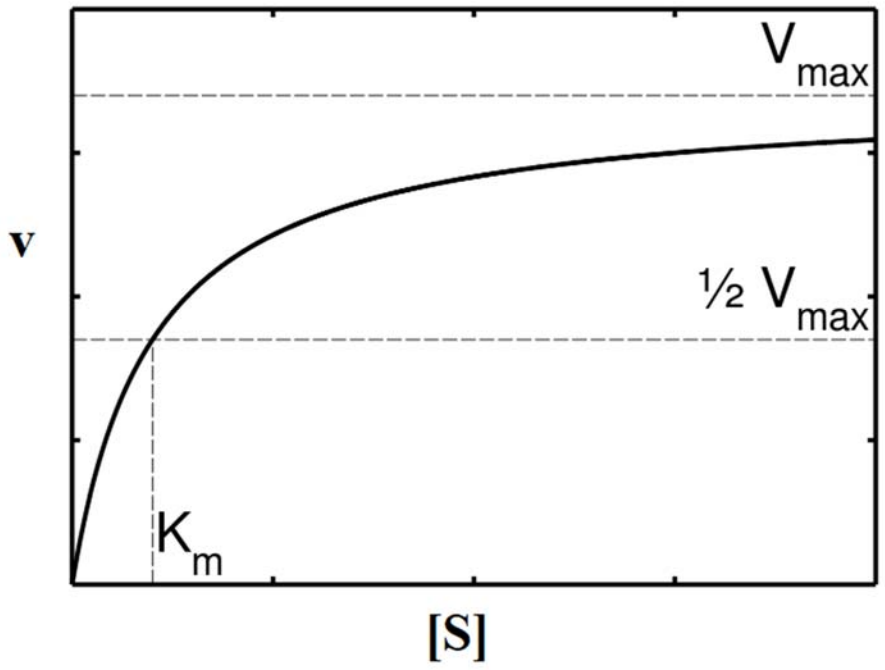

Figure 4.1: Direct fit of initial velocity vs substrate concentration to Michaelis-Menten equation

The Michaelis-Menten equation can be linearize in the following form:

$$\frac{1}{v} = \left(\frac{K_m}{V_{max}} . \frac{1}{[S]}\right) + \frac{1}{V_{max}}$$

Thus, a plot of 1/v vs 1/[S] will produce a straight line with slope of K_m/V_{max}, y-intercept of $1/V_{max}$, and x-intercept of $-1/K_M$ (figure 4.2). Such plots are referred to as double reciprocal or Lineweaver-Burk plots.

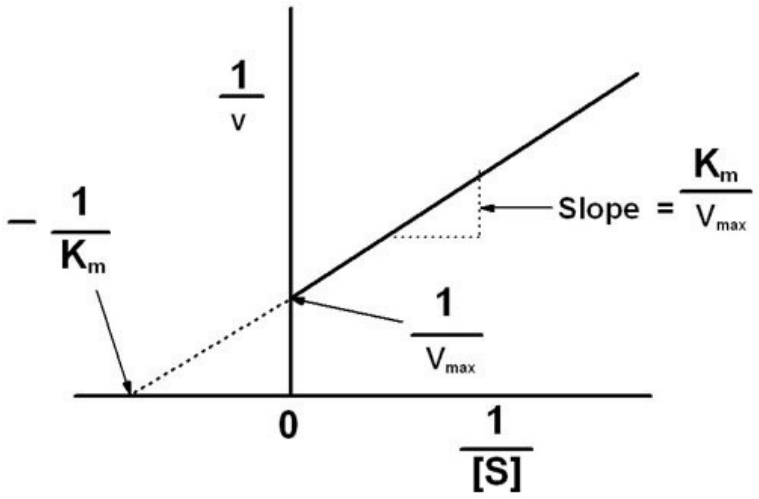

Figure 4.2: Double reciprocal plot of initial velocity vs substrate concentration

The enzymatic reaction equilibrium in presence or absence of inhibitor can be depicted as figure 4.3.

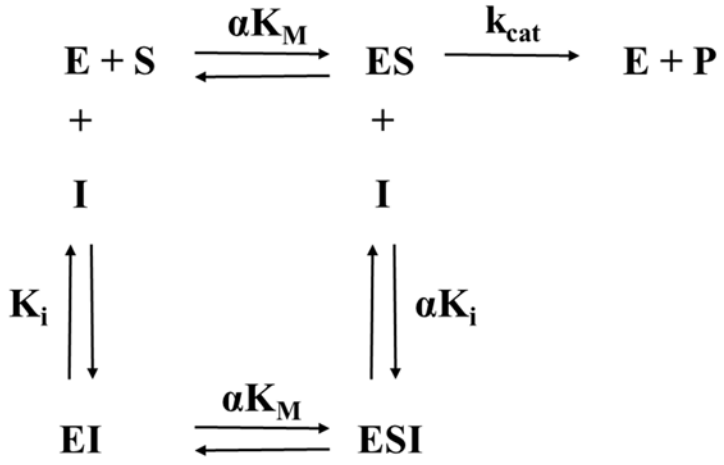

Figure 4.3: Enzymatic reaction equilibrium in presence or absence of inhibitor

I is the inhibitor, EI is the enzyme-inhibitor complex and ESI is the enzyme-substrate-inhibitor complex. k_{cat} is the first-order rate constant for the reaction product formation step. α is a constant that defines the degree to which the affinity of the enzyme (for substrate) is affected by inhibitor binding. $\alpha > 1$, if EI complex decreases the affinity of the enzyme for substrate; $\alpha = 1$, if there is no change in substrate affinity; and $\alpha < 1$, if the affinity of the enzyme for substrate is increased by the formation of EI complex. K_i is the equilibrium dissociation constant for EI complex and αK_i is the equilibrium dissociation constant for ESI complex. There are three potential modes of inhibitor interactions with enzymes: (a) competitive inhibitors, (b) noncompetitive inhibitors, (c) uncompetitive inhibitors (147) (Figure 4.4). Competitive inhibitors bind only to the free enzyme ($\alpha = \infty$). Noncompetitive inhibitors bind to both free enzyme and the enzyme-substrate complex ($\alpha > 1$, when inhibitor binds with the free enzyme with greater affinity; $\alpha = 1$, when inhibitor binds with the free enzyme and the enzyme substrate complex with equal affinity; and $\alpha < 1$, when inhibitor binds with the enzyme-substrate complex with greater affinity). Uncompetitive inhibitors bind only to the enzyme-substrate complex.

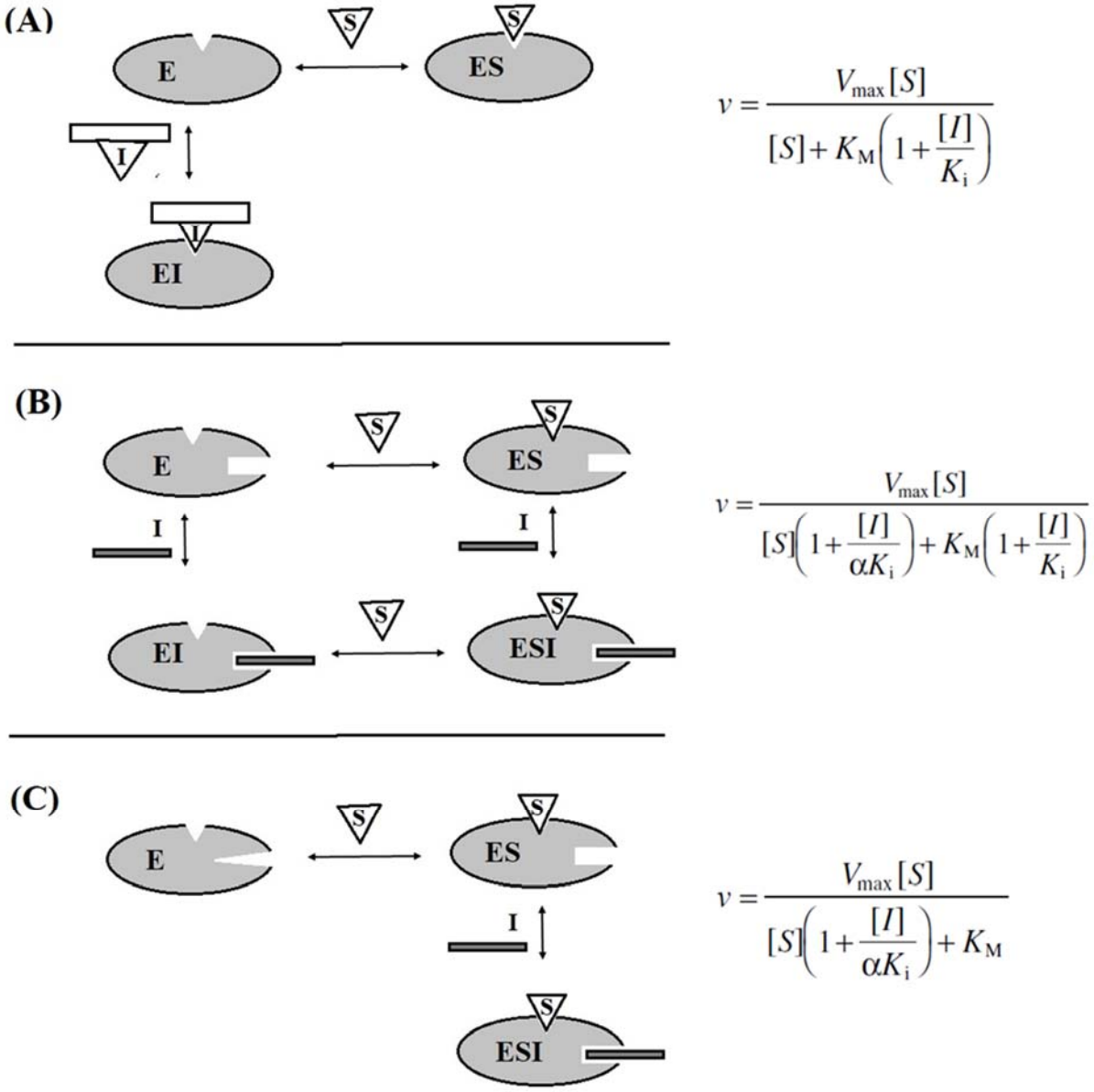

Figure 4.4: Different enzyme inhibition modalities along with equations. (A) Competitive inhibition, (B) noncompetitive inhibition; (C) uncompetitive inhibition.

The mode of inhibition of an inhibitor can be determined experimentally by enzyme kinetic measurements. Generally, the kinetic parameters V_{max} and K_m are determined in the presence of varying inhibitor concentrations. The experimental can be analyzed in the form of double reciprocal Lineweaver-Burk plots. In those plots the deviation of the obtained line from the uninhibited line ([I] = 0) indicates the inhibition mode (figure 4.5). The characteristic signatures of the different inhibition modes in the double reciprocal plots are summarized in table 4.1 (147).

Table 4.1

Characteristic signatures of the different inhibition modes in the double reciprocal plots

Inhibition mode	Diagnostic signature
Competitive	Intersecting lines that converge at y axis
Noncompetitive, $\alpha > 1$	Intersecting lines that converge to the left of y axis and above x axis
Noncompetitive, $\alpha = 1$	Intersecting lines that converge to the left of the y axis and on the x axis
Noncompetitive, $\alpha < 1$	Intersecting lines that converge to the left of the y axis and below the x axis
Uncompetitive	Parallel lines

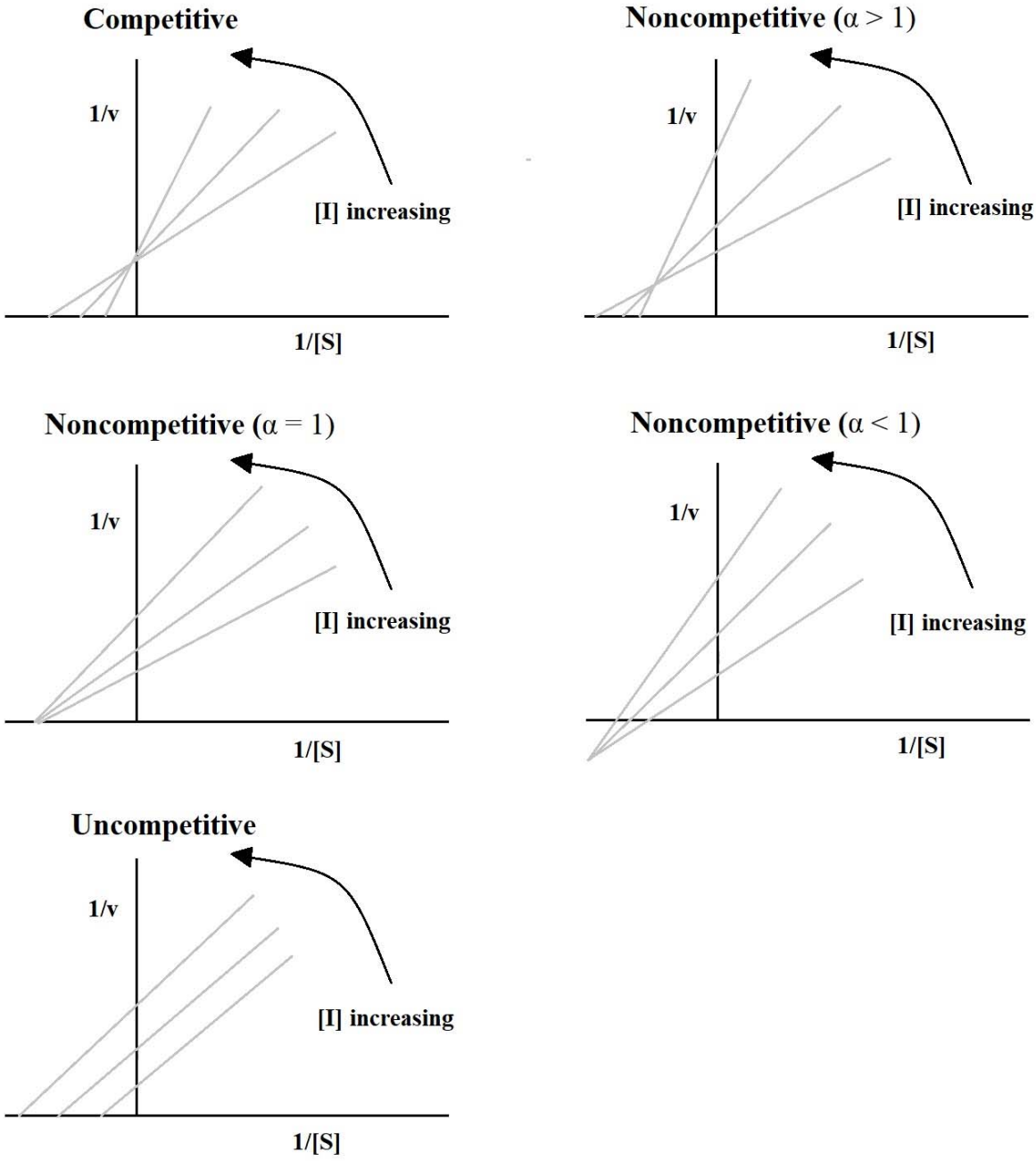

Figure 4.5: Representative double reciprocal plots for different inhibition modes

In addition to the determination of binding affinity and binding site, binding specificity studies are commonly performed to determine the binding selectivity or uptake in the target cells. In pathological conditions like cancers, cells overexpress different receptors/biomarkers which are not present at all or present in very low level in normal cells. This differential receptor expression forms the basis of in vitro cell based studies to determine binding selectivity. CD13 has been found to be upregulated in different cancers (91, 95). To evaluate the binding selectivity of the peptide ligands, cell surface CD13 binding studies (146) and confocal microscopy studies (148, 149) were performed with fluorophore conjugated peptide molecules. The in vitro cell surface binding studies provide information about the abilities of the peptide ligands to bind to CD13 receptor on the cell surface. Confocal microscopy images give the visual confirmation of binding and cellular uptake.

4.2 Materials and Methods

4.2.1 Characterization of CD13 binding affinity and binding site of the peptide ligands.

CD13 catalysis inhibition assays were performed to determine the CD13 binding affinity and to evaluate the binding sites of the peptide ligands. His-tagged human CD13 protein (Sino Biological, Beijing, China) at 2 nM and 172 μM L-Alanine 7-amido-4-methylcoumarin (Ala-MCA) (Santa Cruz Biotechnology, Dallas, TX, USA) were incubated in 96-well polystyrene microplates with 100 μL of binding buffer/well (10 mM HEPES and 0.1% w/v BSA in PBS, pH 7.2) with gradient concentrations of the peptides at 37 °C. The release of fluorescent product 7-amido-4-methylcoumarin was measured using a BioTek Synergy HT microplate reader (BioTek Instruments, Winooski, VT, USA) at λexc of 360 nm and λem of 460 nm. The IC50 is defined as the concentration of the peptide causing 50% inhibition of the CD13 enzymatic activity. The steady-state enzyme kinetic assays were performed at room temperature

as described above, using incremental concentrations of Ala-MCA (33–526 μM), at fixed concentrations of the peptides ranging from 0 to 1304 μM. Initial rates (V_0) were calculated from the slopes of the first 5 minutes of the reaction. The equilibrium dissociation/inhibitory constants (K_i) were calculated using the competitive (or noncompetitive, $\alpha = 1$, depending on the observed inhibition mode in the double reciprocal plots) enzyme inhibition model on GraphPad Prism (La Jolla, CA, USA).

4.2.2 Evaluation of CD13 expression levels in selected cell lines. Western blot studies were carried out to detect the CD13 expression levels in HT-1080 and MCF-7 cells. The cells (ATCC, Manassas, VA, USA) were lysed with cell lysis buffer (Cell Signaling, Boston, MA, USA) and protein concentrations were determined by the bicinchoninic acid assay (BCA assay). Cell proteins (20μg) were then loaded into wells on SDS-PAGE gel (Bio Rad, Hercules, CA, USA). The proteins on gel was then transferred to 0.45 μm nitrocellulose membrane (Bio Rad, Hercules, CA, USA), blocked for 1 h with 5% w/v BSA in 0.1% Tween 20-Tris-buffered saline, and then incubated overnight at 4°C with primary antibody (Anti-CD13 antibody [EPR4058], Abcam, Cambridge, MA, USA). The membrane was incubated with secondary antibody (Donkey anti-Rabbit IgG IRDye 800CW, 1: 10,000) (LI-COR, Lincoln, NE, USA) in the blocking buffer for 1 h at room temperature. The membrane was scanned using a LI-COR Odyssey imaging system (Lincoln, NE, USA). To normalize the protein loading, the blots were incubated with β- actin (Cell Signaling, Boston, MA, USA) as a control.

4.2.3 Evaluation of cell surface CD13 binding of the peptide ligands. For the cell surface CD13 binding assay, CD13 positive HT-1080 cells and CD13 negative MCF-7 cells were seeded at 3 - 4 × 104 cells/well, 48 hours before the experiment in 96-well clear-bottom black plates. On the day of experiment, the cells were washed twice with binding buffer before

incubating 30 minutes (37 °C, 5% CO2) with each peptide conjugate (60 μM) in the binding buffer. The cells were then fixed with 4% paraformaldehyde in PBS for 10 minutes. The fluorescence intensities were measured using the BioTek Synergy HT microplate reader with FITC filter set. The cells were then counterstained with the nuclear stain Hoechst 33342 and analyzed using the same microplate reader with DAPI filter set. Between each step, the cells were washed twice with the binding buffer.

4.2.4 Evaluation of cell internalization and selectivity of the peptide ligands towards CD13. Cell internalization and selectivity of the designed peptides towards CD13 were evaluated in HT-1080 and MCF-7 cell lines using confocal microscopy. HT-1080 and MCF-7 cells were seeded on to coverslips placed inside 6-well culture plates at a density of 100,000 cells/well and incubated for 24 hours. FITC conjugated peptides were added at a concentration of 30 μM at 37 °C, 5% CO2 and incubated for 20 minutes in binding buffer. Cells were then stained with Alexa Fluor 594 (plasma membrane dye) (Invitrogen), fixed with 4% paraformaldehyde in PBS, and visualized under a Leica DMIRE2 confocal laser scanning microscope (Leica Microsystems GmbH, Germany) at 63X magnification with oil immersion. Between each step, the cells were washed twice with the binding buffer.

4.3 Results and Discussions

4.3.1 Characterization of CD13 binding affinity and binding site of the peptide ligands. The designed peptides inhibited the CD13 catalyzed hydrolysis of Ala-MCA substrate, at significantly lower concentrations than NGR-2C peptide (Figure 4.6 and Table 4.2). The illustrated curve-fittings are based on single inhibitor binding site. IC50 values observed for the designed peptides were 2.7 to 7.4 times lower than that of NGR-2C (Table 4.2).

To gain insight into the binding affinity and binding site of the peptide ligands, steady-state enzyme kinetic assays (Figure 4.7, 4.8, 4.9 and Table 4.2) were performed at room temperature. The Lineweaver-Burk double reciprocal plots for PEP20, PEP24, PEP173, and NGR-2C showed series of lines crossing the y-axis ($1/V_0$) at the same point – i.e. V_{max} unchanged, but with increasing values of Michaelis constant (K_m). These data were consistent with competitive inhibition model (PEP20, K_i = 54.0 ± 11.9 μM; PEP24, K_i = 74.3 ± 12.0 μM; PEP173, K_i = 38.8 ± 5.21 μM; NGR-2C, K_i = 773 ± 157 μM), suggesting that PEP20, PEP24, PEP173, and NGR-2C bind to the catalytic site of CD13. On the other hand, PEP293 and PEP308 were found to lower the V_{max}, without affecting K_m (Figure 4.9), suggesting that they can bind to CD13 in presence of the substrate. This indicates non-competitive inhibition mode for PEP293 (K_i = 137 ± 8.31 μM) and PEP308 (K_i = 234 ± 14.3 μM).

The three identified peptides [PEP173 (GYPAVYLF), PEP20 (GYPAY) and PEP24 (GFPAY)] showed 10 – 20 times higher binding affinity (K_i) towards hCD13 as compared to NGR-2C peptide. PEP20, 24 and 173 were found to bind to the catalytic active site of CD13 -the intended target site of the designed peptide ligands. The nonspecific control peptides [PEP293 (GYPAYVEF) and PEP308 (GFPAVYEF)] were found to bind to sites distant from the intended catalytic active site.

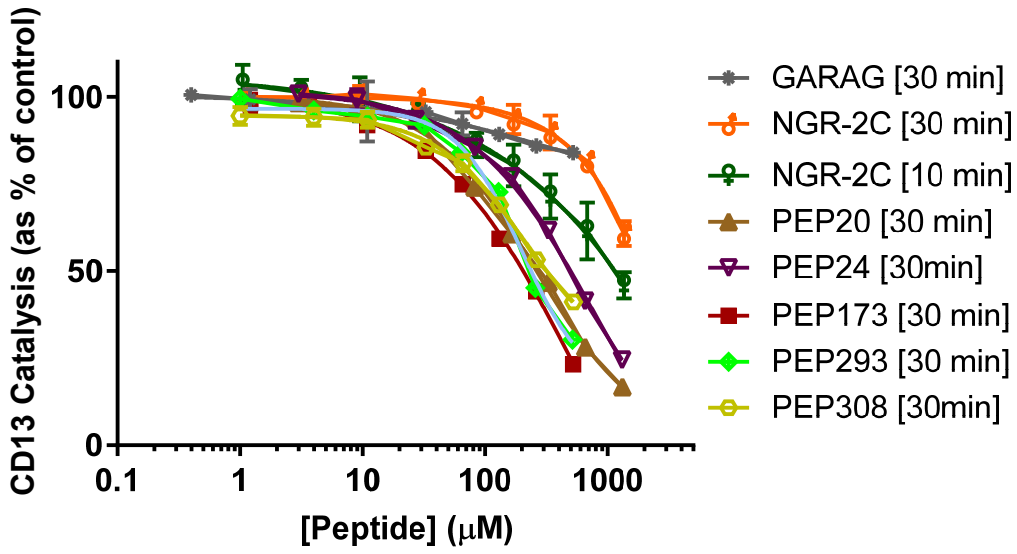

Figure 4.6: CD13 catalysis inhibition by the peptides (n = 3, mean ± SE in duplicate or triplicate)

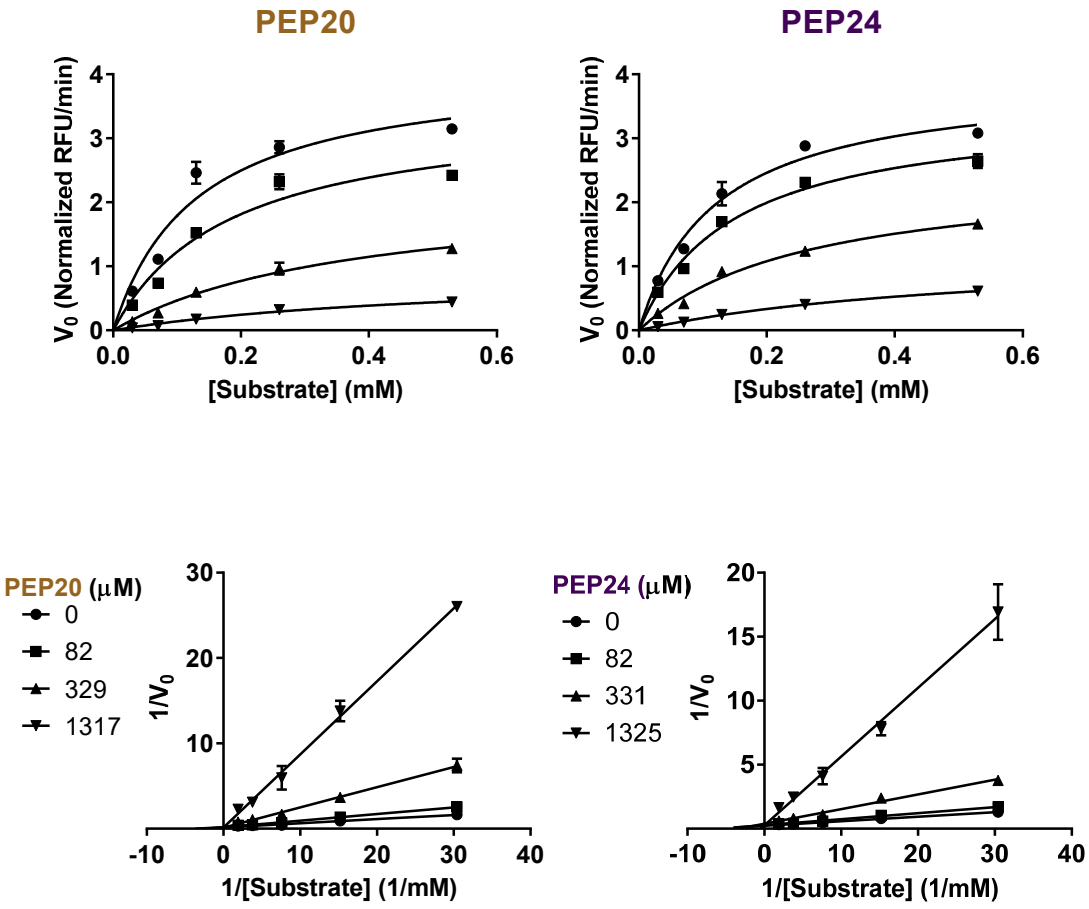

Figure 4.7: Steady state kinetic analysis of CD13 in presence of Ala-MCA substrate, and PEP20 and PEP24; plots of initial velocity (V_0) versus Ala-MCA concentration (upper panels) and double reciprocal plots (lower panels) (mean ± SE, in triplicate).

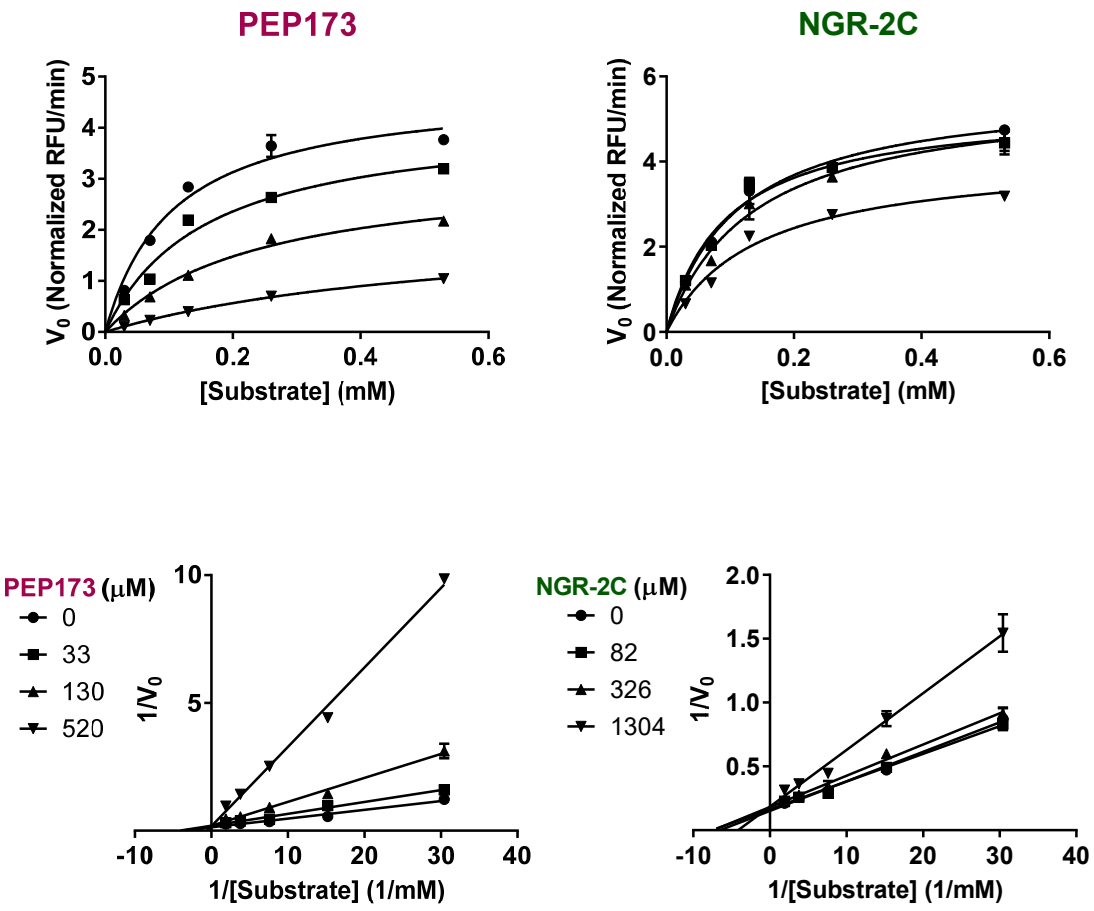

Figure 4.8: Steady state kinetic analysis of CD13 in presence of Ala-MCA substrate, and PEP173 and NGR-2C; plots of initial velocity (V_0) versus Ala-MCA concentration (upper panels) and double reciprocal plots (lower panels) (mean ± SE, in triplicate).

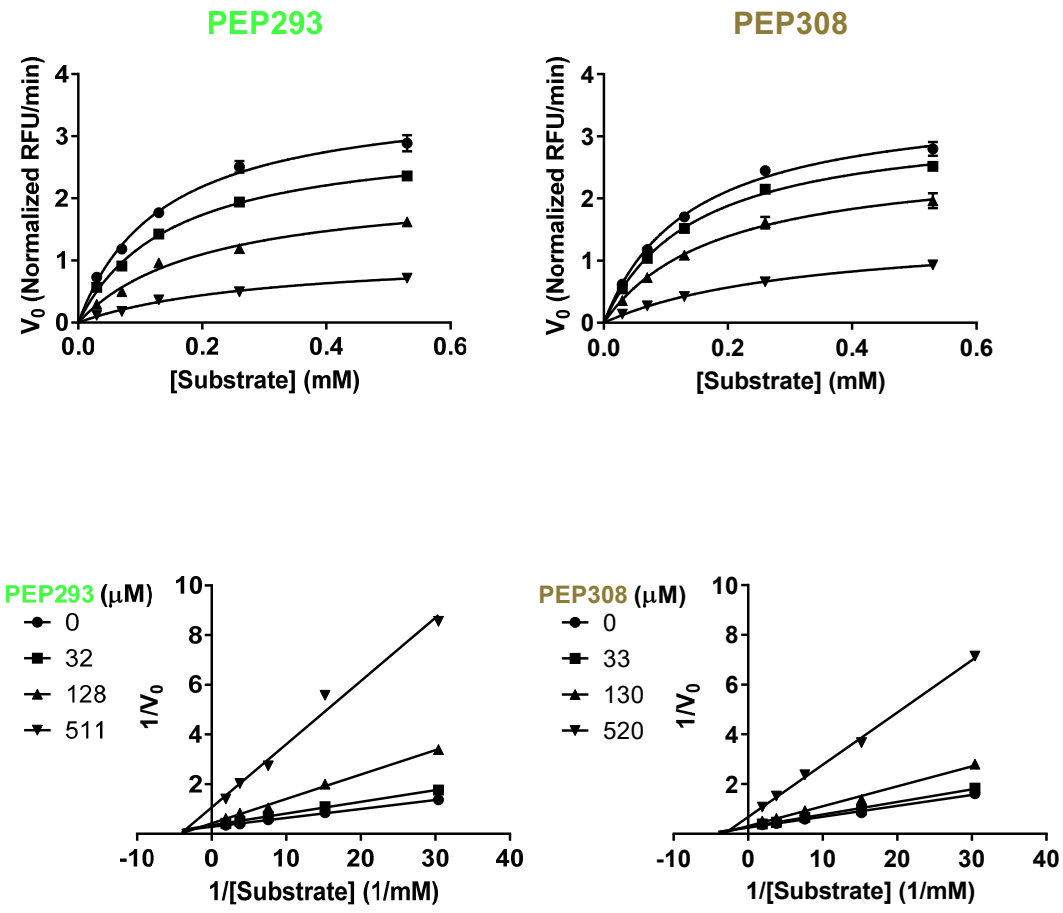

Figure 4.9: Steady state kinetic analysis of CD13 in presence of Ala-MCA substrate, and PEP293 and PEP308; plots of initial velocity (V_0) versus Ala-MCA concentration (upper panels) and double reciprocal plots (lower panels) (mean ± SE, in triplicate).

Table 4.2

CD13 catalysis inhibition assay data

Peptides	Sequence	IC_{50} (μM)[a, b]	Binding Affinity, K_i (μM)[c, d]	Inhibition mode
PEP20	GYPAY	227 ± 6.67	54.0 ± 11.9	Competitive
PEP24	GFPAY	463 ± 21.8	74.3 ± 12.0	Competitive
PEP173	GYPAVYLF	170 ± 23.0	38.8 ± 5.21	Competitive
NGR-2C (+ve control)	CNGRC (C1-C5)	1260 ± 80.0	772.6 ± 157	Competitive
GARAG (-ve control)	GARAG	-	-	-
PEP293	GYPAYVEF	213 ± 6.67	137 ± 8.31	Non-competitive
PEP308	GFPAVYEF	300 ± 40.0	234 ± 14.3	Non-competitive

[a] n = 3, Mean ± SE, [b] All after 30 minutes except NGR-2C after 10 minutes, [c] Mean ± SE, d For PEP20, 24, 173 and NGR-2C, competitive inhibition model was used in Prism 7 to determine the K_i; for PEP293 and 308, noncompetitive inhibition model (α = 1) was used

4.3.2 Evaluation of CD13 expression levels in selected cell lines. While HT-1080 cells exhibited clear CD13 bands, MCF-7 cells did not show significantly identifiable band of CD13 in the blots (Figure 4.10). Based on the band intensity, HT-1080 cells showed ten-fold greater CD13 expression than MCF-7 cells. These data showed the suitability of using HT-1080 and MCF-7 cells as the CD13 positive and negative cell lines, respectively.

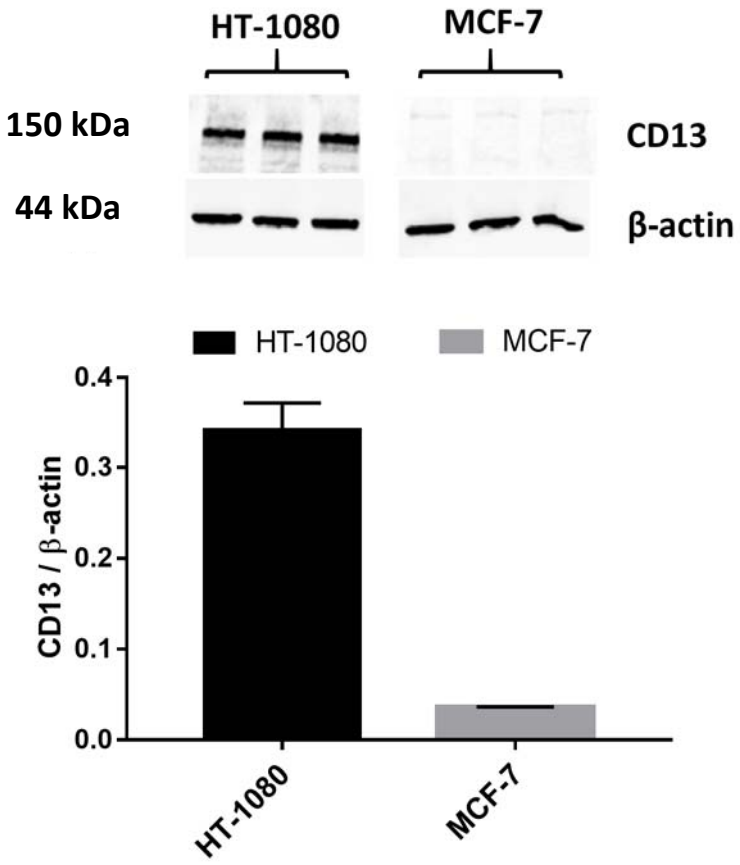

Figure 4.10: CD13 expression levels in HT-1080 and MCF-7 cells (mean ± SE, in triplicate)

4.3.3 Evaluation of cell surface CD13 binding of the peptide ligands. The ability of the peptides to recognize cell surface CD13 receptor was evaluated by measuring the fluorescence intensity (cell number normalized) after incubating the FITC-conjugated peptides in CD13 positive HT-1080 cells and CD13 negative MCF-7 cells. In the cell binding assay, all the FITC conjugated peptides except the negative control conjugate (GARAG-FITC), showed significantly higher cell surface binding to CD13 positive HT-1080 cells as compared to the CD13 negative MCF-7 cells (Figure 4.11). Additionally, the designed peptide (PEP20, PEP24,

and PEP173) conjugates were found to exhibit slightly higher cell surface binding compared to NGR-2C conjugate in HT-1080 cells. These data suggested that the designed peptides could recognize and bind to the CD13 receptors on the cell surface.

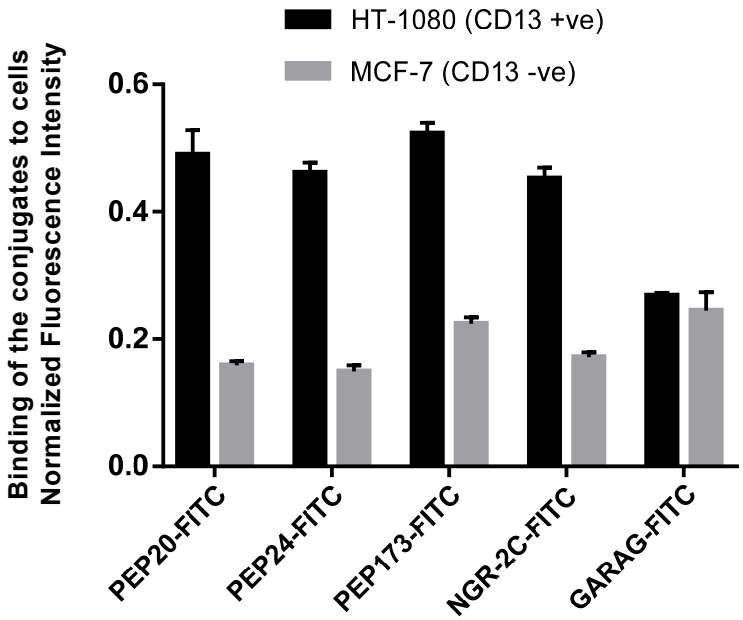

Figure 4.11: Binding of the peptide conjugates to HT-1080 and MCF-7 cells (mean ± SE, in quadruplicate)

4.3.4 Evaluation of cell internalization and selectivity of the peptide ligands towards CD13. Cell internalization and selectivity of the designed peptides towards CD13 were evaluated in HT-1080 and MCF-7 cell lines using confocal microscopy. Confocal microscopic imaging was performed after incubating the cells with the FITC conjugated peptides for 20 minutes. In the HT-1080 cell images (upper panels of Figures 4.12. 4.13, 4.14, and 4.15),

significant green fluorescence was observed inside the cells and some fluorescence was detected on the cell surface for the designed peptides (PEP20-FITC, PEP24-FITC and PEP173-FITC) and NGR-2C-FITC. The same molecules resulted in only background green fluorescence in MCF-7 cell images (lower panels of Figures 4.12. 4.13, 4.14, and 4.15). FITC labeled control peptide GARAG showed no binding to both the cell lines (Figure 4.16). These data demonstrated that the designed FITC labeled peptides and the positive control NGR-2C-FITC bound and got internalized in the CD13 positive HT-1080 cells, but not in CD13 negative MCF-7 cells.

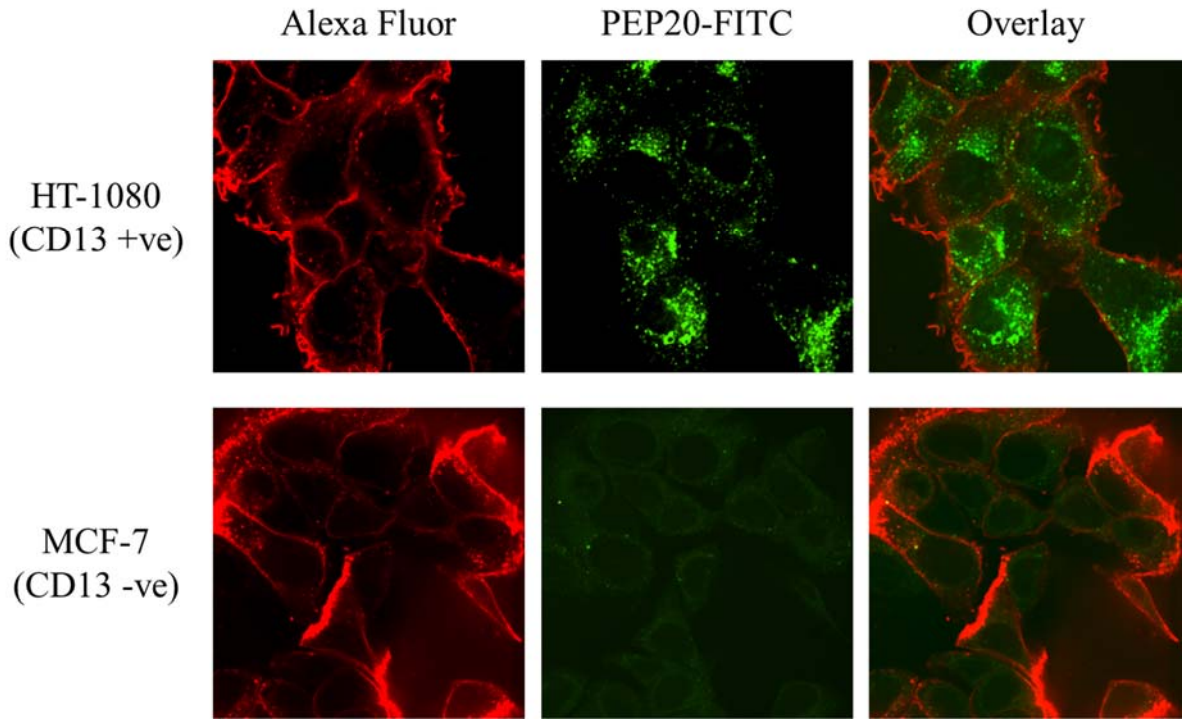

Figure 4.12: Confocal images of PEP20-FITC. Left Alexa Fluor column shows the cell treated with membrane dye (red), middle FITC column shows the cells treated with FITC conjugated peptide (green), and right overlay column displays the two images overlaid.

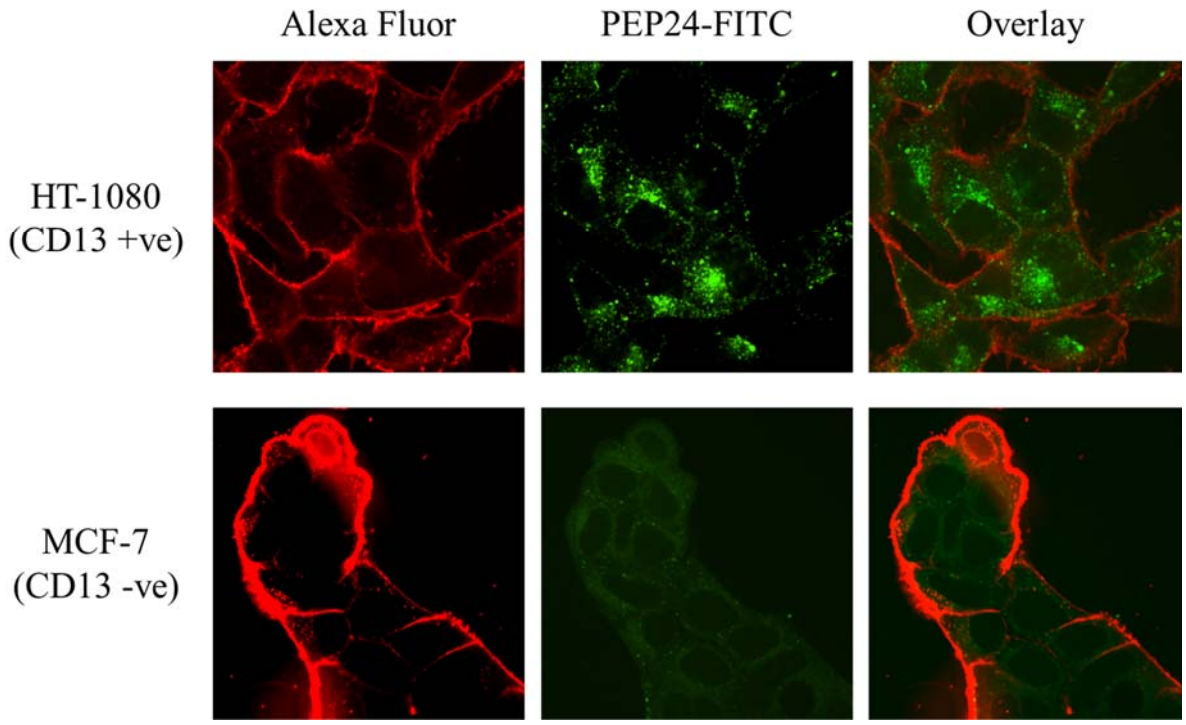

Figure 4.13: Confocal images of PEP24-FITC. Left Alexa Fluor column shows the cell treated with membrane dye (red), middle FITC column shows the cells treated with FITC conjugated peptide (green), and right overlay column displays the two images overlaid.

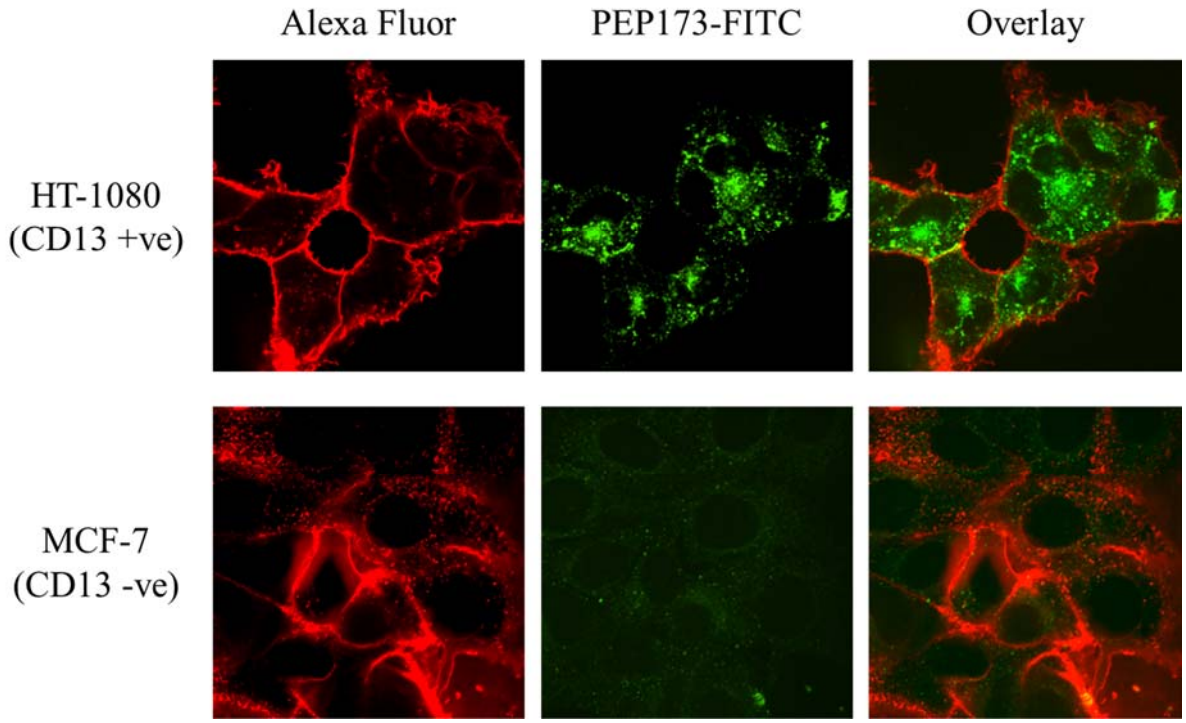

Figure 4.14: Confocal images of PEP173-FITC. Left Alexa Fluor column shows the cell treated with membrane dye (red), middle FITC column shows the cells treated with FITC conjugated peptide (green), and right overlay column displays the two images overlaid.

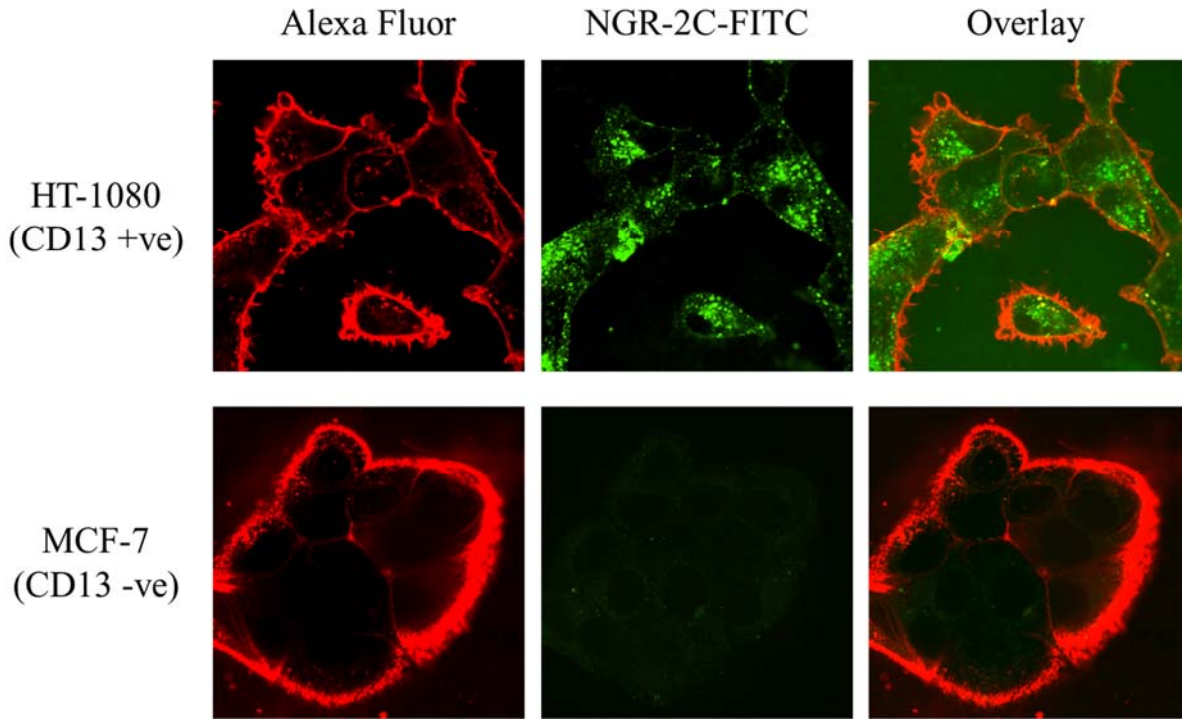

Figure 4.15: Confocal images of NGR-2C-FITC. Left Alexa Fluor column shows the cell treated with membrane dye (red), middle FITC column shows the cells treated with FITC conjugated peptide (green), and right overlay column displays the two images overlaid.

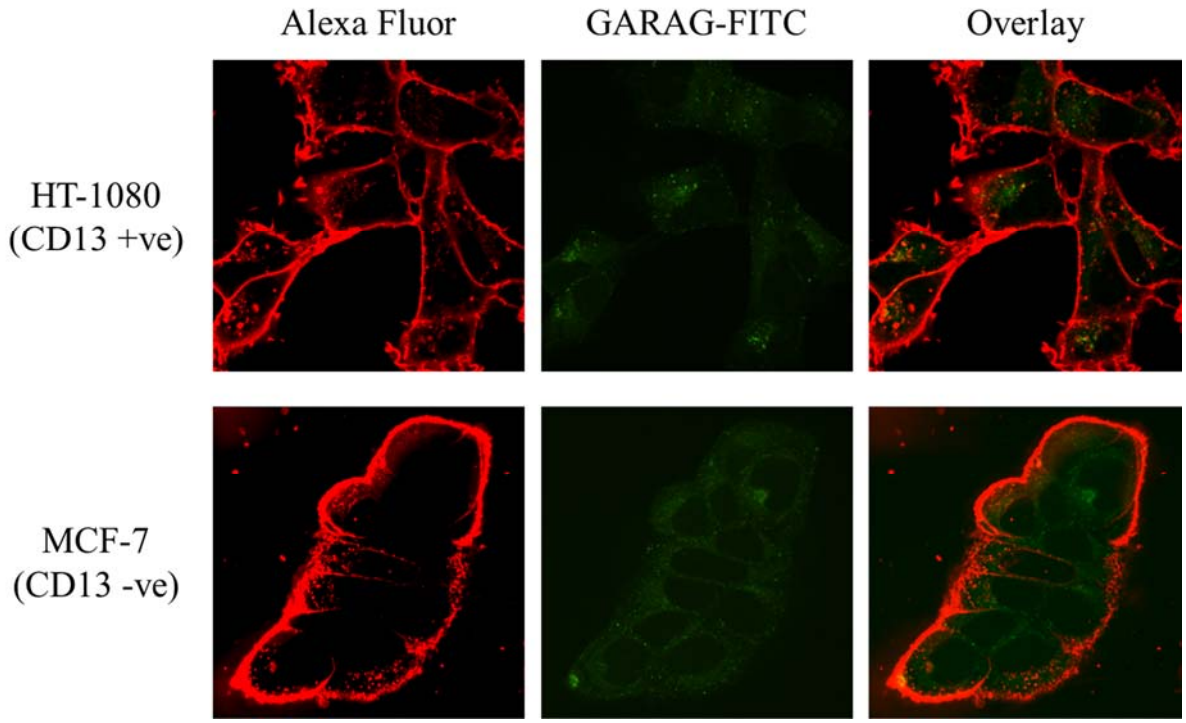

Figure 4.16: Confocal images of GARAG-FITC. Left Alexa Fluor column shows the cell treated with membrane dye (red), middle FITC column shows the cells treated with FITC conjugated peptide (green), and right overlay column displays the two images overlaid.

Chapter 5: Designed Peptide - Drug Conjugate

5.1 Introduction

In cancer therapy, the primary objective of targeted drug delivery is to transport drug to the cancer sites while minimizing their exposure to normal tissues. Two key strategies have been extensively studied to achieve this goal, both of which rely on modifying the pharmacokinetic properties of the drug to some extent. The first strategy uses a delivery vehicle, like nanoparticles, that carries the drug and determines the drug biodistribution via its own physicochemical characteristics. The second one is the prodrug strategy, where covalent modification of the drug with a moiety that momentarily disguises the drug's bioactivity and confers desirable pharmacokinetic properties. The prodrug approach have several advantages over delivery vehicle approach: (a) significantly lower amount of inert materials that results in decreased metabolic burden of the patient (b) minimize premature drug release, (c) relatively straightforward and simple preparation/manufacturing (150-152).

Peptide-drug conjugate (PDC) is an emerging type of prodrug. It is formed by covalent attachment of a specific peptide sequence to a drug through a linker. The use of peptides would enable the incorporation of many functionalities into PDCs. The amino acid sequences can be selected to regulate the physicochemical properties of the conjugate, as well as to impart active targeting towards a specific receptor expressed at the target cancer tissue. PDCs are biodegradable and generally show no or minimum undesired immunogenic responses because they are composed of amino acids and typically have short peptide sequences. Different amino acid combinations allow simplistic preparation of different PDCs. A number of tumor targeting peptides have been developed till date for different types of cancers. The peptide sequence can

be easily modified to facilitate drug conjugation and, to tune the conjugate molecule ionization and hydrophobicity, which in turn impact the bioavailability. Additionally, owing to their low molecular weight, PDCs can be purified by simple HPLC technique (153, 154).

The main building blocks of a PDC include a cytotoxic drug, a targeting peptide ligand and a linker between them (Figure 5.1). The therapeutic efficacy of the PDC is primarily governed by the potency of the cytotoxic drug and the targeting efficiency of the conjugate. The process of synthesizing PDCs is generally fast and simple. And since an already approved drug can be selected as the therapeutic payload, the overall cost of production of PDCs is significantly lower than that of synthesizing a new drug (155).

Figure 5.1: Typical structure of a peptide-drug conjugate (PDC)

The general mechanism of action of a PDC in cancer therapy is illustrated in Figure 5.2. After administration into plasma (step 1), the PDC interacts with the specific antigen on target cell surface (step 2). Then the PDC-antigen complex gets internalized into the cell (step 3). Inside the target cell, PDC undergoes lysosomal degradations and release the cytotoxic agent (step 4). Majority of the cytotoxic drugs cause cell death via either DNA intercalation or binding to microtubulins (step 5).

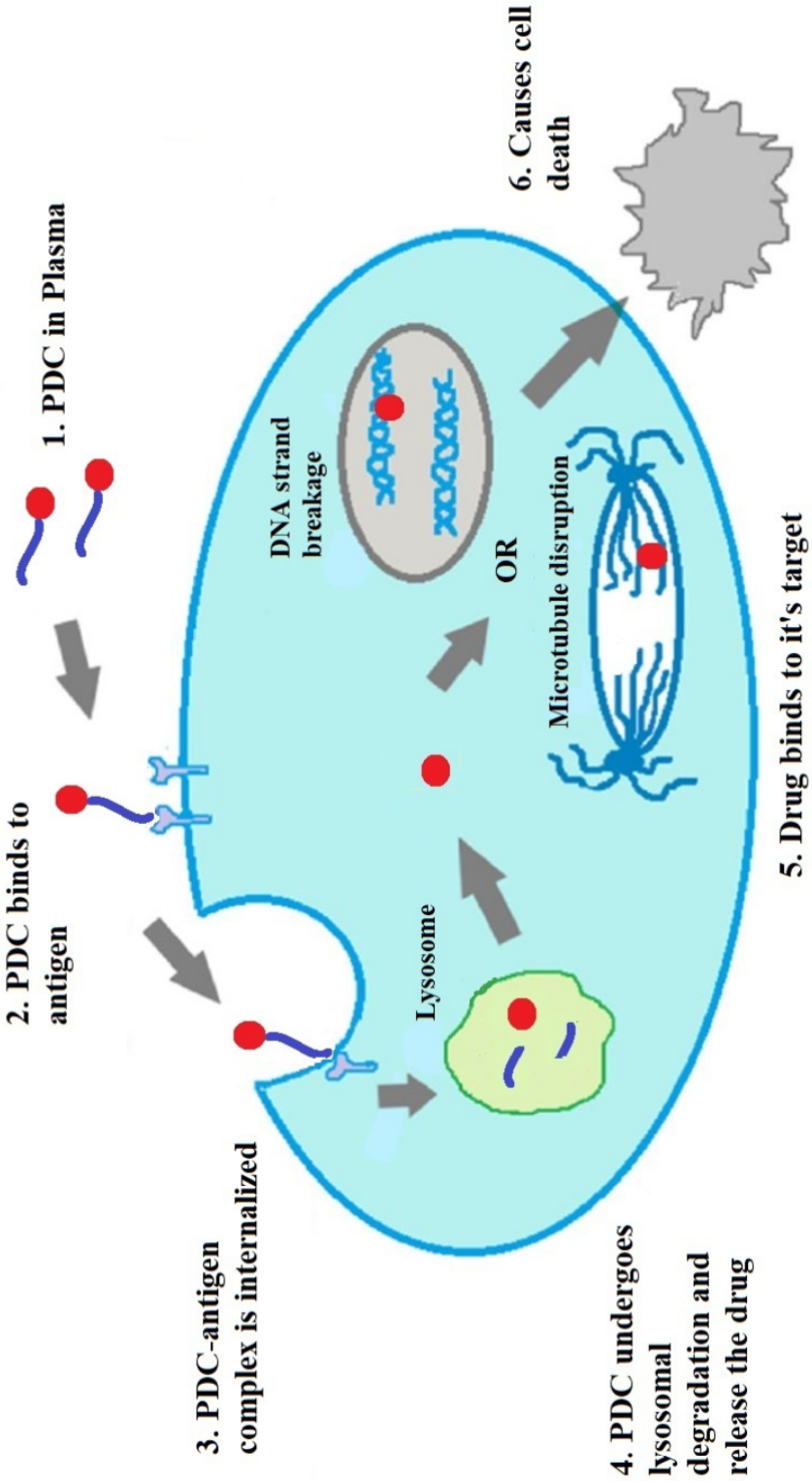

Figure 5.2: Mechanism of action of PDCs. The peptide portion of the PDC homes onto a cell-surface antigen that is specific to certain cancer.

The role of linker is very important in the design of PDCs. There are two classes of linkers: (a) cleavable linkers, and (b) non-cleavable linkers. While cleavable linkers get cleaved extracellularly or intracellularly at the target site by different endogenous or exogenous stimuli, non-cleavable linkers do not get cleaved. The non-cleavable linkers undergo degradation in lysosome along with the whole conjugate. The most widely used cleavable linkers are hydrazone and disulphide linkers. Drug-linker moiety is typically linked to peptide or antibody using the lysine or thiol groups on the targeting moiety (156, 157).

Doxorubicin, chlorambucil, camptothecin, and paclitaxel are some of the chemotherapeutic drugs that have been used in PDC development (111). But these drugs are relatively low potency cytotoxic drugs. Currently, very potent cytotoxic agents, like auristatins, are used in drug conjugate development (158). Auristatins leads to cell apoptosis by inhibiting the polymerization of tubulin in dividing cells (159).

Design of a novel peptide-doxorubicin conjugate was reported by Soudy et al. They made two different conjugates having ester and amide bonds between doxorubicin and linker. The PDC with ester bond showed 4 times more toxicity than doxorubicin in MDA-MB-435 cells and 40 times better selectivity towards breast cancer cell lines when compared to normal cells (160). Polyak et al reported the development of integrin targeted cyclic RGD-PEG-Dox conjugate. The PDC inhibited the cell proliferation at lower IC_{50} as compared to doxorubicin or control conjugate without RGD peptide (161). An EGFR-binding peptide-doxorubicin conjugate was developed and evaluated in-vitro and in-vivo for anti-cancer efficacy. The study showed improved anticancer efficacy and lower systemic toxicity of PDC with EGFR upregulated tumor cells (162).

In this study, PDCs were prepared by conjugating the drug monomethyl auristatin E (MMAE) to the designed CD13 targeting peptides via cleavable linker. The linker-drug construct contains a spacer, maleimidocaproyl (mc); a protease degradable dipeptide, valine-citrulline (vc); a self-immolative moiety, para-amino benzyloxycarbonyl (PABC); and the antimitotic drug, MMAE (Figure 5.3). This construct is termed as mc-vc-PABC-MMAE. The linker-drug construct can be conjugated to a cysteine residue in the peptide sequence using the specific thiol-maleimide coupling reaction (163, 164). The PDCs were studied to evaluate the cytotoxicity and determine the IC_{50} values. The studies were performed in CD13 overexpressing HT-1080 cells, and CD13 negative MCF-7 cells, and a control normal cell line HEK 293.

In this study targeting ability of the designed peptide ligands in living host was also evaluated by studying the in-vivo anti-tumor efficacy of the synthesized peptide-drug conjugates. The use of animal models enables researchers to study disease conditions in ways which would be unapproachable in a human patient. To study cancer efficacy, different animal models are available. These models are typically used to study the reasons of malignant transformation, metastasis, and invasion, and to evaluate the response to different anticancer therapies.

The most extensively used model for studying cancer states is the xenograft model. In xenograft model, tumor cells or tissues are introduced in immunocompromised mice, either under the skin or directly into the organ where the tumor originates. The immunocompromised mice do not reject the transplanted exogenous cells. Xenograft can be developed in athymic nude mice, severely compromised immunodeficient (SCID) mice, or other immunocompromised mice breeds (165). The tumor develops in 1 week to 4 months depending on the number of cells transplanted, or the size of the transplanted tumor tissue. The response to therapeutics can then be investigated in vivo.

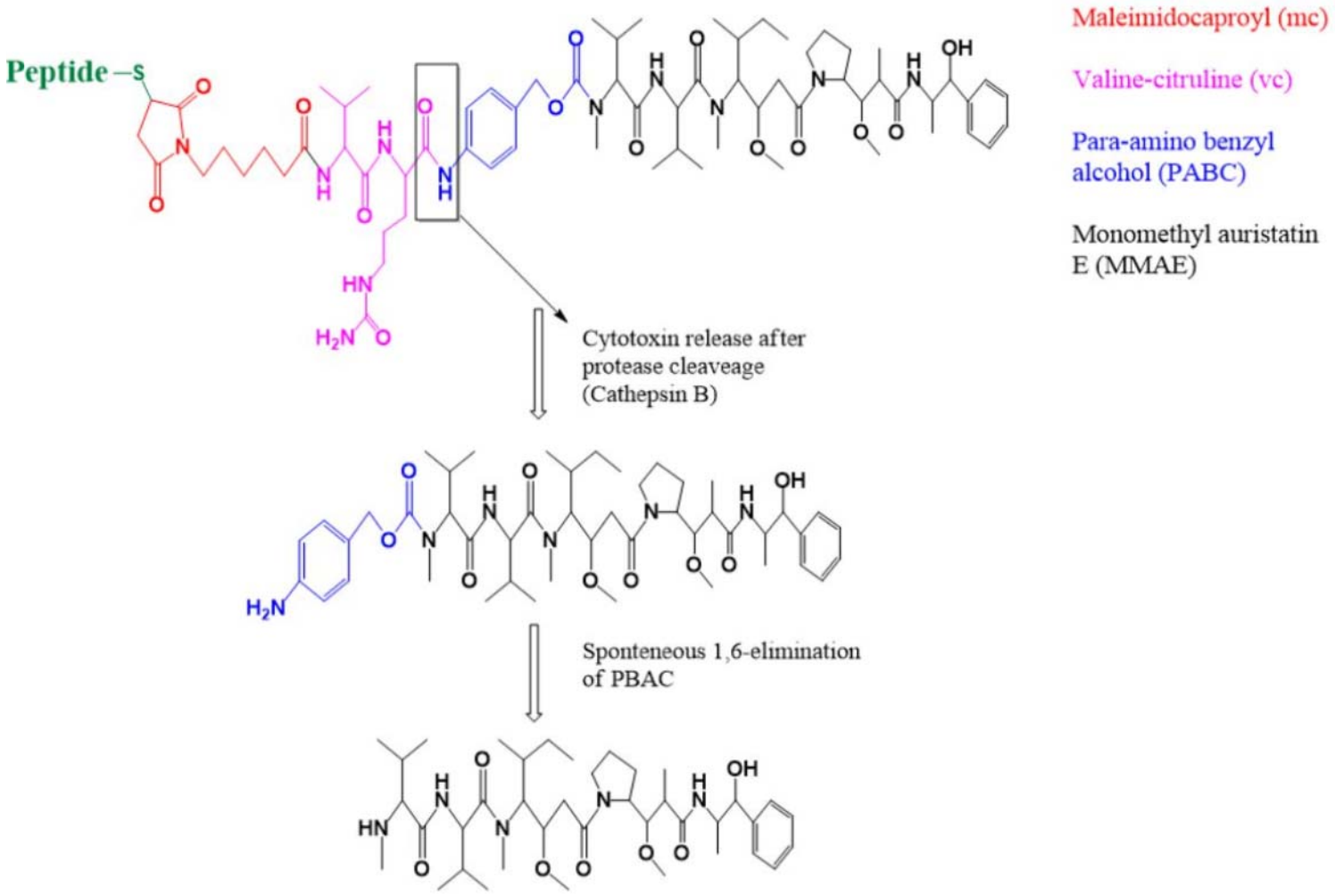

Figure 5.3: Peptide-mc-vc-PABC-MMAE conjugate structure and the drug release mechanism

5.2 Materials

Fmoc-L-Cys(Trt)-2-chlorotrityl resin, Fmoc-amino acids, Boc-amino acids, Fmoc-aminohexanoic acid, N, N′-diisopropylcarbodiimide (DIC), diisopropylethylamine (DIPEA), triisopropylsilane (TIS), N-hydroxybenzotriazole (HOBT) were purchased from Chem-Impex International Ltd (Wood Dale, IL, USA). Maleimidocaproyl-valine-citrulline-p-aminobenzoyloxycarbonyl-monomethyl auristatin E (mc-vc-PABC-MMAE) and monomethyl auristatin E (MMAE) were obtained from MuseChem (Fairfield, NJ, USA) and MedKoo Biosciences (Morrisville, NC, USA), respectively. Sulforhodamine B (SRB) assay kit was purchased from Abcam (Cambridge, UK). All chemicals and solvents were used without further purification.

HT-1080, MCF-7, and HEK 293 cells were purchased from ATCC (Manassas, VA, USA). Cells were cultured in dulbecco's modified eagle medium (DMEM) (high glucose, with L-glutamine, and sodium pyruvate) (Thermo Fisher Scientific, Waltham, MA, USA) with 10% fetal bovine serum (Gemini Bio-Products, West Sacramento, CA, USA) and 1% penicillin-streptomycin (Gemini Bio-Products, West Sacramento, CA, USA). TrypLE Express was obtained from Thermo Fisher Scientific (Waltham, MA, USA).

Four to six weeks old female athymic nude mice (nu/nu) were purchased from Simonsen Laboratories (Santa Clara, CA, USA). The medical supplies like syringes, and alcohol swabs were purchased from Beckton Dickinson (Franklin Lakes, NJ, USA). Isoflurane was obtained from Patterson Veterinary (Patterson, CA, USA).

5.3 Methods

5.3.1 Synthesis of the peptide-drug conjugates (PDCs). The peptides (PEP20-Ahx-Cys, GYPAY-Ahx-C; and PEP173-Ahx-Cys, GYPAVYLF-Ahx-C) were synthesized by standard solid phase synthesis method (0.2 to 0.4 mmol scale). The synthesis was started with Fmoc-L-Cys(Trt)-2-chlorotrityl resin to place a cysteine residue at the C-terminal so that the drug-linker construct can be conjugated at the C-terminal side of the peptide (Figure 5.4). A spacer (e.g. 6-aminohexanoic acid/ Ahx) was added between the designed peptide sequence and the C-terminal cysteine residue using same DIC/HOBt coupling method. Coupling of subsequent amino acids was performed with 3 to 5 fold excess of 1-hydroxy-benzotriazole (HOBt) and diisopropyl-carbodiimide (DIC). Each coupling was done for 3 hours, followed by Kaiser test to confirm the completeness of reaction. Fmoc group was removed in each step by treating the resins was solution of 20% piperidine in DMF. Kaiser tests were also performed after each deprotection step. Boc protected amino acids were used only for the last N-terminal amino acids to eliminate the necessity of last Fmoc deprotection step. Cleavage of the peptides were done by treating the resins with trifluoroacetic acid – water – triisopropylsilane (95: 2.5: 2.5) cocktail for 3 hours. The obtained TFA-peptide solution was cooled and evaporated under nitrogen flow until it became thick viscous oily liquid. Ice cold ether was added to the oily liquid to precipitate the peptide. The peptides are then freeze dried and stored in −20° C freeze until further use. The peptides were used to synthesize the PDCs without further purification.

The PDCs were prepared using thiol-maleimide coupling reaction. To synthesize each PDC (Figure 5.4), 5mg of the peptide was dissolved in 2.5 ml of PBS-ACN (70:30) mixture, and equimolar amount of mc-vc-PABC-MMAE was dissolved separately in 2.5 ml PBS-ACN (70:30) mixture. The peptide solution and the drug-linker solution were mixed thoroughly by

vortexing. The pH of the reaction mixture was adjusted to 6.5 – 7 using HCl (aq). The reaction mixture was shaken for 1 hour at room temperature, and solidified by freeze drying.

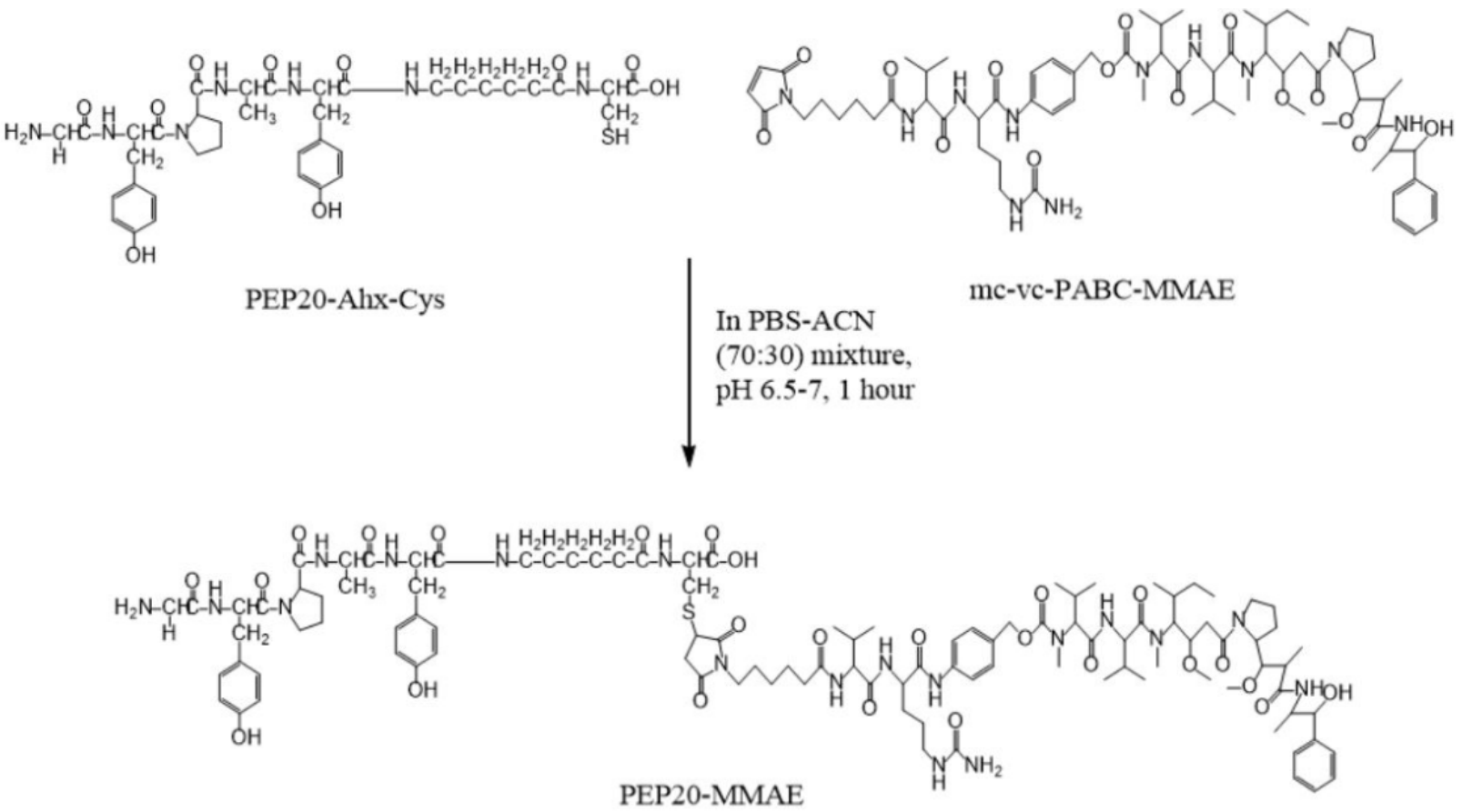

Figure 5.4: Peptide-drug conjugate (PDC) synthesis scheme

5.3.2 Characterization of the synthesized molecules. Synthesized molecules were characterized by Electron Spray Ionization Mass Spectrometry (ESI-MS, AB Sciex PI 3000). Samples were made in acetonitrile and water mixture (50:50).

The purity of the synthesized molecules was determined using high pressure liquid chromatography (HPLC) (Agilent 1100). The column used was Agilent Zorbax C18, 5 μm, 4.6×150 mm, and the wavelengths used for detection were 210, 254 and 280 nm. The samples were eluted with a mobile phase consisting of water (A) and acetonitrile (B) using a linear gradient from 10 to 90% B over 30 to 35 minutes, at 1.0 mL/min flow rate. The purified compounds were freeze dried and stored at -80° C.

5.3.3 In vitro cytotoxicity of peptide-drug conjugates. The cytotoxicity study of MMAE and peptide-drug conjugates was performed using CD13 overexpressing HT-1080 cells, CD13 non-expressing MCF-7 cells, and a control normal cell line HEK293. The cells were grown in 75 cm^2 flasks in DMEM with 10% FBS and 1% penicillin-streptomycin at 37° C and 5% CO_2. The cells were detached using TrypLE Express and the cell density was counted using Scepter Automated Handheld Cell Counter (MilliporeSigma, Burlington, MA, USA). The cells were seeded into clear 96 well plates at 5000 cells/well (0.2 mL cell suspension/well) and incubated overnight to allow them to attach to the wells. Then the cells were incubated with drug MMAE and peptide-drug conjugates at various concentrations ranging from 0.0000302 to 30200 nM for 72 h at 37° C and 5% CO_2 (in complete growth media). The Sulforhodamine B (SRB) Cell cytotoxicity assays were performed following the company recommended protocol (SRB assay kit, Abcam, ab235935). The SRB absorbance was measured at 490 nm wavelength by using a microplate reader (BioTek Instruments, Inc., VT, USA).

Percent cytotoxicity was calculated by the following formula:

$$Cytotoxicity\ (\%) = \frac{O.D.(DMSO) - O.D.(Smaple)}{O.D.(DMSO)} \times 100$$

Where,

O.D. (DMSO) = absorbance of the DMSO control after background correction.

O.D. (Sample) = absorbance of the sample after background correction.

The IC50 values were determined using Graph Pad Prism 7 software (GraphPad Software Inc., CA, USA) with nonlinear regression dose-response - inhibition curve fit (variable slope four parameter).

5.3.4 In vivo anti-tumor efficacy of peptide-drug conjugates. The in vivo study was performed as per the animal protocol (No. 17R02) reviewed and approved by the Institutional Animal Care and Use Committee, University of the Pacific.

5.3.4.1 Determining maximum tolerated dose (MTD) of the drug MMAE. The MTD of the drug MMAE was determined in four to six weeks old female athymic nude (homozygous, nu/nu) mice. Five healthy mice were given a single dose of 0.375 mg/kg, 0.5 mg/kg, 0.7 mg/kg, 1 mg/kg, and 1.5 mg/kg of MMAE, respectively via tail vein injection using 29 gauge needles. Following administration, the mice were observed daily for their general health and the body weight was measured every three days.

5.3.4.2 Xenograft model. CD13 overexpressing HT-1080 cells were cultured as described previously in Section 5.3.3. On the day of tumor transplantation, cells were detached using TrypLE Express and re-suspended in DMEM. The cell density was counted using Scepter Automated Handheld Cell Counter. The cells were centrifuged at 125xG for 5 minutes and the supernatant was discarded. The cell pellet was washed once with sterile PBS and re-suspended in 50:50 PBS – Matrigel (High Concentration) (Corning Life Sciences, Tewksbury, MA, USA) so that 0.1 mL of the suspension contains approximately 1,000,000 cells. The cell suspension was maintained on ice until injection.

Four to six weeks old female athymic nude mice (homozygous, nu/nu) were used for tumor xenograft model development. All mice were anaesthetized using isoflurane. 0.1 mL of cell suspension was injected subcutaneously on the right flank of each mouse using a 27 gauge needle. Following inoculation, the mice were observed daily for their general health and tumor appearance.

5.3.4.3 Anti-tumor efficacy study. Tumors in mice were grown to reach an average of approximately 100 mm^3. The tumor bearing mice were then divided in to four groups each having four mice. The groups were PBS group, MMAE group, PEP20-MMAE group, and PEP173-MMAE group. Treatment was started 9 or 12 days after cancer cell transplantation and was administered intravenously via tail vein using 29 gauge needles every 4 days for a total of 4 doses (q4d X 4). The dose was 975 nmol/kg for each compound which is equivalent to 0.7 mg/kg MMAE. The greatest longitudinal diameter (L) and the greatest transverse diameter (W) of the tumor were measured using Vernier caliper every four days from the day of first dosing. Tumor volume was determined using the formula $(L \times W^2)/2$. The body weights were also measured every four days.

5.4 Results and Discussions

5.4.1 Synthesis and characterization of peptide-drug conjugates (PDCs). Designed peptides PEP20 and PEP173 were chosen as the targeting peptide moieties for the synthesis of PDCs. The anticipated binding mode of the designed peptides indicates that the N-terminal side binds deep inside the peptide binding channel of CD13 (Figures 2.6, 2.7, and 2.8). Moreover, it has been reported that, any modification at the N-terminal of the conventional CD13 targeting peptide ligand CNGRC (C1-C5) hampers its binding ability (166). Therefore, a cysteine conjugation site was incorporated at the C-terminal side of the peptides (PEP20 and PEP173) under study. A spacer (6-aminohexanoic acid) was added in between the designed peptide sequence and the cysteine conjugation site to have spatial separation between the targeting peptide moiety and the linker-drug moiety.

The peptides (PEP20-Ahx-Cys and PEP173-Ahx-Cys) were conjugated to monomethyl auristatin E (MMAE), a highly potent but non-selective tubulin polymerization inhibitor, through a maleimidocaproyl-valine-citrulline-p-aminobenzoyloxycarbonyl (mc-vc-PABC) linker. The maleimidocaproyl (mc) part of the linker-drug motif (mc-vc-PABC-MMAE) utilizes maleimide chemistry for cysteine linkage, which takes advantage of exceptional reactivity of maleimide towards sulfhydryl groups to form stable thioester bond. Valine-citrulline (vc) dipeptide is an intracellular protease, cathepsin B, sensitive linker. This protease sensitive approach uses the main proteases found in the tumor cell lysosome for identification and cleavage of a specific peptide sequence. The para-amino benzyloxycarbonyl (PABC) moiety in the linker-drug motif is a self-immolative spacer (164, 167).

All the products were characterized by ESI-MS as shown in table 5.1. The mass spectra of PEP20-Ahx-Cys and PEP173-Ahx-Cys were observed as singly charged species and are displayed in figures 5.5, and 5.7. Peptide drug conjugates PEP20-MMAE (PEP20-Ahx-Cys-mc-vc-PABC-MMAE), and PEP173-MMAE (PEP173-Ahx-Cys-mc-vc-PABC-MMAE) were observed as double and triple charged species and are displayed in Figures 5.9, and 5.11, respectively. The HPLC analysis of the compounds used after purification were greater than 98% pure (Figures 5.6, 5.8, 5.10, 5.12 and Table 5.1).

Table 5.1

MS and HPLC data for the peptides and PDCs

Molecule	MS (g/mol) Calculated	MS (g/mol) Observed	HPLC Purity (%)
PEP20-Ahx-Cys	808.9 $[M+Na]^{+}$	808.8	80.5
PEP173-Ahx-Cys	1144.3 $[M-H]^{-}$	1144.2	80.9
PEP20-MMAE (PEP20-Ahx-Cys-mc-vc-PABC-MMAE)	1062.5 $[M+H+Na]^{+2}$	1062.9	98.1
PEP173-MMAE (PEP173-Ahx-Cys-mc-vc-PABC-MMAE)	835.8 $[M+H+2Na]^{+3}$	834.1	98.3

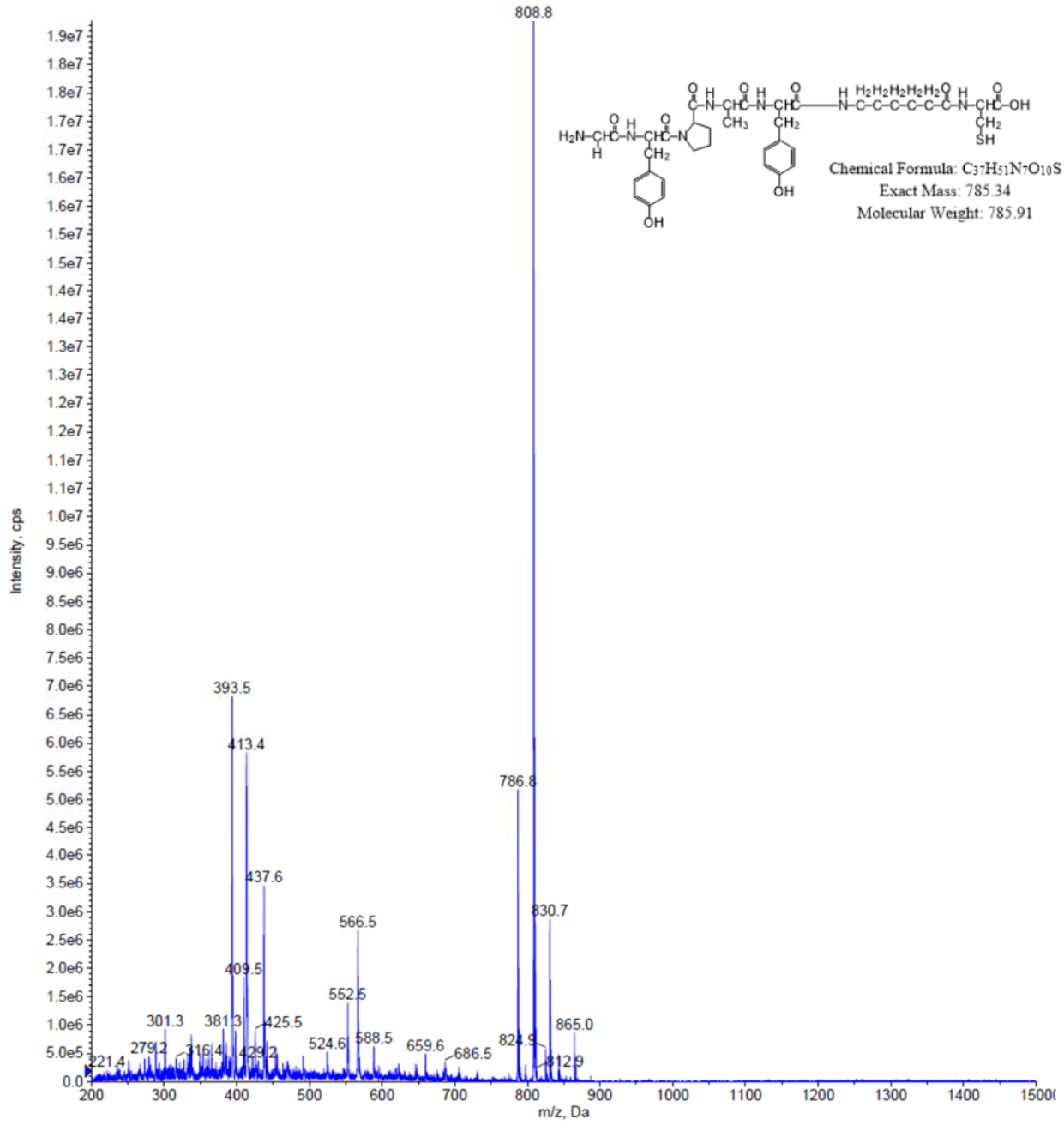

Figure 5.5: MS spectrum of PEP20-Ahx-Cys

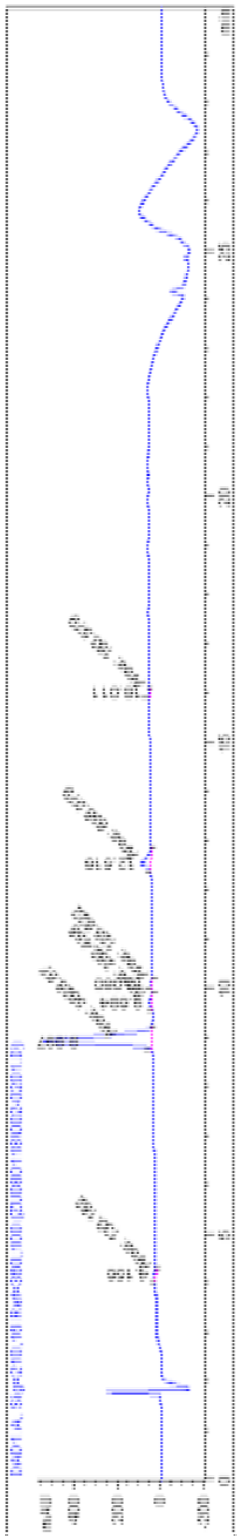

Figure 5.6: HPLC chromatogram of PEP20-Ahx-Cys

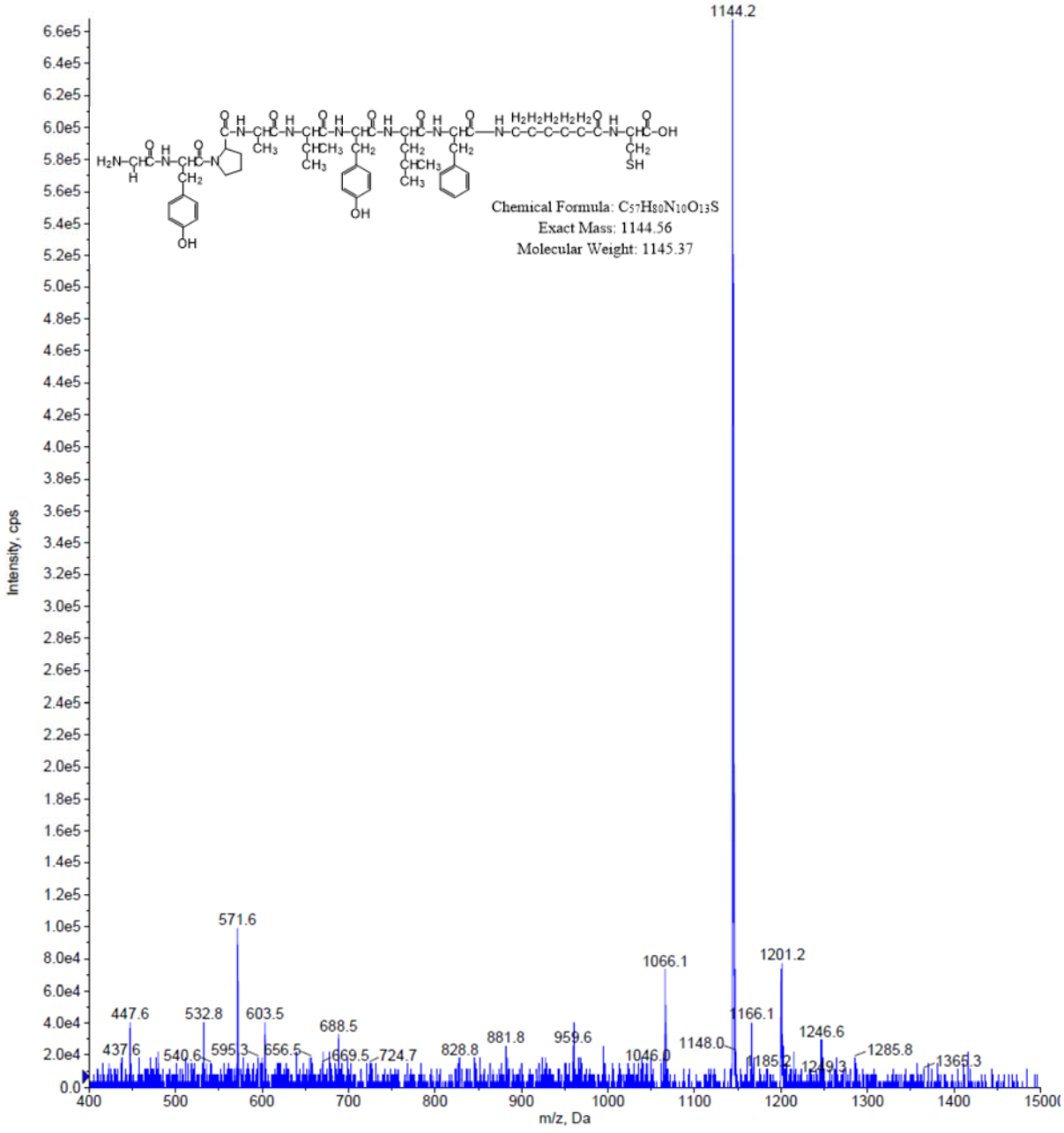

Figure 5.7: MS spectrum of PEP173-Ahx-Cys

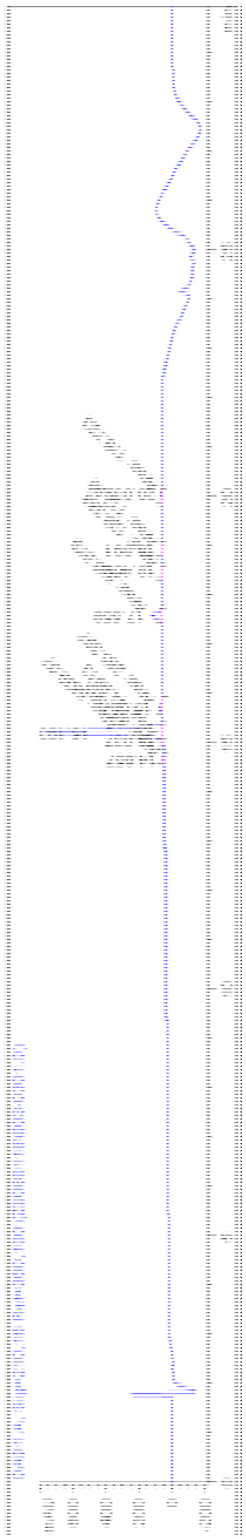

Figure 5.8: HPLC chromatogram of PEP173-Ahx-Cys

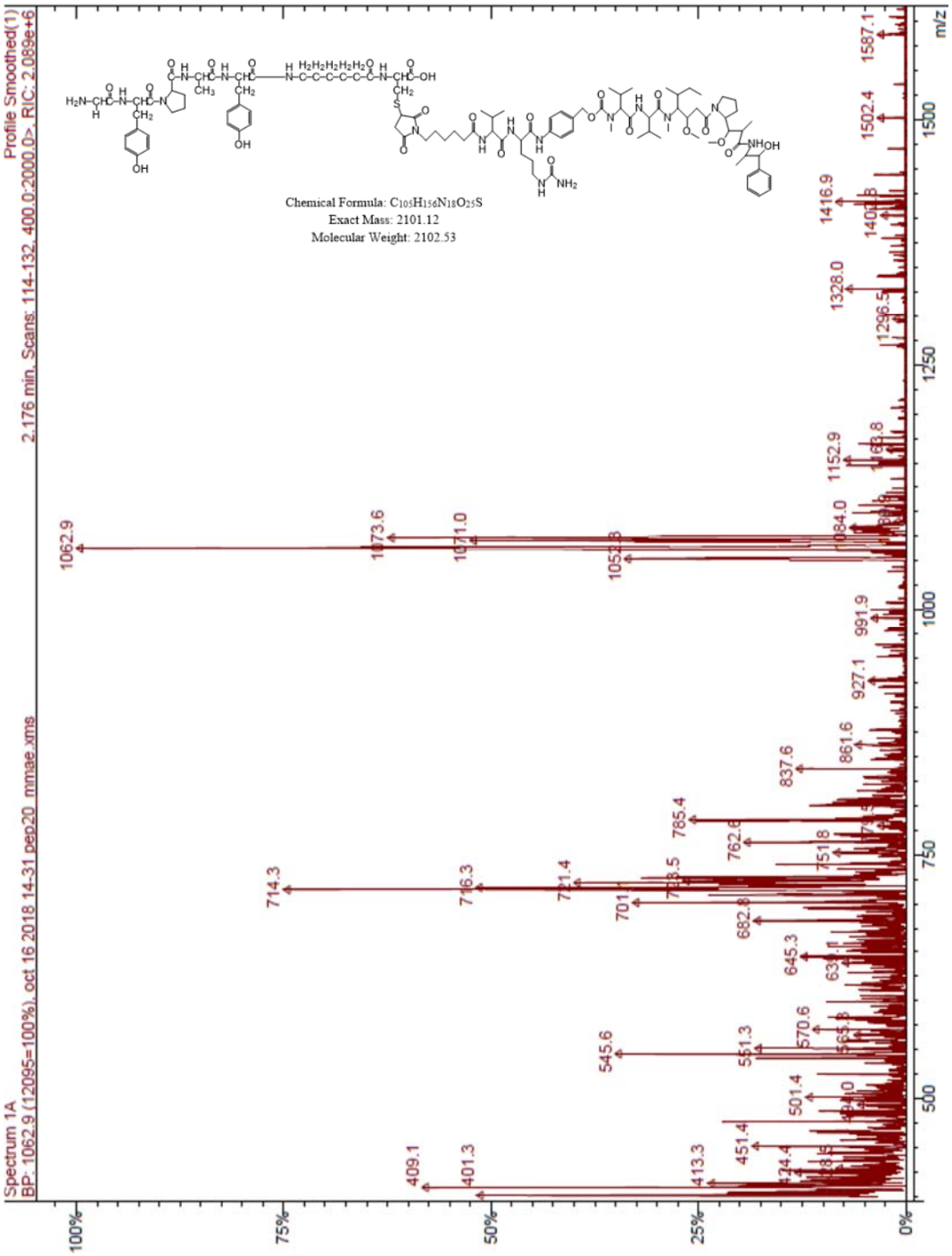

Figure 5.9: MS spectrum of PEP20-MMAE

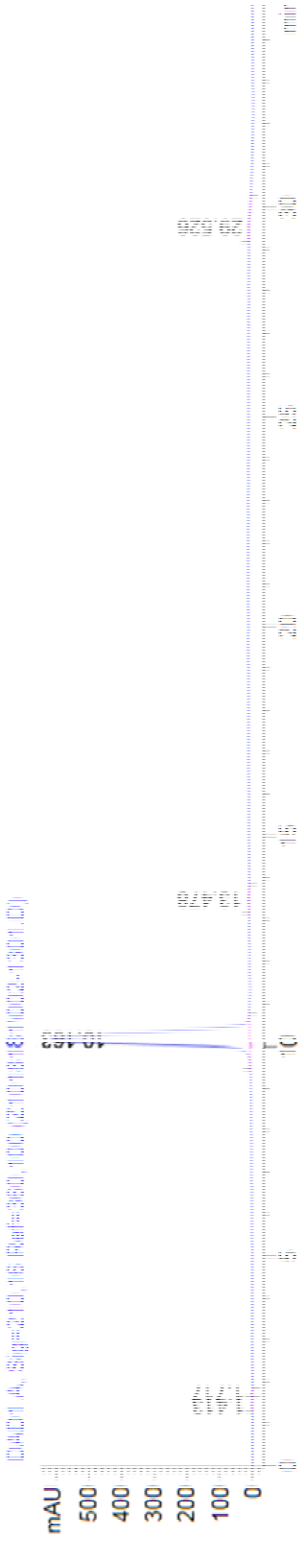

Figure 5.10: HPLC chromatogram of PEP20-MMAE

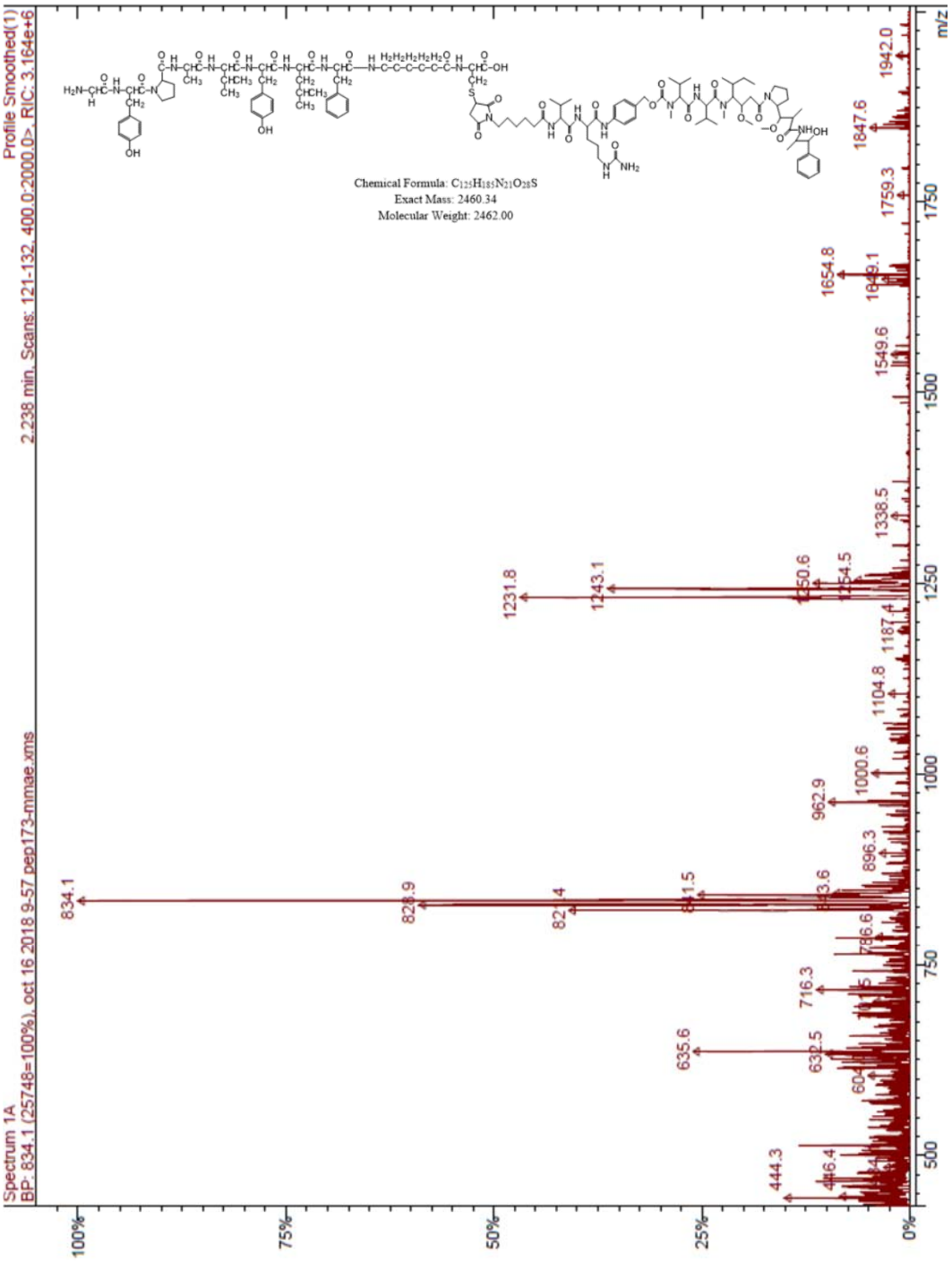

Figure 5.11: MS spectrum of PEP173-MMAE

Figure 5.12: HPLC chromatogram of PEP173-MMAE

5.4.2 In vitro cytotoxicity studies. Cytotoxicity studies were carried out to evaluate the potency of the free drug, and peptide drug conjugates. Percentage cytotoxicity was calculated using sulphorhodamine B assay.

MMAE showed very high potency (low IC50 values) across all three cell lines (Table 5.2). For all three cells lines, PDCs (PEP20-MMAE and PEP173-MMAE) showed significantly lower cytotoxicity than MMAE in the cell culture medium (Figures 5.13, 5.14 and 5.15, and Table 5.2).

PEP20-MMAE showed 5.2 and 4.3 times lower cytotoxicity in CD13 negative MCF-7 and control normal HEK-293 cells, respectively, when compared to that in CD13 positive HT-1080 cells (Figures 5.13, 5.14 and 5.15, and Table 5.2). PEP173-MMAE was found to have approximately 2.4 times less cytotoxicity both in MCF-7 cells and HEK-293 cells as compared to HT-1080 cells (Figures 5.13, 5.14 and 5.15, and Table 5.2). The PDCs seemed to have specificity trend towards CD13 positive HT-1080 cells as evidence by the lower IC50 in the HT-1080 cells. However, as compared to the HT-1080 cells, the drug MMAE was also found to be 4.5 and 8.9 times less cytotoxic (in terms of IC_{50}) in MCF-7 cells and HEK-293 cells, respectively (Figures 5.13, 5.14 and 5.15, and Table 5.2). This indicates that the conjugation of peptide-linker construct to the drug decreased the potency of MMAE rather than improving selectivity.

There could be several reasons behind the lower cytotoxicity of the PDCs as compared to MMAE. One possibility could be higher protein binding of the PDCs or interference by fetal bovine serum present in the cell culture medium in which the cells were incubated with PDCs/drug. Liraglutide, a human glucagon-like peptide-1, was reported to exhibit

approximately 99% serum protein binding in vitro (168). Hsiao IL and Huang YJ observed significantly lower in vitro cytotoxicity of ZnO particles in serum containing medium as compared to the serum free medium (169). A dual targeting NGR-peptide−drug conjugate also showed significantly lower in vitro cytotoxicity than the drug itself in serum containing medium (170). The designed peptides might also lose their targeting ability after conjugating to the linker-drug construct owing to the large size of the construct. The size of the drug-linker construct (mc-vc-PABC-MMAE) is bigger than the peptides. While, the molar weight of PEP20-Ahx-Cys and PEP173-Ahx-Cys are 785.91 and 1145.3 g/mol, respectively, the molar weight of the linker-drug construct is 1316.6 g/mol. It has been reported that conjugation induced perturbations in the peptide structural microenvironment can lead to diminished binding affinity to the target receptor (155). Peng ZH and Kopeček J have shown that the cell penetrating cyclic peptide iRGD (CRGDKGPDC) lose its targeting ability after conjugating to linker-drug (valproic acid) construct (171).

Table 5.2

In-vitro cytotoxicity study data

Cell Line	IC_{50} (nM)		
	MMAE	PEP20-MMAE	PEP173-MMAE
HT-1080 (CD13 +ve)	0.09358 ± 0.01086	92.54 ± 13.38	72.68 ± 9.910
MCF-7 (CD13 -ve)	0.4250 ± 0.08300	477.9 ± 89.67	175.0 ± 21.30
HEK-293 (normal cell line)	0.8354 ± 0.1101	399.7 ± 51.89	172.8 ± 23.93

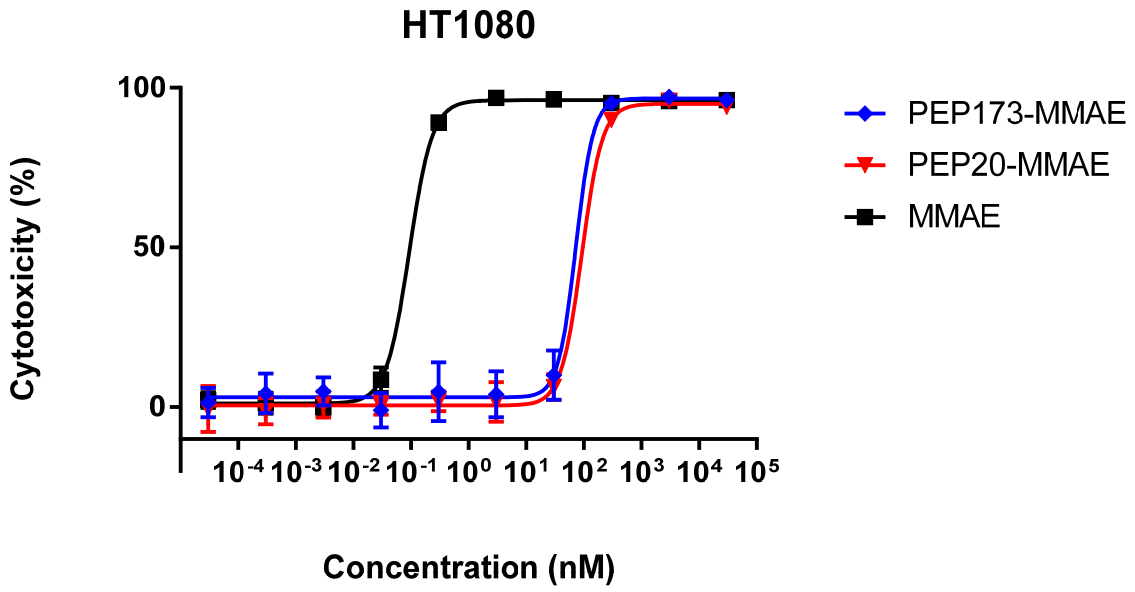

Figure 5.13: Percent cytotoxicity of MMAE, PEP20-MMAE, and PEP173-MMAE in HT-1080 cells

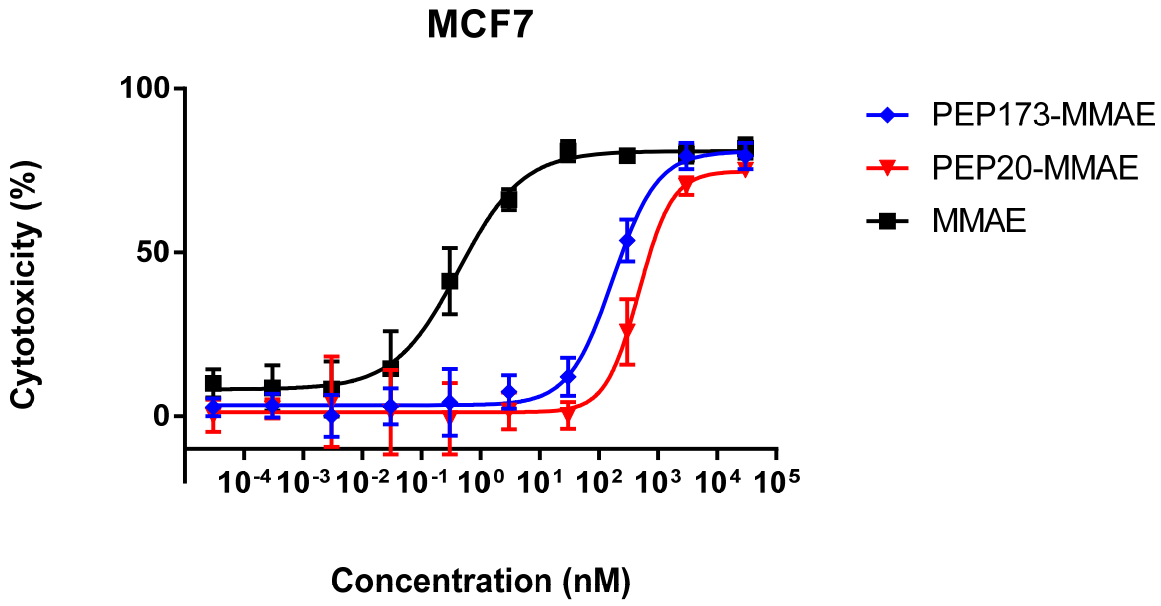

Figure 5.14: Percent cytotoxicity of MMAE, PEP20-MMAE, and PEP173-MMAE in MCF-7 cells

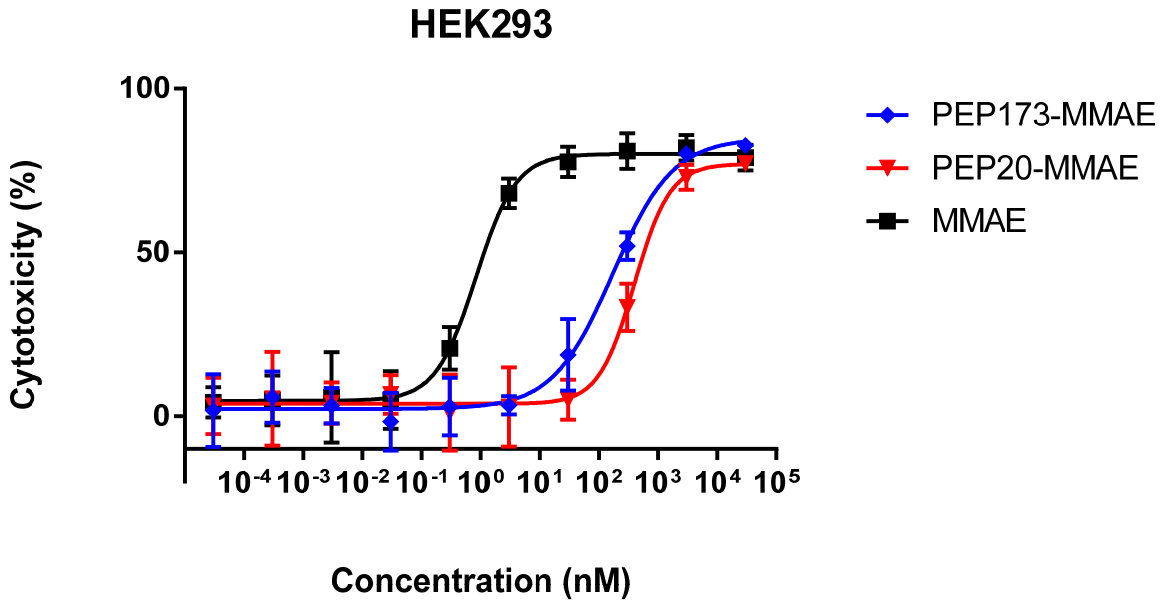

Figure 5.15: Percent cytotoxicity of MMAE, PEP20-MMAE, and PEP173-MMAE in HEK-293 cells

5.4.3 In vivo anti-tumor efficacy study. To select the therapeutic doses of the compounds in the in vivo study a maximum tolerated dose (MTD) was determined. MMAE was injected into healthy athymic nude mice at doses ranging from 0.375 mg/kg to 1.5 mg/kg (n=1 for all doses, except for 0.70 mg/kg n=2). General health and body weight of the mice were monitored for 15 days after injection (Figure 5.16). Doses up to 0.70 mg/kg of MMAE were well tolerated with no apparent sign of toxicity. At 1.0 mg/kg dose, the mouse experienced around 20% weight loss within 6 days of injection and then started regaining weight. The mouse returned to initial body weight by day 15. The mouse receiving 1.5 mg/kg of MMAE lost more than 30% of the body weight by day 6 at which point the mouse was euthanized. Thus, the MTD of MMAE in female athymic nude mice (4-6 weeks old) was determined to be between 1.0 mg/kg and 1.5 mg/kg. The maximum tolerated dose (MTD) of dolastatin 10 in mice was reported to be approximately 0.45 mg/kg (172). Dolastatin 10 is a cytotoxic agent whose structure is similar to MMAE (173). Francisco et al reported the MTD of MMAE in SCID mice to be between 0.50 mg/kg and 1.0 mg/kg (163).

For this anti-tumor efficacy study, 975 nmol/kg, which is equivalent to 0.70 mg/kg of MMAE, was selected as the treatment dose (MMAE, PEP20-MMAE, and PEP173-MMAE). Treatment was started when the average tumor volume reached approximately 100 mm^3 (9 or 12 days after tumor cell injection). Mice were administered with the drug or PBS treatment every 4 days for a total of 4 doses (q4d x 4). In the mice treated with only PBS, the tumor grew rapidly and reached approximately 450 mm3 by day 28 after tumor implantation (Figure 5.17). MMAE, PEP20-MMAE, and PEP173-MMAE all showed almost complete tumor regression during the study (Figure 5.17). PEP20-MMAE and PEP173-MMAE showed slightly higher tumor regression than MMAE, but the difference was not significant. As described before in section

5.4.2, the insignificant difference in antitumor activity between the drug MMAE and PDCs may also be due to higher plasma protein binding of the PDCs or the diminished targeting ability of the peptides after conjugating with the larger linker-drug construct. Additionally the degradation of PDCs in circulation by different enzymes may have contributed to this observation. Enzymatic degradation in systemic circulation has long been one of the major challenges for the peptide based drugs (174).

Although, the PDCs have comparable anti-cancer efficacy in mouse as compared to the drug MMAE, the groups treated with PEP20-MMAE and PEP173-MMAE showed a body weight increase of 4% and 8%, respectively, even after fourth dose (25 and 28 days after tumor implantation) (Figure 5.18). On the other hand, the drug MMAE treated group lost body weight after dosing started and had a maximum weight loss of 10% after 28 days of tumor implantation (Figure 5.18). Weight loss is one of major adverse effects of anticancer agents due to high and non-selective cytotoxic potency (175). The PDCs (PEP20-MMAE and PEP173-MMAE) have shown significantly reduced side effects in terms of weight loss.

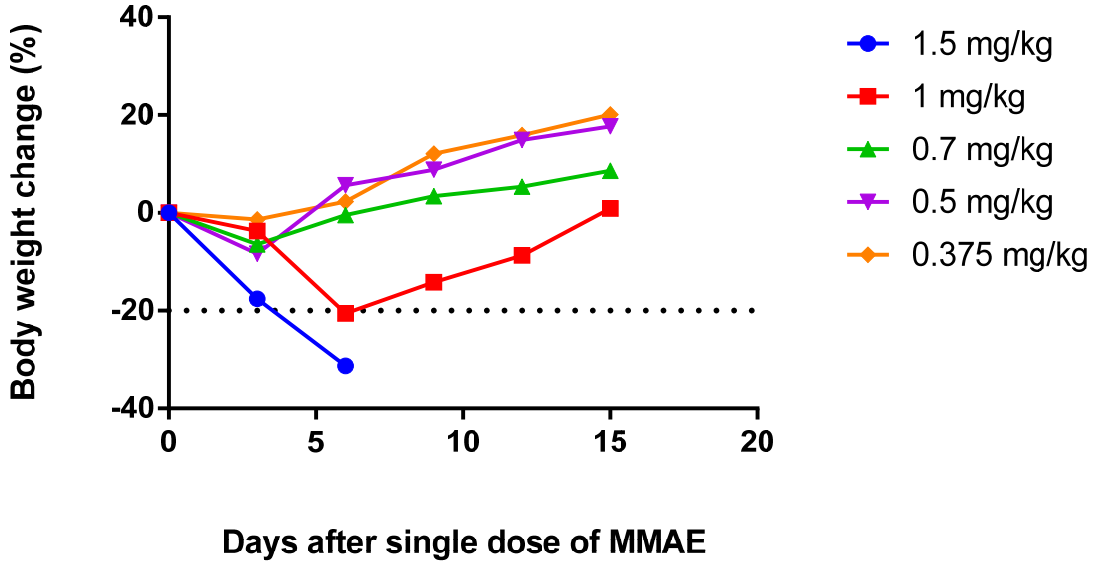

Figure 5.16: Maximum tolerated dose (MTD) study for the drug MMAE

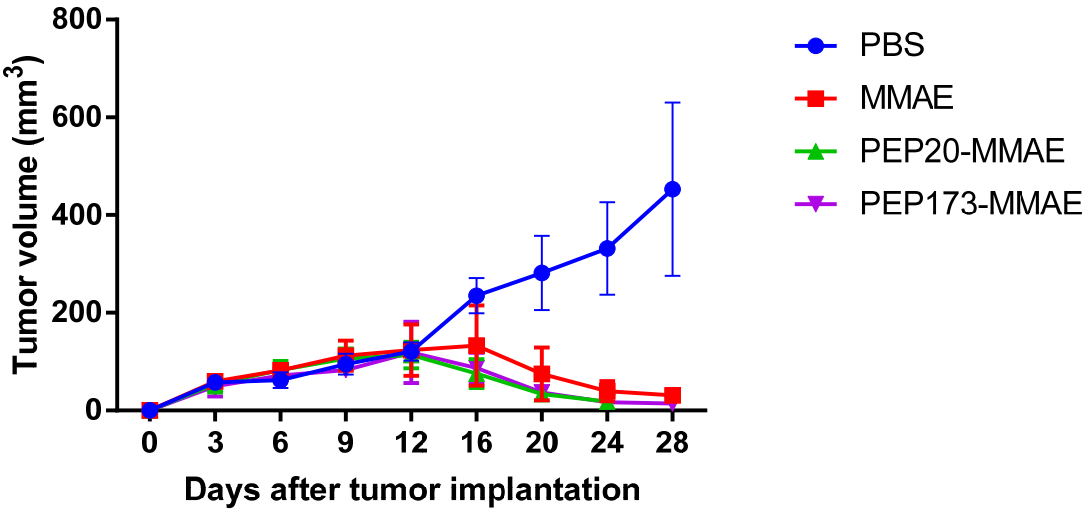

Figure 5.17: Tumor volume vs days after tumor implantation

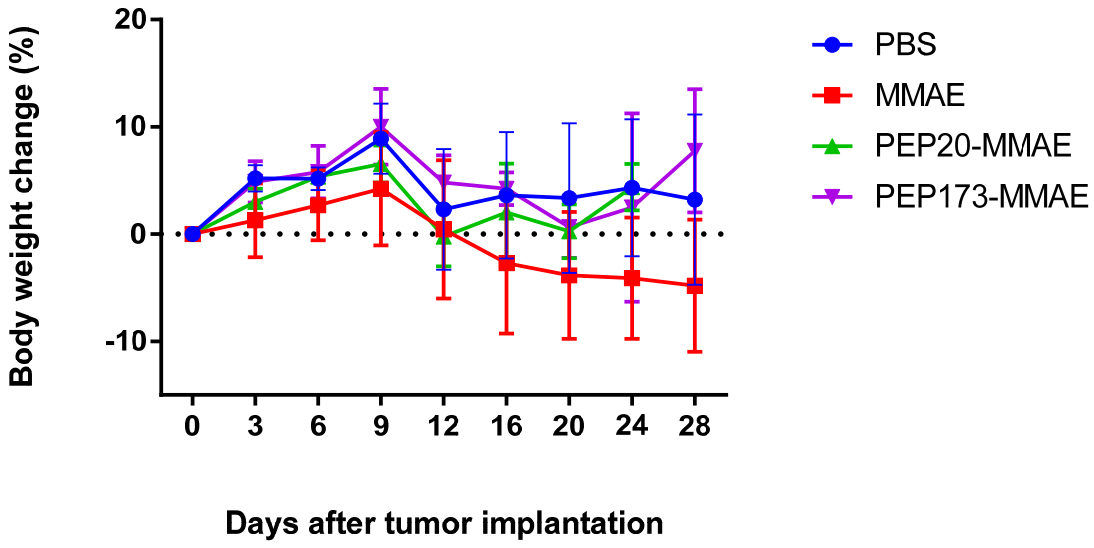

Figure 5.18: Body weight change (%) vs days after tumor implantation

Chapter 6: Summary and Conclusions

Structure based design plays a crucial role in developing novel molecules/drugs. This approach to ligand design utilizes three-dimensional information of a target protein to improve recognition and discrimination by identifying favorable residue interactions. The first therapeutic peptide designed from crystal structure analysis was enfuvirtide, which received the US-FDA approval as an anti-HIV peptide in 2003 (76). Foy et al (176) designed vaccines against EGFR by selecting different regions from the crystal structure of the protein. A VEGFR-3 targeted peptide ligand was developed by analyzing the crystal structure of the extracellular domain of VEGFR-3 (177). Recently, Joshi et al (178) reported the design of a peptide that inhibits the enzymatic activity of CD13. The peptide was developed by a substrate-based approach where crystal structures of CD13 with different amino acids were solved to determine the structural basis of the substrate specificity. The structural insights of the protein-ligand interaction obtained from the crystal structures have culminated in several computational peptide design approaches. However, it is quite evident that most of these approaches are based on either sequence motifs or protein complexes (59). A rational design method based on the predicted interaction between target and ligand molecule will significantly speed up this development process.

In this study, a Knob-Socket analysis of protein packing structure was used to rationally design peptide ligands with specificity for the CD13 active site. The method begins with mapping the target protein binding site to characterize the amino acid packing arrangements in terms of three residue sockets on the target receptor that pack ligand knob residues- in this study the prototype receptor used was CD13. From the sockets identified as important for ligand binding on the surface of CD13, a set of knobs with high propensity interactions were selected.

This set of amino acids enabled peptide sequences to be designed rationally by predicting the packing of the peptide ligand at the binding site. The peptides were screened in silico by a docking programs to identify the best peptide candidates.

From the design approach, 412 potential peptide sequences were reduced to just 3 candidates. The three identified peptides showed selective binding to human CD13 receptor in vitro. In the enzymatic assay, the designed peptides exhibited higher CD13 catalysis inhibition than the CNGRC (C1-C5) peptide (NGR-2C). NGR-2C showed significantly reduced inhibition of CD13 enzymatic activity within 30 minutes (Figure 4.6), suggestive of its' unstable physicochemical characteristics at the assay condition. This phenomenon is not unexpected since the NGR-2C peptide has been reported to lose CD13 binding ability rapidly through deamidation of the Asn residue (179). The success of therapeutic peptides or peptide ligands depends on the delivery of their active form at the target site. The physicochemical stability of the peptides is largely influenced by the amino acid composition and sequences of the peptides (180-182). In our rational design method peptides having potentially unstable amino acids or sequences can be excluded at the very beginning of the development works during peptide screening phase.

The three identified peptides [PEP173 (GYPAVYLF), PEP20 (GYPAY) and PEP24 (GFPAY)] showed 10 – 20 times higher binding affinity (K_i) towards hCD13 as compared to NGR-2C peptide (773 μM) (Table 4.2). In other reported studies, IC_{50} of the NGR-2C peptide was 300-515 μM, and the K_i was 134μM (145, 146). Unlike the fluorescence-based method used in the present study, those reported experiments used either L-leucine-p-nitroanilide or L-alanine-p-nitroanilide as the catalysis substrate, and the formation of p-nitroaniline product was measured by the absorbance at 405 nm. The compositions of the assay buffer were also different

in these studies. But generally, fluorescence-based detection techniques are more sensitive than the absorbance-based methods (183).

Ranking of the three peptides (PEP173, PEP20 and PEP24, respectively) according to their experimental binding affinities, K_i, (38.8 μM, 54.0 μM, 74.3 μM, respectively) was in agreement with the ranking predicted by the MOE docking scores (-16.2385 kcal/mol, -13.9095 kcal/mol, -11.9234 kcal/mol, respectively). Additionally, as predicted by the AutoDock Vina (Figure 2.8 and Table 2.4), PEP20, PEP24 and PEP173 were found to bind to the catalytic active site of CD13 in the experimental steady-state enzyme kinetic assay (Figures 4.7 and 4.8, and Table 4.2). AutoDock Vina also accurately predicted the distant binding sites of the nonspecific control peptides [PEP293 (GYPAYVEF) and PEP308 (GFPAVYEF)] as experimentally confirmed by their observed noncompetitive inhibition mode in enzymatic assay (Figure 4.9 and Table 4.2). These findings suggest that the combination of multiple docking platforms in our design method could accurately predict the binding characteristics (affinity ranking and binding site) of the designed peptide ligands. Data from the cell binding and confocal microscopy assays (Figures 4.11 – 4.16) further demonstrated that the designed peptides could recognize and selectively bind to the CD13 on the cell membrane.

The NGR-motif containing peptide ligand (i.e. CNGRC) for CD13 was first identified by an in vivo phage display selection study in a mouse model (98, 103). Thus, the prototype target, CD13 receptor, allowed us to compare the performance of our rational peptide ligand design method with the structure free design technique in terms of in vitro binding affinity and selectivity of the identified peptide ligands. A typical in vivo phage display screening starts with generating a large library of phage particles expressing a wide array of peptides on their surface. The size of the library can reach up to 100,000,000 – 1,000,000,000 different variants (184). The

phage display library proceeds through several enrichment screening cycles, which involves binding, phage amplification, and plaque isolation. The final step is sequencing. Additional validation of the interaction may involve immunohistochemistry, real time PCR, bio-distribution and homing inhibition studies (185). On the other hand, our design method rationally identified CD13 selective peptide ligands having better in vitro binding affinity with much less screening and experimental complexity.

The in vitro cytotoxicity studies of the designed peptide-drug conjugates (PEP20-MMAE and PEP173-MMAE) indicated that the conjugation of peptide-linker construct to the drug might have just decreased the potency of MMAE rather than providing selectivity. This was further observed in the in vivo anti-tumor efficacy studies where the peptide-drug conjugates (PDCs) and the drug MMAE showed insignificant difference in antitumor activity. One possible reason could be higher protein binding of the PDCs or interference by fetal bovine serum present in the cell culture medium in which the cells were incubated with PDCs or drug for the cytotoxicity assays. Secondly, the peptides might have lost their targeting ability after conjugating to the linker-drug construct owing to the large size of the construct. The size of the drug-linker construct (mc-vc-PABC-MMAE) is bigger than both the peptides. Therefore, there is a possibility that the bigger and hydrophobic linker-drug moiety might have altered the binding properties of the CD13 targeted peptides. One additional reason could be the degradation of PDCs in circulation by different enzymes. van Hensbergen et al previously reported the CD13 targeted peptide-drug conjugate, Doxorubicin-CNGRC (C1-C5), to show no added advantage as compared to the drug, doxorubicin, in terms of in vitro cytotoxicity and in vivo antitumor effects (186). In the in vivo study, weight loss was higher in the doxorubicin treated group as compared to PDC group (186).

In conclusion, in the present study a rational peptide ligand design method based on the Knob-Socket model of protein packing was developed and successfully employed to identify 3 novel peptide ligands for the model receptor, CD13. The identified peptides showed good selectivity and higher binding affinity towards the hCD13 receptor in vitro as compared to the known peptide ligand CNGRC (C1-C5). Our study demonstrated the feasibility of the rational method to design novel peptide ligands. Most importantly, the rational method excluded the need of long experimental screening of a vast library of peptide sequences, and thus significantly reduces the time and resources traditionally employed to identify such molecules.

The limited effectiveness of peptide drug conjugates in the in vivo mice tumor model suggested the need to improve the designed peptide-MMAE drug conjugates. Future research should focus on achieving the optimal chemical configuration of the conjugates for in vivo targeting and receptor mediated cellular uptake. The current computational simulation studies is limited to project binding of the peptides to the target protein. In future, peptide design with higher number of amino acids in the targeting moiety, and smaller linker-drug construct (especially small molecules) may be used to conserve the target binding ability of the PDCs. Serum stability and plasma protein binding of the PDCs should be carried out to explain a more detailed in vivo efficacy study.

References

1. Hillery AM, Lloyd AW, Swarbrick J. Drug delivery and targeting for pharmacists and pharmaceutical scientists. London; New York: Taylor & Francis; 2001.

2. Torchilin VP. European journal of pharmaceutical sciences. European journal of pharmaceutical sciences. 2000 October 1,;11:S91.

3. Key Targeting Approaches for Pharmaceutical Drug Delivery [Internet]. [cited Jan 9, 2019]. Available from: http://www.americanpharmaceuticalreview.com/Featured-Articles/148744-Key-Targeting-Approaches-for-Pharmaceutical-Drug-Delivery/.

4. Fahmy TM, Fong PM, Goyal A, Saltzman WM. Targeted for drug delivery. Materials Today. 2005;8(8):18-26.

5. Peer D, Karp JM, Hong S, Farokhzad OC, Margalit R, Langer R. Nanocarriers as an emerging platform for cancer therapy. Nat Nanotechnol. 2007 Dec;2(12):751-60.

6. Gregoriadis G. Targeting of drugs. Nature. 1977;265(5593):407-11.

7. Poste G, Kirsh R. Site–Specific (Targeted) Drug Delivery in Cancer Therapy. Nature Biotechnology. 1983;1(10):869-78.

8. Francis GE(. Drug targeting: strategies, principles and applications. Totowa, N.J. : Humana Press; 2000.

9. Formulation Considerations and Applications of Solid Lipid Nanoparticles [Internet]. [cited Jan 9, 2019]. Available from: http://www.americanpharmaceuticalreview.com/Featured-Articles/131176-Formulation-Considerations-and-Applications-of-Solid-Lipid-Nanoparticles/.

10. Williams AS, Camilleri JP, Goodfellow RM, Williams BD. A SINGLE INTRA-ARTICULAR INJECTION OF LIPOSOMALLY CONJUGATED METHOTREXATE SUPPRESSES JOINT INFLAMMATION IN RAT ANTIGEN-INDUCED ARTHRITIS. Rheumatology (Oxford). 1996 /08/01;35(8):719-24.

11. Marchal-Heussler L, Sirbat D, Hoffman M, Maincent P. Poly(epsilon-caprolactone) nanocapsules in carteolol ophthalmic delivery. Pharm Res. 1993 Mar;10(3):386-90.

12. El C, Mateeva LS, Mazaev AV. Intracoronary administration of fibrinolysin in acute myocardial infarction. Ter Arkh. 1976;48:8-19.

13. Jain RK. Transport of molecules across tumor vasculature. Cancer Metastasis Rev. 1987;6(4):559-93.

14. Palmer TN, Caldecourt MA, Kingaby RO. Liposomal drug delivery in chronic ischaemia. Biochem Soc Trans. 1984 Apr;12(2):344-5.

15. Yuan F, Dellian M, Fukumura D, Leunig M, Berk DA, Torchilin VP, et al. Vascular permeability in a human tumor xenograft: molecular size dependence and cutoff size. Cancer Res. 1995 Sep 01,;55(17):3752-6.

16. Gabizon AA. Selective tumor localization and improved therapeutic index of anthracyclines encapsulated in long-circulating liposomes. Cancer Res. 1992;52(4):891-6.

17. Weissig V, Whiteman KR, Torchilin VP. Accumulation of protein-loaded long-circulating micelles and liposomes in subcutaneous Lewis lung carcinoma in mice. Pharm Res. 1998;15(10):1552-6.

18. Torchilin VP, Narula J, Halpern E, Khaw BA. Poly (ethylene glycol)-coated anti-cardiac myosin immunoliposomes: factors influencing targeted accumulation in the infarcted myocardium. Biochimica et Biophysica Acta (BBA)-Biomembranes. 1996;1279(1):75-83.

19. Ganta S, Devalapally H, Shahiwala A, Amiji M. A review of stimuli-responsive nanocarriers for drug and gene delivery. J Control Release. 2008 Mar 20,;126(3):187-204.

20. Weinstein JN, Magin RL, Yatvin MB, Zaharko DS. Liposomes and local hyperthermia: selective delivery of methotrexate to heated tumors. Science. 1979;204(4389):188-91.

21. Torchilin VP, Zhou F, Huang L. pH-sensitive liposomes. J Liposome Res. 1993;3(2):201-55.

22. Widder KJ, Marino PA, Morris RM, Senyei AE. Targeting antineoplastic agents using magnetic albumin microspheres. Targeted Drugs.Wiley, New York. 1983:201-30.

23. Torchilin VP, Papisov MI, Orekhova NM, Belyaev AA, Petrov AD, Ragimov SE. Magnetically driven thrombolytic preparation containing immobilized streptokinase-targeted transport and action. Pathophysiology of Haemostasis and Thrombosis. 1988;18(2):113-6.

24. Vitetta ES, Krolick KA, Miyama-Inaba M, Cushley W, Uhr JW. Immunotoxins: a new approach to cancer therapy. Science. 1983:644-50.

25. Torchilin VP. Targeted pharmaceutical nanocarriers for cancer therapy and imaging. AAPS J. 2007 May 11,;9(2):128.

26. Liu R, Kay BK, Jiang S, Chen S. Nanoparticle Delivery: Targeting and Nonspecific Binding. MRS Bulletin. 2009 /06;34(6):432-40.

27. Friedman AD, Claypool SE, Liu R. The Smart Targeting of Nanoparticles. Curr Pharm Des. 2013 Jan 1,;19(35):6315-29.

28. Herrington-Symes AP, Farys M, Khalili H, Brocchini S. Antibody fragments: Prolonging circulation half-life special issue-antibody research. Advances in Bioscience and Biotechnology. 2013 -05-27;04:689.

29. Schmidt MM, Wittrup KD. A modeling analysis of the effects of molecular size and binding affinity on tumor targeting. Mol Cancer Ther. 2009 Oct;8(10):2861-71.

30. Yuan F, Dellian M, Fukumura D, Leunig M, Berk DA, Torchilin VP, et al. Vascular permeability in a human tumor xenograft: molecular size dependence and cutoff size. Cancer Res. 1995 Sep 01,;55(17):3752-6.

31. Srinivasarao M, Low PS. Ligand-Targeted Drug Delivery. Chem Rev. 2017 Oct 11,;117(19):12133-64.

32. Low PS, Henne WA, Doorneweerd DD. Discovery and development of folic-acid-based receptor targeting for imaging and therapy of cancer and inflammatory diseases. Acc Chem Res. 2008 Jan;41(1):120-9.

33. Zhao X, Li H, Lee RJ. Targeted drug delivery via folate receptors. Expert Opin Drug Deliv. 2008 Mar;5(3):309-19.

34. Mach RH, Huang Y, Freeman RA, Wu L, Vangveravong S, Luedtke RR. Conformationally-flexible benzamide analogues as dopamine D3 and sigma 2 receptor ligands. Bioorg Med Chem Lett. 2004 Jan 05,;14(1):195-202.

35. Banerjee R, Tyagi P, Li S, Huang L. Anisamide-targeted stealth liposomes: a potent carrier for targeting doxorubicin to human prostate cancer cells. Int J Cancer. 2004 Nov 20,;112(4):693-700.

36. Cruz LJ, Tacken PJ, Pots JM, Torensma R, Buschow SI, Figdor CG. Comparison of antibodies and carbohydrates to target vaccines to human dendritic cells via DC-SIGN. Biomaterials. 2012 Jun;33(16):4229-39.

37. Paul WE. Fundamental immunology. New York: Raven Press; 1989.

38. Jr CAJ, Travers P, Walport M, Shlomchik MJ, Jr CAJ, Travers P, et al. Immunobiology. 5th ed. Garland Science; 2001.

39. Alley SC, Okeley NM, Senter PD. Antibody–drug conjugates: targeted drug delivery for cancer. Current Opinion in Chemical Biology. 2010;14(4):529-37.

40. Liu X, Wang Y, Hnatowich DJ. A nanoparticle for tumor targeted delivery of oligomers. Methods Mol Biol. 2011;764:91-105.

41. Popov J, Kapanen AI, Turner C, Ng R, Tucker C, Chiu G, et al. Multivalent rituximab lipid nanoparticles as improved lymphoma therapies: indirect mechanisms of action and in vivo activity. Nanomedicine (Lond). 2011 Nov;6(9):1575-91.

42. Yang K, Zhang F, Tang H, Zhao C, Cao Y, Lv X, et al. In-vivo imaging of oral squamous cell carcinoma by EGFR monoclonal antibody conjugated near-infrared quantum dots in mice. Int J Nanomedicine. 2011;6:1739-45.

43. Skerra A. Alternative non-antibody scaffolds for molecular recognition. Curr Opin Biotechnol. 2007 Aug;18(4):295-304.

44. Vazquez-Lombardi R, Phan TG, Zimmermann C, Lowe D, Jermutus L, Christ D. Challenges and opportunities for non-antibody scaffold drugs. Drug Discov Today. 2015 Oct;20(10):1271-83.

45. Jayasena SD. Aptamers: an emerging class of molecules that rival antibodies in diagnostics. Clin Chem. 1999 Sep;45(9):1628-50.

46. Khati M. The future of aptamers in medicine. J Clin Pathol. 2010 Jun;63(6):480-7.

47. Lopes de Campos, Walter Rangel, Coopusamy D, Morris L, Mayosi BM, Khati M. Cytotoxicological analysis of a gp120 binding aptamer with cross-clade human immunodeficiency virus type 1 entry inhibition properties: comparison to conventional antiretrovirals. Antimicrob Agents Chemother. 2009 Jul;53(7):3056-64.

48. Pagratis NC, Bell C, Chang YF, Jennings S, Fitzwater T, Jellinek D, et al. Potent 2'-amino-, and 2'-fluoro-2'-deoxyribonucleotide RNA inhibitors of keratinocyte growth factor. Nat Biotechnol. 1997 Jan;15(1):68-73.

49. Wilson N. Chapter 2 - Market Evolution of Topical Anti-aging Treatments. In: Dayan N, editor. Skin Aging Handbook. Norwich, NY: William Andrew Publishing; 2009. p. 15-34.

50. IUPAC Gold Book - amino-acid residue in a polypeptide [Internet]. [cited Jan 13, 2019]. Available from: http://goldbook.iupac.org/html/A/A00279.html.

51. David A. Peptide ligand-modified nanomedicines for targeting cells at the tumor microenvironment. Adv Drug Deliv Rev. 2017 09 15,;119:120-42.

52. Borghouts C, Kunz C, Groner B. Current strategies for the development of peptide-based anti-cancer therapeutics. Journal of peptide science: an official publication of the European Peptide Society. 2005;11(11):713-26.

53. Lee S, Xie J, Chen X. Peptide-based probes for targeted molecular imaging. Biochemistry. 2010;49(7):1364-76.

54. Pasqualini R, Ruoslahti E. Organ targeting in vivo using phage display peptide libraries. Nature. 1996;380(6572):364.

55. Ruoslahti E. Peptides as targeting elements and tissue penetration devices for nanoparticles. Adv Mater. 2012;24(28):3747-56.

56. Thayer AM. Improving peptides. Chemical & Engineering News. 2011;89(22):13.

57. Sugahara KN, Teesalu T, Karmali PP, Kotamraju VR, Agemy L, Girard OM, et al. Tissue-penetrating delivery of compounds and nanoparticles into tumors. Cancer cell. 2009;16(6):510-20.

58. McDonald DM, Baluk P. Significance of Blood Vessel Leakiness in Cancer. Cancer Res. 2002 -09-15 00:00:00;62(18):5381-5.

59. Vanhee P, van der Sloot, Almer M., Verschueren E, Serrano L, Rousseau F, Schymkowitz J. Computational design of peptide ligands. Trends Biotechnol. 2011 May;29(5):231-9.

60. Aina OH, Liu R, Sutcliffe JL, Marik J, Pan C, Lam KS. From combinatorial chemistry to cancer-targeting peptides. Molecular pharmaceutics. 2007;4(5):631-51.

61. Liu R, Enstrom AM, Lam KS. Combinatorial peptide library methods for immunobiology research. Exp Hematol. 2003;31(1):11-30.

62. Liu T, Qian Z, Xiao Q, Pei D. High-throughput screening of one-bead-one-compound libraries: identification of cyclic peptidyl inhibitors against calcineurin/NFAT interaction. ACS combinatorial science. 2011;13(5):537-46.

63. Cwirla SE, Peters EA, Barrett RW, Dower WJ. Peptides on phage: a vast library of peptides for identifying ligands. Proceedings of the National Academy of Sciences. 1990;87(16):6378-82.

64. Sela-Culang I, Kunik V, Ofran Y. The structural basis of antibody-antigen recognition. Frontiers in immunology. 2013;4:302.

65. Laune D, Molina F, Ferrieres G, Mani J, Cohen P, Simon D, et al. Systematic exploration of the antigen binding activity of synthetic peptides isolated from the variable regions of immunoglobulins. J Biol Chem. 1997;272(49):30937-44.

66. Kunik V, Peters B, Ofran Y. Structural consensus among antibodies defines the antigen binding site. PLoS computational biology. 2012;8(2):e1002388.

67. Lam KS, Salmon SE, Hersh EM, Hruby VJ, Kazmierski WM, Knapp RJ. A new type of synthetic peptide library for identifying ligand-binding activity. Nature. 1991;354(6348):82.

68. Lam KS, Liu R, Miyamoto S, Lehman AL, Tuscano JM. Applications of one-bead one-compound combinatorial libraries and chemical microarrays in signal transduction research. Acc Chem Res. 2003;36(6):370-7.

69. Salmon SE, Liu-Stevens RH, Zhao Y, Lebl M, Krchňák V, Wertman K, et al. High-volume cellular screening for anticancer agents with combinatorial chemical libraries: a new methodology. Mol Divers. 1996;2(1-2):57-63.

70. Cho C, Behnam Azad B, Luyt LG, Lewis JD. High-Throughput Screening of One-Bead–One-Compound Peptide Libraries Using Intact Cells. ACS combinatorial science. 2013;15(8):393-400.

71. Aina OH, Marik J, Gandour-Edwards R, Lam KS. Near-infrared optical imaging of ovarian cancer xenografts with novel α3-integrin binding peptide "OA02". Molecular imaging. 2005;4(4):7290.2005. 05169.

72. Smith GP. Filamentous fusion phage: novel expression vectors that display cloned antigens on the virion surface. Science. 1985;228(4705):1315-7.

73. Barry MA, Dower WJ, Johnston SA. Toward cell–targeting gene therapy vectors: Selection of cell–binding peptides from random peptide–presenting phage libraries. Nat Med. 1996;2(3):299.

74. Christianson DR, Ozawa MG, Pasqualini R, Arap W. Techniques to decipher molecular diversity by phage display. In: Cardiovascular Proteomics. Springer; 2007. p. 385-406.

75. Watt PM. Screening for peptide drugs from the natural repertoire of biodiverse protein folds. Nat Biotechnol. 2006 Feb;24(2):177-83.

76. Naider F, Anglister J. Peptides in the treatment of AIDS. Current Opinion in Structural Biology. 2009;19(4):473-82.

77. Moellering RE, Cornejo M, Davis TN, Del Bianco C, Aster JC, Blacklow SC, et al. Direct inhibition of the NOTCH transcription factor complex. Nature. 2009 Nov 12,;462(7270):182-8.

78. Schafmeister CE, Po J, Verdine GL. An All-Hydrocarbon Cross-Linking System for Enhancing the Helicity and Metabolic Stability of Peptides. J Am Chem Soc. 2000 June 1,;122(24):5891-2.

79. Walensky LD, Kung AL, Escher I, Malia TJ, Barbuto S, Wright RD, et al. Activation of apoptosis in vivo by a hydrocarbon-stapled BH3 helix. Science. 2004 Sep 03,;305(5689):1466-70.

80. Reina J, Lacroix E, Hobson SD, Fernandez-Ballester G, Rybin V, Schwab MS, et al. Computer-aided design of a PDZ domain to recognize new target sequences. Nat Struct Biol. 2002 Aug;9(8):621-7.

81. van der Sloot, Almer M., Tur V, Szegezdi E, Mullally MM, Cool RH, Samali A, et al. Designed tumor necrosis factor-related apoptosis-inducing ligand variants initiating apoptosis exclusively via the DR5 receptor. Proc Natl Acad Sci U S A. 2006 Jun 06,;103(23):8634-9.

82. Smith CA, Kortemme T. Structure-based prediction of the peptide sequence space recognized by natural and synthetic PDZ domains. J Mol Biol. 2010 Sep 17,;402(2):460-74.

83. Raveh B, London N, Schueler-Furman O. Sub-angstrom modeling of complexes between flexible peptides and globular proteins. Proteins. 2010 Jul;78(9):2029-40.

84. King CA, Bradley P. Structure-based prediction of protein-peptide specificity in Rosetta. Proteins. 2010 Dec;78(16):3437-49.

85. Petsalaki E, Stark A, García-Urdiales E, Russell RB. Accurate prediction of peptide binding sites on protein surfaces. PLoS Comput Biol. 2009 Mar;5(3):e1000335.

86. Abe K, Kobayashi N, Sode K, Ikebukuro K. Peptide ligand screening of alpha-synuclein aggregation modulators by in silico panning. BMC Bioinformatics. 2007 Nov 16,;8:451.

87. Unal EB, Gursoy A, Erman B. VitAL: Viterbi algorithm for de novo peptide design. PLoS ONE. 2010 Jun 02,;5(6):e10926.

88. Wong AHM, Zhou D, Rini JM. The X-ray crystal structure of human aminopeptidase N reveals a novel dimer and the basis for peptide processing. J Biol Chem. 2012 Oct 26,;287(44):36804-13.

89. Luan Y, Xu W. The structure and main functions of aminopeptidase N. Curr Med Chem. 2007;14(6):639-47.

90. O'Connell PJ, Gerkis V, d'Apice AJ. Variable O-glycosylation of CD13 (aminopeptidase N). J Biol Chem. 1991 Mar 05,;266(7):4593-7.

91. Wickström M, Larsson R, Nygren P, Gullbo J. Aminopeptidase N (CD13) as a target for cancer chemotherapy. Cancer Sci. 2011 Mar;102(3):501-8.

92. Ghosh M, McAuliffe B, Subramani J, Basu S, Shapiro LH. CD13 regulates dendritic cell cross-presentation and T cell responses by inhibiting receptor-mediated antigen uptake. J Immunol. 2012 Jun 01,;188(11):5489-99.

93. Mina-Osorio P, Winnicka B, O'Conor C, Grant CL, Vogel LK, Rodriguez-Pinto D, et al. CD13 is a novel mediator of monocytic/endothelial cell adhesion. J Leukoc Biol. 2008 Aug;84(2):448-59.

94. Mina-Osorio P. The moonlighting enzyme CD13: old and new functions to target. Trends Mol Med. 2008 Aug;14(8):361-71.

95. Corti A, Curnis F. Tumor vasculature targeting through NGR peptide-based drug delivery systems. Curr Pharm Biotechnol. 2011 Aug;12(8):1128-34.

96. Dixon J, Kaklamanis L, Turley H, Hickson ID, Leek RD, Harris AL, et al. Expression of aminopeptidase-n (CD 13) in normal tissues and malignant neoplasms of epithelial and lymphoid origin. J Clin Pathol. 1994 Jan;47(1):43-7.

97. Curnis F, Arrigoni G, Sacchi A, Fischetti L, Arap W, Pasqualini R, et al. Differential binding of drugs containing the NGR motif to CD13 isoforms in tumor vessels, epithelia, and myeloid cells. Cancer Res. 2002 Feb 01,;62(3):867-74.

98. Pasqualini R, Koivunen E, Kain R, Lahdenranta J, Sakamoto M, Stryhn A, et al. Aminopeptidase N is a receptor for tumor-homing peptides and a target for inhibiting angiogenesis. Cancer Res. 2000 Feb 01,;60(3):722-7.

99. Buehler A, van Zandvoort, Marc A. M. J., Stelt BJ, Hackeng TM, Schrans-Stassen, Bianca H. G. J., Bennaghmouch A, et al. cNGR: a novel homing sequence for CD13/APN targeted molecular imaging of murine cardiac angiogenesis in vivo. Arterioscler Thromb Vasc Biol. 2006 Dec;26(12):2681-7.

100. Fukasawa K, Fujii H, Saitoh Y, Koizumi K, Aozuka Y, Sekine K, et al. Aminopeptidase N (APN/CD13) is selectively expressed in vascular endothelial cells and plays multiple roles in angiogenesis. Cancer Lett. 2006 Nov 08,;243(1):135-43.

101. Zhang X, Xu W. Aminopeptidase N (APN/CD13) as a target for anti-cancer agent design. Curr Med Chem. 2008;15(27):2850-65.

102. Hashida H, Takabayashi A, Kanai M, Adachi M, Kondo K, Kohno N, et al. Aminopeptidase N is involved in cell motility and angiogenesis: its clinical significance in human colon cancer. Gastroenterology. 2002 Feb;122(2):376-86.

103. Arap W, Pasqualini R, Ruoslahti E. Cancer treatment by targeted drug delivery to tumor vasculature in a mouse model. Science. 1998 Jan 16,;279(5349):377-80.

104. Wang RE, Niu Y, Wu H, Hu Y, Cai J. Development of NGR-based anti-cancer agents for targeted therapeutics and imaging. Anticancer Agents Med Chem. 2012 Jan;12(1):76-86.

105. Zou M, Zhang L, Xie Y, Xu W. NGR-based strategies for targeting delivery of chemotherapeutics to tumor vasculature. Anticancer Agents Med Chem. 2012 Mar;12(3):239-46.

106. Ashley EA. Towards precision medicine. Nat Rev Genet. 2016 08 16,;17(9):507-22.

107. Muro S. Challenges in design and characterization of ligand-targeted drug delivery systems. J Control Release. 2012 Dec 10,;164(2):125-37.

108. Bae YH, Park K. Targeted drug delivery to tumors: myths, reality and possibility. J Control Release. 2011 Aug 10,;153(3):198-205.

109. Danhier F, Feron O, Préat V. To exploit the tumor microenvironment: Passive and active tumor targeting of nanocarriers for anti-cancer drug delivery. J Control Release. 2010 Dec 01,;148(2):135-46.

110. Zhang X, Eden HS, Chen X. Peptides in cancer nanomedicine: drug carriers, targeting ligands and protease substrates. J Control Release. 2012 Apr 10,;159(1):2-13.

111. Gilad Y, Firer M, Gellerman G. Recent Innovations in Peptide Based Targeted Drug Delivery to Cancer Cells. Biomedicines. 2016 May 26,;4(2).

112. Fosgerau K, Hoffmann T. Peptide therapeutics: current status and future directions. Drug Discov Today. 2015 Jan;20(1):122-8.

113. Smith GP, Petrenko VA. Phage Display. Chem Rev. 1997 Apr 01,;97(2):391-410.

114. Koivunen E, Arap W, Rajotte D, Lahdenranta J, Pasqualini R. Identification of receptor ligands with phage display peptide libraries. J Nucl Med. 1999 May;40(5):883-8.

115. Campa MJ, Kuan CT, O'Connor-McCourt MD, Bigner DD, Patz EF. Design of a novel small peptide targeted against a tumor-specific receptor. Biochem Biophys Res Commun. 2000 Aug 28,;275(2):631-6.

116. Park BW, Zhang HT, Wu C, Berezov A, Zhang X, Dua R, et al. Rationally designed anti-HER2/neu peptide mimetic disables P185HER2/neu tyrosine kinases in vitro and in vivo. Nat Biotechnol. 2000 Feb;18(2):194-8.

117. Song S, Liu D, Peng J, Deng H, Guo Y, Xu LX, et al. Novel peptide ligand directs liposomes toward EGF-R high-expressing cancer cells in vitro and in vivo. FASEB J. 2009 May;23(5):1396-404.

118. Joo H, Chavan AG, Phan J, Day R, Tsai J. An amino acid packing code for α-helical structure and protein design. J Mol Biol. 2012 Jun 08,;419(3-4):234-54.

119. Joo H, Tsai J. An amino acid code for β-sheet packing structure. Proteins. 2014 Sep;82(9):2128-40.

120. Joo H, Chavan AG, Fraga KJ, Tsai J. An amino acid code for irregular and mixed protein packing. Proteins. 2015 Dec;83(12):2147-61.

121. Voronoi G. Nouvelles applications des paramètres continus à la théorie des formes quadratiques. Deuxième mémoire. Recherches sur les parallélloèdres primitifs. Journal für die reine und angewandte Mathematik. 1908;134:198-287.

122. Delaunay B. Sur la sphère vide. A la mémoire de Georges Voronoï. Bulletin de l'Académie des Sciences de l'URSS. 1934(6):793-800.

123. Abdollahi A, Folkman J. Evading tumor evasion: current concepts and perspectives of anti-angiogenic cancer therapy. Drug Resist Updat. 2010 Feb-Apr;13(1-2):16-28.

124. Corti A, Pastorino F, Curnis F, Arap W, Ponzoni M, Pasqualini R. Targeted drug delivery and penetration into solid tumors. Med Res Rev. 2012 Sep;32(5):1078-91.

125. Liu C, Yang Y, Chen L, Lin Y, Li F. A unified mechanism for aminopeptidase N-based tumor cell motility and tumor-homing therapy. J Biol Chem. 2014 Dec 12,;289(50):34520-9.

126. Pettersen EF, Goddard TD, Huang CC, Couch GS, Greenblatt DM, Meng EC, et al. UCSF Chimera--a visualization system for exploratory research and analysis. J Comput Chem. 2004 Oct;25(13):1605-12.

127. Kabsch W, Sander C. Dictionary of protein secondary structure: pattern recognition of hydrogen-bonded and geometrical features. Biopolymers. 1983 Dec;22(12):2577-637.

128. Plaxco KW, Simons KT, Baker D. Contact order, transition state placement and the refolding rates of single domain proteins. J Mol Biol. 1998 Apr 10,;277(4):985-94.

129. Beck A, Bussat MC, Klinguer-Hamour C, Goetsch L, Aubry JP, Champion T, et al. Stability and CTL activity of N-terminal glutamic acid containing peptides. J Pept Res. 2001 Jun;57(6):528-38.

130. Martin AN, Sinko PJ. Martin's Physical Pharmacy and Pharmaceutical Sciences: Physical Chemical and Biopharmaceutical Principles in the Pharmaceutical Sciences. 6th ed. Lippincott Williams & Wilkins; 2011.

131. Li S, Schöneich C, Borchardt RT. Chemical instability of protein pharmaceuticals: Mechanisms of oxidation and strategies for stabilization. Biotechnol Bioeng. 1995 Dec 05,;48(5):490-500.

132. Trott O, Olson AJ. AutoDock Vina: improving the speed and accuracy of docking with a new scoring function, efficient optimization and multithreading. J Comput Chem. 2010 -1-30;31(2):455-61.

133. Hauser AS, Windshügel B. LEADS-PEP: A Benchmark Data Set for Assessment of Peptide Docking Performance. J Chem Inf Model. 2016 Jan 25,;56(1):188-200.

134. Chen L, Lin Y, Peng G, Li F. Structural basis for multifunctional roles of mammalian aminopeptidase N. Proc Natl Acad Sci U S A. 2012 Oct 30,;109(44):17966-71.

135. Chandrudu S, Simerska P, Toth I. Chemical methods for peptide and protein production. Molecules. 2013 Apr 12,;18(4):4373-88.

136. Amblard M, Fehrentz J, Martinez J, Subra G. Fundamentals of modern peptide synthesis. Methods Mol Biol. 2005;298:3-24.

137. Mäde V, Els-Heindl S, Beck-Sickinger AG. Automated solid-phase peptide synthesis to obtain therapeutic peptides. Beilstein J Org Chem. 2014;10:1197-212.

138. Isidro-Llobet A, Alvarez M, Albericio F. Amino acid-protecting groups. Chem Rev. 2009 Jun;109(6):2455-504.

139. Kaiser E, Colescott RL, Bossinger CD, Cook PI. Color test for detection of free terminal amino groups in the solid-phase synthesis of peptides. Anal Biochem. 1970 Apr;34(2):595-8.

140. Anizon F, Boyle FT, Fisher J, Kocienski PJ. Synthesis and Characterisation of a Doxorubicin-CNGRC Peptide Conjugate that Targets Tumour Vasculature. Synthesis. 2002 /12;2002(18):2733-6.

141. Chhabra SR, Khan AN, Bycroft BW. Versatile Dde-based primary amine linkers for solid phase synthesis. Tetrahedron Letters. 1998 May 21,;39(21):3585-8.

142. Zheng Y, Ji S, Czerwinski A, Valenzuela F, Pennington M, Liu S. FITC-conjugated cyclic RGD peptides as fluorescent probes for staining integrin αvβ3/αvβ5 in tumor tissues. Bioconjug Chem. 2014 Nov 19,;25(11):1925-41.

143. Yakimchuk K. Receptor-Ligand Binding Assays. Materials and Methods. 2018 /12/11.

144. van Hensbergen Y, Broxterman HJ, Hanemaaijer R, Jorna AS, van Lent NA, Verheul HMW, et al. Soluble aminopeptidase N/CD13 in malignant and nonmalignant effusions and intratumoral fluid. Clin Cancer Res. 2002 Dec;8(12):3747-54.

145. Plesniak LA, Salzameda B, Hinderberger H, Regan E, Kahn J, Mills SA, et al. Structure and activity of CPNGRC: a modified CD13/APN peptidic homing motif. Chem Biol Drug Des. 2010 Jun;75(6):551-62.

146. Curnis F, Fiocchi M, Sacchi A, Gori A, Gasparri A, Corti A. NGR-tagged nano-gold: A new CD13-selective carrier for cytokine delivery to tumors. Nano Res. 2016 May;9(5):1393-408.

147. Reversible Modes of Inhibitor Interactions with Enzymes. In: Evaluation of Enzyme Inhibitors in Drug Discovery. John Wiley & Sons, Ltd; 2013. p. 57-121.

148. Li G, Xing Y, Wang J, Conti PS, Chen K. Near-infrared fluorescence imaging of CD13 receptor expression using a novel Cy5.5-labeled dimeric NGR peptide. Amino Acids. 2014 Jun;46(6):1547-56.

149. Liang J, Wu W, Xu X, Zhuo R, Zhang X. pH responsive micelle self-assembled from a new amphiphilic peptide as anti-tumor drug carrier. Colloids Surf B Biointerfaces. 2014 Feb 01,;114:398-403.

150. Langer R. Drug delivery and targeting. NATURE-LONDON-. 1998:5-10.

151. Su H, Koo JM, Cui H. One-component nanomedicine. J Controlled Release. 2015;219:383-95.

152. Khandare J, Minko T. Polymer–drug conjugates: progress in polymeric prodrugs. Progress in polymer science. 2006;31(4):359-97.

153. Wang Y, Cheetham AG, Angacian G, Su H, Xie L, Cui H. Peptide–drug conjugates as effective prodrug strategies for targeted delivery. Advanced Drug Delivery Reviews. 2017 February 1,;110-111:112-26.

154. Kapoor P, Singh H, Gautam A, Chaudhary K, Kumar R, Raghava GPS. TumorHoPe: a database of tumor homing peptides. PLoS ONE. 2012;7(4):e35187.

155. Vrettos EI, Mező G, Tzakos AG. On the design principles of peptide–drug conjugates for targeted drug delivery to the malignant tumor site. Beilstein J Org Chem. 2018 -4-26;14:930-54.

156. Jaracz S, Chen J, Kuznetsova LV, Ojima I. Recent advances in tumor-targeting anticancer drug conjugates. Bioorg Med Chem. 2005 Sep 01,;13(17):5043-54.

157. Sato H. Enzymatic procedure for site-specific pegylation of proteins. Adv Drug Deliv Rev. 2002 Jun 17,;54(4):487-504.

158. Alley SC, Zhang X, Okeley NM, Anderson M, Law C, Senter PD, et al. The pharmacologic basis for antibody-auristatin conjugate activity. J Pharmacol Exp Ther. 2009 Sep;330(3):932-8.

159. Doronina SO, Toki BE, Torgov MY, Mendelsohn BA, Cerveny CG, Chace DF, et al. Development of potent monoclonal antibody auristatin conjugates for cancer therapy. Nat Biotechnol. 2003 Jul;21(7):778-84.

160. Soudy R, Gill A, Sprules T, Lavasanifar A, Kaur K. Proteolytically stable cancer targeting peptides with high affinity for breast cancer cells. J Med Chem. 2011 Nov 10,;54(21):7523-34.

161. Polyak D, Ryppa C, Eldar-Boock A, Ofek P, Many A, Licha K, et al. Development of PEGylated doxorubicin-E-[c(RGDfK)2] conjugate for integrin-targeted cancer therapy. Polymers for Advanced Technologies. 2011;22(1):103-13.

162. Ai S, Duan J, Liu X, Bock S, Tian Y, Huang Z. Biological evaluation of a novel doxorubicin-peptide conjugate for targeted delivery to EGF receptor-overexpressing tumor cells. Mol Pharm. 2011 Apr 04,;8(2):375-86.

163. Francisco JA, Cerveny CG, Meyer DL, Mixan BJ, Klussman K, Chace DF, et al. cAC10-vcMMAE, an anti-CD30-monomethyl auristatin E conjugate with potent and selective antitumor activity. Blood. 2003 Aug 15,;102(4):1458-65.

164. Jain N, Smith SW, Ghone S, Tomczuk B. Current ADC Linker Chemistry. Pharm Res. 2015 Nov;32(11):3526-40.

165. Morton CL, Houghton PJ. Establishment of human tumor xenografts in immunodeficient mice. Nat Protoc. 2007;2(2):247-50.

166. Graziadio A, Zanda M, Frau S, Fleming IN, Musolino M, Dall'Angelo S, et al. NGR Tumor-Homing Peptides: Structural Requirements for Effective APN (CD13) Targeting. Bioconjugate Chem. 2016 May 18,;27(5):1332-40.

167. Dubowchik GM, Firestone RA, Padilla L, Willner D, Hofstead SJ, Mosure K, et al. Cathepsin B-labile dipeptide linkers for lysosomal release of doxorubicin from internalizing immunoconjugates: model studies of enzymatic drug release and antigen-specific in vitro anticancer activity. Bioconjug Chem. 2002 Jul-Aug;13(4):855-69.

168. Plum A, Jensen LB, Kristensen JB. In vitro protein binding of liraglutide in human plasma determined by reiterated stepwise equilibrium dialysis. J Pharm Sci. 2013 Aug;102(8):2882-8.

169. Hsiao I-, Huang Y. Effects of serum on cytotoxicity of nano- and micro-sized ZnO particles. J Nanopart Res. 2013;15:1829.

170. Enyedi KN, Tóth S, Szakács G, Mező G. NGR-peptide−drug conjugates with dual targeting properties. PLOS ONE. 2017 Jun 2,;12(6):e0178632.

171. Peng Z, Kopeček J. Synthesis and activity of tumor-homing peptide iRGD and histone deacetylase inhibitor valproic acid conjugate. Bioorg Med Chem Lett. 2014 Apr 15,;24(8):1928-33.

172. Mirsalis JC, Schindler-Horvat J, Hill JR, Tomaszewski JE, Donohue SJ, Tyson CA. Toxicity of dolastatin 10 in mice, rats and dogs and its clinical relevance. Cancer Chemother Pharmacol. 1999;44(5):395-402.

173. Poncet J. The dolastatins, a family of promising antineoplastic agents. Curr Pharm Des. 1999 Mar;5(3):139-62.

174. Böttger R, Hoffmann R, Knappe D. Differential stability of therapeutic peptides with different proteolytic cleavage sites in blood, plasma and serum. PLOS ONE. 2017 Jun 2,;12(6):e0178943.

175. Wahlang JB, Laishram PD, Brahma DK, Sarkar C, Lahon J, Nongkynrih BS. Adverse drug reactions due to cancer chemotherapy in a tertiary care teaching hospital. Ther Adv Drug Saf. 2017 -2;8(2):61-6.

176. Foy KC, Wygle RM, Miller MJ, Overholser JP, Bekaii-Saab T, Kaumaya PTP. Peptide vaccines and peptidomimetics of EGFR (HER-1) ligand binding domain inhibit cancer cell growth in vitro and in vivo. J Immunol. 2013 Jul 01,;191(1):217-27.

177. Li HM, Dong ZP, Wang QY, Liu LX, Li BX, Ma XN, et al. De Novo Computational Design for Development of a Peptide Ligand Oriented to VEGFR-3 with High Affinity and Long Circulation. Mol Pharm. 2017 07 03,;14(7):2236-44.

178. Joshi S, Chen L, Winter MB, Lin Y, Yang Y, Shapovalova M, et al. The Rational Design of Therapeutic Peptides for Aminopeptidase N using a Substrate-Based Approach. Sci Rep. 2017 05 02,;7(1):1424.

179. Curnis F, Cattaneo A, Longhi R, Sacchi A, Gasparri AM, Pastorino F, et al. Critical role of flanking residues in NGR-to-isoDGR transition and CD13/integrin receptor switching. J Biol Chem. 2010 Mar 19,;285(12):9114-23.

180. Lai MC, Topp EM. Solid-state chemical stability of proteins and peptides. J Pharm Sci. 1999 May;88(5):489-500.

181. Pernot M, Vanderesse R, Frochot C, Guillemin F, Barberi-Heyob M. Stability of peptides and therapeutic success in cancer. Expert Opin Drug Metab Toxicol. 2011 Jul;7(7):793-802.

182. Adessi C, Soto C. Converting a peptide into a drug: strategies to improve stability and bioavailability. Curr Med Chem. 2002 May;9(9):963-78.

183. Lakowicz JR. Principles of Fluorescence Spectroscopy. 3rd ed. Springer US; 2006.

184. Kuzmicheva GA, Belyavskaya VA. [Peptide phage display in biotechnology and biomedicine]. Biomed Khim. 2016 Jul;62(5):481-95.

185. Bábíčková J, Tóthová Ľ, Boor P, Celec P. In vivo phage display--a discovery tool in molecular biomedicine. Biotechnol Adv. 2013 Dec;31(8):1247-59.

186. van Hensbergen Y, Broxterman HJ, Elderkamp YW, Lankelma J, Beers JCC, Heijn M, et al. A doxorubicin-CNGRC-peptide conjugate with prodrug properties. Biochem Pharmacol. 2002 Mar 01,;63(5):897-908.